

学位論文

*Microwave Spectroscopy of the Complexes
containing the NaCl Molecule*

(NaCl分子を含む分子錯体のマイクロ波分光)

Asao Mizoguchi

溝口 麻雄

Thesis

Microwave Spectroscopy of the Complexes
containing the NaCl Molecule

Asao Mizoguchi

Department of Basic Science,
Graduate School of Arts and Sciences,
The University of Tokyo

February 1998

Acknowledgments

I wish to thank Professor Yasuki Endo for his helpful guidance, valuable suggestions, and kind encouragement throughout this study. I wish also to express my gratitude to Professor Yasuhiro Ohshima for his valuable suggestions and great encouragement. I am also grateful to Dr. Yoshihiro Sumiyoshi for many helpful discussions and encouragement.

I am grateful to Drs. Hiroshi Kohguchi, Kennosuke Hoshina, and Yasuko Kasai for their helpful advice and kind encouragement. I am grateful to all members in Endo laboratory in the University of Tokyo for their much help throughout my study.

I am grateful to Drs. Toshio Asada and Kichisuke Nishimoto for their helpful advice and giving us their result of the simulation of MX-(H₂O).

Finally, I would like to express my special thanks to my parents for their encouragement and the support of my living expenses and school expenses.

Contents

Chapter 1. General Introduction	
§ 1.1 Introduction	2
§ 1.2 Experimental Method	7
1.2.1 Production of complexes	
1.2.2 Detection of complexes	
References, Table, Figures	13
Appendix	23
Chapter 2. The rotation spectra of the Rg-NaCl (Rg = Ar, Kr) complexes	
§ 2.0 Abstract	26
§ 2.1 Experiment	27
§ 2.2 Results and Analysis	29
2.2.1 Ar-NaCl	
2.2.2 Kr-NaCl	
§ 2.3 Discussion	33
2.3.1 Structure of the Rg-NaCl complex	
2.3.2 Induction effect in the Rg-NaCl complex	
2.3.3 Intermolecular potential energy surface of the Rg-NaCl complex	
References, Tables, Figures	41
Appendixes	52

Chapter 3. Microwave Spectroscopy of the $\text{NaCl}-(\text{H}_2\text{O})_n$ ($n = 1, 2, 3$) complexes and Microsolvation process on NaCl	
§ 4.0 Abstract	80
§ 4.2 Experimental	81
§ 4.3 Results and Analysis	82
4.3.1 $\text{NaCl}-\text{H}_2\text{O}$	
4.3.2 $\text{NaCl}-(\text{H}_2\text{O})_2$	
4.3.3 $\text{NaCl}-(\text{H}_2\text{O})_3$	
§ 4.4 Discussion	88
4.4.1 <i>Structures of the $\text{NaCl}-(\text{H}_2\text{O})_n$ complexes</i>	
4.4.2 <i>Intermolecular interaction in the $\text{NaCl}-(\text{H}_2\text{O})_n$ complexes</i>	
4.4.3 <i>Microsolvation process on NaCl</i>	
References, Figures, Tables	99
Appendixes	117

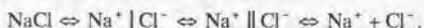
Chapter 1
General Introduction

§ 1.1 Introduction	2
§ 1.2 Experimental Method	7
1.2.1 Production of complexes	
1.2.2 Detection of complexes	
References, Table, Figures	13
Appendix	23

§ 1.1 Introduction

Solvation effects can profoundly alter chemical and physical interactions between molecules. Alkali halides near the vicinity of the equilibrium structure in the electronic ground state have an ionic character and are strongly bound with each other by their electrostatic forces (about 100 to 140 kcal/mol). In the gas phase, alkali halides dissociate into neutral atoms because the potential curve in the ground state changes from ionic character to covalent character as a result of non-crossing rule as the nuclei are separated [1]. However, it is known that, in aqueous solutions, most of their corresponding crystals are easily dissolved into ions. Understanding of the behavior of ion pairs in water is one of the fundamental and important issues in chemistry because association of oppositely charged ions is an important step in many chemical reactions. In the present work, complexes of an ion pair, NaCl, with up to three water molecules have been investigated in order to understand microscopic mechanisms of solution. While this model system cannot be expected to predict quantitatively the solvation effects, it can provide valuable insights into forces controlling the arrangement of the solvent molecules around the Na⁺ and Cl⁻ ions, which govern the solvation effect on the NaCl bond. In addition, results of this investigation will provide information on potential functions of the ionic exit channel in an initial process of solvation.

A general scheme for the solvation process of an ion pair may be written as follows



where two intermediate states, Na⁺ | Cl⁻ and Na⁺ || Cl⁻, denotes the contact ion-pair (CIP) and the solvent-separated ion-pair (SSIP) states, respectively. Existence of the two intermediate states was first proposed by Winstein *et al.* [2] in 1957 to interpret the dependence of the rate constants for solvolysis of several electrolytes on the addition of salt. However, no detailed information on the role of

the two intermediate states has been obtained yet.

To date, the $\text{NaCl}-(\text{H}_2\text{O})_n$ system which consists of an isolated NaCl molecule and a few H_2O molecules has been studied using several computational and experimental methods.

On the experimental side, however, only one paper has been reported for the system. In 1978 Ault [3] measured infrared spectra of several Ar matrix-isolated complexes, which are made up of one alkali halide (NaCl, KCl, CsCl, CsBr, or CsI) and one H_2O molecule. On the basis of the dependence of the vibrational frequency shift on the change of the alkali halide in each complex, he determined the structure of the alkali halide-water complex to be form (I) among four possible structures (I), (V), (VI), and (VII) of Fig. 1.1.

On the computational side, Smith and Dang [4] have performed a molecular dynamics computer simulation of NaCl in water. They calculated the potential of mean force (PMF) shown in Fig. 1.2, which expresses the free energy of an ion pair as a function of the separation $r(\text{NaCl})$. The PMF showed existence of two minima corresponding to the two intermediate states, CIP and SSIP. They estimated from the PMF that the distances $r(\text{NaCl})$ between Na and Cl were 2.7–2.8 Å and ~5 Å for the CIP and SSIP states, respectively.

So far, several *ab initio* calculations have been performed on the $\text{NaCl}-(\text{H}_2\text{O})_n$ complexes. Kulkarni and Rao [5] have calculated several possible structures of the $\text{MX}-\text{H}_2\text{O}$ ($M = \text{Li, Na}$; $X = \text{F, Cl}$) complexes, (I), (II), (V), (VI), and (VII) as shown in Fig. 1.1, with low level basis functions (HF/STO-3G). Although the most stable structure was calculated to be (I) for $\text{NaCl}-\text{H}_2\text{O}$, which is in agreement with the experimental result of Ault, the most stable structure was determined to be (II) for other alkali halide-water complexes. Recently, Woon and Dunning, Jr [6] have calculated the most stable structures of four species of $M^+X^--(\text{H}_2\text{O})_n$ ($M = \text{Li, Na}$; $X = \text{F, Cl}$) from $n = 1$ up to 2 or 3 using the second-order Møller-Plesset perturbation

method with rather high level basis functions (cc-pVDZ and aug-cc-pVDZ). They calculated energies for four possible structures (II), (III), (IV), and (VI) in Fig. 1.1. and determined the most stable structure to be (III) for all the $\text{MX}-\text{H}_2\text{O}$ complexes. They explained the difference of the result of Kuklarni and Rao as the effects of excessive basis set superposition error and/or over estimation of the electrostatic properties in the smaller basis sets. Furthermore, they assumed that $\text{MX}-(\text{H}_2\text{O})_2$ has C_2 symmetry and the structure for $\text{MX}-(\text{H}_2\text{O})_2$ to be the one with the second H_2O located that it is rotated by 180° around the MX axis from the first H_2O . Similarly, $\text{MX}-(\text{H}_2\text{O})_3$ has C_n symmetry with the second and third water molecules to be located by $\pm 120^\circ$ away from the first H_2O , as shown in Fig. 1.3. The most stable structures were derived for $\text{LiX}-(\text{H}_2\text{O})_n$ ($n = 1, 2, 3$) and $\text{NaX}-(\text{H}_2\text{O})_n$ ($n = 1, 2$). They reported that, for all the complexes they calculated, $r(\text{MX})$ increases gradually with the increase of the number of the H_2O molecules. From the fact that the change of the distance $r(\text{LiX})$ from $\text{LiX}-(\text{H}_2\text{O})_2$ to $\text{LiX}-(\text{H}_2\text{O})_3$ is slightly larger than that from $\text{LiX}-\text{H}_2\text{O}$ to $\text{LiX}-(\text{H}_2\text{O})_2$ in the $\text{LiX}-(\text{H}_2\text{O})_n$ complexes, they estimated that the change due to adding the third H_2O molecule to NaCl will be larger than the change observed upon adding the second H_2O molecule. As a result, $r(\text{NaCl})$ in $\text{NaCl}-(\text{H}_2\text{O})_3$ was expected to be approaching to the distance estimated for CIP in the simulation of Smith and Dang. They also reported that substantial charge is transferred from the halides to water molecules. From a comparison of the stability of LiCl with that of $\text{Li}^+ + \text{Cl}^-$ when one water was added, the energy required to dissociate $\text{LiCl}-\text{H}_2\text{O}$ into $\text{Li}^+(\text{H}_2\text{O}) + \text{Cl}^-$ was calculated to be 136 kcal/mol. The second and third waters further lower the energy to 126 and 120 kcal/mol, respectively. Although this change was dramatic, it was far from that observed in solution, where CIP is bound by only a few kcal/mol.

In an independent study, Asada and Nishimoto [7,8] have carried out a Monte Carlo simulation of $\text{NaCl}-(\text{H}_2\text{O})_n$ ($n = 1 \sim 8$) with bond-bond potential

functions, which were proposed by Honda and Kitaura [9]. Their optimized structures derived from their potential functions are shown in Fig. 1.4. The most stable structures for $n = 1$ and 2 of $\text{NaCl}-(\text{H}_2\text{O})_n$ are nearly the same as those of Woon and Dunning, Jr. They showed that, from the Monte Carlo simulation, average distance between Na and Cl changes monotonously with the increase of the number of water molecules. Furthermore, they have proposed a possible solvation model that water molecules are first hydrated with the Na ion, and then the water molecules are shared with the Na ion and the Cl ion.

No study on the complexes containing ion pairs such as alkali halide molecules have been carried out in the gas phase. There may be two reasons. The first one is the difficulty of efficient production of such complexes because alkali halides are solid with a high melting point, being not easy to obtain sufficient vapor pressure of the alkali halide to produce complexes. Another reason we can consider is as follows. Since the first excited electronic state of alkali halides is very shallow or dissociative [10], the excited states of the complexes are also expected to be shallow or dissociative. Thus the spectroscopic methods, such as laser-induced fluorescence spectroscopy, which has very high sensitivity in the visible or ultraviolet region, cannot be applied in investigating the spectrum of the complex containing alkali halide molecules.

In this thesis, $\text{Rg}-\text{NaCl}$ ($\text{Rg} = \text{Ar}, \text{Kr}$) and $\text{NaCl}-(\text{H}_2\text{O})_n$ ($n = 1, 2, 3$) have been studied by using a Fourier-transform microwave (FTMW) spectrometer coupled with a laser ablation source, as will be discussed in section 1.2. The characteristic features of this spectrometer, high sensitivity and high resolution, will give us detailed information on these complexes. For example, the determined rotational constants will be used to determine the structures of the complexes, and the nuclear quadrupole coupling constants of the Na and Cl atoms will be used to obtain information on the NaCl bond. In the present study we expect that the

intermolecular interactions between NaCl and H₂O can be discussed on the basis of the detailed information on the structures including the bond length of NaCl.

In chapter 2, pure rotational spectra of the Rg-NaCl complexes (Rg = Ar, Kr) are described in detail. The purpose of the observation of Rg-NaCl was to examine the possibility to detect complexes containing NaCl and, if possible, to investigate the intermolecular interaction between Rg and NaCl. Since the NaCl molecule has a large dipole moment as shown in Table 1.A1.1 of Appendix I, it may be very important to consider the electrostatic effects on the field around Na and Cl by complex formation in understanding the intermolecular interaction. The Rg-NaCl system is one of the best systems to investigate the electrostatic effects on NaCl because Rg does not affect the field by itself. We expect that detailed information on the intermolecular interaction is also very useful to discussions on NaCl-(H₂O)_n.

In chapter 3, pure rotational spectra of the NaCl-(H₂O)_n (n = 1, 2, 3) complexes are described in detail. The main purpose of this investigation is to clarify how NaCl dissolves into the Na⁺ and Cl⁻ ions microscopically by complex formation with a few H₂O molecules, as mentioned above. The pure rotational spectra of the NaCl-(H₂O)_n complexes are observed for the first time in this work. We have determined the molecular structures by using the precisely determined rotational constants, and have obtained information on the electric field around Na and Cl from the nuclear quadrupole coupling constants of Na and Cl. We will discuss in detail how the molecular structure and the charge distribution around Na and Cl are changed with increase of the number of water molecules.

§ 1.2 Experimental Method

1.2.1 Production of complexes

A large number of spectroscopic studies for molecules with high melting points in the gas phase have been performed by means of vaporization of the molecules heated up at high temperatures. NaCl has been studied by this conventional method by heating absorption cells at about 900°C, and its detailed molecular constants have been determined, as shown in Appendix I. However, it is impossible to produce complexes by using the conventional method because the internal energy of the complex is larger than the binding energy between the constituent molecules. In principle, we can use a high temperature pulsed nozzle to produce a supersonic beam containing molecules with high melting points. Such a nozzle was used for the observations of molecules with relatively low melting points such as alkali metals. In this work, however, we used a laser ablation method, which easily produce complexes containing a molecule with a high melting point. A spectroscopic study using the laser ablation method was performed by Powers *et al.* for the first time [11]. They vaporized the Cu metal, and observed an electronic spectrum of Cu₂ in the visible region. Since then the method is extensively applied in various spectroscopic studies. As will be given below, a few studies have already been reported even in the microwave region, where sensitivity is much lower compared to optical spectroscopy.

The laser ablation nozzle assembly used in the present work is shown in Fig. 1.5. We attached an ablation nozzle unit in front of a commercially available solenoid valve (General Valve Co.) with an orifice 0.8 mmφ in diameter. The shape of the nozzle unit was selected among several units with different sizes in order to maximize the intensity of the signal. The fundamental or second harmonic of a Nd³⁺:YAG laser (Spectra Physics Co. Quanta-Ray GCR-3 or GCR-230) was used as a

laser ablation source. The laser beam (100 – 200 mJ/pulse) was focused by a 50 cm focal-length lens onto a target rod through a hole with about 1 mm in diameter. The rod was rotated and translated through a mechanical coupling with a 0.5 mm pitch screw driven by a stepping motor in order to provide a fresh surface of the material for each laser shot.

1.2.2 Detection of complexes

As discussed in section 1.1, we are mainly interested in experimentally clarifying the change of the structures of the $\text{NaCl}-(\text{H}_2\text{O})_n$ ($n = 1, 2, 3$) complexes predicted by ab initio calculations. Therefore, we used an FTMW spectrometer which has resolution high enough to precisely determine the molecular constants of the complexes.

In 1976 Ekkers and Flygare of University of Illinois have constructed an FTMW spectrometer for the first time [12]. Its principle of operation is analogous to that of a Fourier-transform NMR. When an incident microwave pulse was irradiated onto molecules, the molecules are polarized coherently and a macroscopic polarization is produced. When the incident microwave pulse disappeared, the macroscopic polarization oscillates with a frequency corresponding to a rotational transition and decays. This emission in the time domain is called the free induction decay (FID). The FID signal in the time domain is detected and Fourier-transformed to obtain a frequency domain spectrum. In order to maximize the macroscopic polarization, that is, to mix two levels corresponding to the transition with equivalent weights, the microwave pulse width (Δt) must satisfy the condition that Rabi frequency equals to $\pi/2\Delta t$,

$$\frac{\mu E}{\hbar} = \frac{\pi}{2\Delta t} \quad (1.1)$$

where μ and E are the permanent dipole moment of the molecule and the intensity

of the electric field in the cavity, respectively.

In 1981 Balle and Flygare reported a new type of standing wave FTMW spectrometer [13]. This spectrometer has two characteristics. The first is that a Fabry-Perot cavity in a large vacuum chamber was used as a sample cell. It means that the power of the incident microwave pulse can be considerably reduced to simplify the electronics in the apparatus. The second is that it was combined with a pulsed solenoid valve as a molecular source. The use of a pulsed valve in the vacuum chamber, i.e., the use of the supersonic expansion extended the applicability of the system by increasing the number of observable species to not only stable monomer species but transient species such as free radicals, ions, and molecular complexes.

In 1992 Xu *et al.* reported a new type of FTMW spectrometer [14]. Their spectrometer has the arrangement that the molecular beam and MW beam run in parallel. This parallel type of FTMW spectrometer results in a higher sensitivity and a higher resolution compared to the original Balle-Flygare type of setup using a perpendicularly mounted nozzle.

So far, there are a few examples of the FTMW spectrometers coupled to a laser ablation source. For example, the group of NIST has observed rotational spectra of transient molecules such as SiC_2 [15] or metal oxides [16] by using a Balle-Flygare type of FTMW spectrometer. Our group also has observed the MgCl radical [17] by using the same type of spectrometer. The group of the University of British Columbia has observed metal chlorides [18] by using the parallel type of FTMW spectrometer. Although the parallel type of FTMW spectrometer is more sensitive, it has a disadvantage that it was not possible to move the target rod to provide a fresh surface. In the present work, we used a Balle-Flygare type of FTMW spectrometer with perpendicular beam because the "freshness" of the surface was found to have a significant effect for the study of NaCl complexes.

A schematic diagram of the spectrometer used in the present study is shown in Fig. 1.6. The microwave components (mixer, amplifier, circulator and so on) used are listed in Table 1.1. Two aluminum mirrors are located inside the chamber confronted with each other to form a microwave cavity. Two sets of mirrors with 300 mm and 390 mm in diameter were used, all with the radius of curvature of mirrors, 600 mm. The Q-value of the cavity was about 10^4 . One of the mirrors is fixed at the vacuum chamber, and the other can be moved by a stepping motor, which is controlled by a personal computer to adjust the separation to keep the resonance condition of the cavity with the TEM_{001} mode. The resonance condition was checked by monitoring the reflected power of the incident microwave from the cavity by using a microwave circulator. The position with minimum reflected power corresponds to the resonance position. The vacuum chamber is pumped by an 18-inch diffusion pump (DALAVAC LIMITED DPF-18Z; 9000 l/sec), which is backed up by a mechanical buster pump (ULVAC Co. PMB-006CM; 167 l/sec) and a rotary pump (EDWARDS E2M80; 25 l/sec) which are connected in series. The pressure in the vacuum chamber is less than 1×10^{-6} Torr when a gas is not expanded. In the present study the direction of gas pulse emitted is perpendicular to the axis of the Fabry-Perot cavity.

The experimental timing is controlled by TTL pulses from a timing generator as shown in Fig. 1.7. Pulses to the molecular valve are repeated at 10 Hz. The time t_v is the width of the output pulse for the pulsed valve and is fixed at 0.3 ms. The amplitude of the pulse to the pulsed valve is adjusted by a driver in order to optimize the condition of the pressure in the chamber. A gas is expanded from a distance about 25 cm above the center of the cavity. The time td_1 in Fig. 1.7 is a delay time between the opening of the pulsed valve and firing the flash lamp of the ablation laser. The time td_2 is a delay time between the opening of the pulsed valve and the opening of a PIN diode switch 1 (PIN 1). Delay times, td_1 and td_2 , have to

be adjusted to maximize the signal amplitude of the molecule to be measured. The velocity of the emitted gas depends on the carrier gas and that gives an estimate of the delay times. For example, as the velocity is about 500 m/s in Ar carrier gas, the time difference between td_1 and td_2 is estimated to be about 0.5 ms. A CW microwave synthesizer (HP 83711B; frequency range, 1 - 20 GHz with averaged output power of +14 dBm) was used as a microwave source. We consider a case that microwave with a frequency ν is emitted from the synthesizer to explain the operation of the detection system. The time t_1 represents the width of the incident microwave pulse, which is formed by opening a PIN diode (PIN 1) switch. Both the pulse width (t_1) and the incident microwave power are adjusted to satisfy the condition given in Eq. (1.1). After a time t_2 from turning the incident microwave off, the gate of another PIN diode (PIN 2) switch is opened for a time t_3 . The local oscillator (LO) is phase locked using a frequency stabilizer (MICROWAVE/SYSTEMS INC. PLS-60) with a constant frequency difference (60 MHz) with a fixed phase relation with respect to that of the synthesizer. The FID signal is mixed with the LO signal by a mixer (M2) and the IF signal out of M2 is divided into two signals with π phase difference by a π -divider. These two signals are mixed with two 60 MHz local signals with $\pi/2$ phase differences using a mixer (M3 & M4). As a result, we can get two signals of DC \sim 1 MHz and $\pi/2$ phase difference. After a time t_4 from opening of PIN 2, two signals are digitized to digital data with 2560-points by two 8-bit analog-digital converters (THAMWAY AD-8H50AT) with a sampling rate of 50 ns in the personal computer (IBM Aptiva DX4-100MHz). The digital data with 2560-points for each signal is reduced to 512-points by averaging successive 5-points. Assuming that one of the two signals to be a real part and the other as an imaginary part, the complex Fourier-transformation is performed, giving a spectrum spreading around the center frequency ν , where a frequency range of about 1 MHz can be observed at a time. In

order to cancel out the background noise, two signals corresponding to the circumstances when the gas is emitted and not emitted are obtained and subtracted.

For the measurement above 20 GHz, the microwave radiation in the 20 – 40 GHz is obtained by taking a second harmonic of the synthesizer output by using a coaxial frequency doubler (MITEQ MAX2M260400). The output power of the MW radiation is approximately 10 mW for the second harmonic.

We observed spectra of OCS isotopes to check the sensitivity of our spectrometer. As shown in Fig. 1.8, we could observe a rotational spectrum of the $^{18}\text{O}^{13}\text{C}^{32}\text{S}$ (natural abundance: 20.9 ppm). But $^{18}\text{O}^{13}\text{C}^{34}\text{S}$ (natural abundance: 0.93 ppm) could not be observed.

References

- [1] G. Herzberg, *Molecular Spectra and Molecular Structure Volume I - Spectra of Diatomic Molecules*, Krieger Publishing Co., Malabar Florida (1989)
- [2] S. Winstein, E. Clippinger, A. H. Fainberg, and G. C. Robinson, *J. Am. Chem. Soc.*, **76**, 2597(1954)
- [3] B. S. Ault, *J. Am. Chem. Soc.*, **100**, 2426 (1978)
- [4] D. E. Smith and L. X. Dang, *J. Chem. Phys.*, **100**, 3757(1994)
- [5] G. V. Kulkarni and C. N. R. Rao, *J. Mol. Struct.*, **100**, 531(1983)
- [6] D. E. Woon and T. H. Dunning, Jr., *J. Am. Chem. Soc.*, **117**, 1090(1995)
- [7] T. Asada and K. Nishimoto, *Chem. Phys. Letters*, **232**, 518(1995)
- [8] T. Asada and K. Nishimoto, *Molecular Simulation*, **16**, 307(1996)
- [9] K. Honda and K. Kitaura, *Chem. Phys. Letters*, **140**, 53 (1987)
- [10] W. S. Struve, *Fundamentals of Molecular Spectroscopy*, A Wiley-Interscience Publication., New York (1989)
- [11] D. E. Powers, S. G. Hansen, M. E. Gesic, A. C. Pulu, J. B. Hopkins, T. G. Dietz, M. A. Duncan, P. R. R. Langridge-Smith and R. E. Smalley, *J. Phys. Chem.*, **86**, 2556 (1982)
- [12] J. Ekkers and W. H. Flygare, *Rev. Sci. Instrum.*, **47**, 448 (1976)
- [13] T. J. Balle and W. H. Flygare, *Rev. Sci. Instrum.*, **52**, 33 (1981)
- [14] J. Xu, W. Jäger and M. C. L. Gerry, *J. Mol. Spectrosc.*, **151**, 206(1992)
- [15] R. D. Suenram, F. J. Lovas and K. Matsumura, *Ap. J.*, **342**, L103(1989)
- [16] C. E. Blom, H. G. Hedderich, F. J. Lovas, R. D. Suenram and A. G. Maki, *J. Mol. Spectrosc.*, **152**, 109(1992)
- [17] Y. Ohshima and Y. Endo, *Chem. Phys. Letters*, **213**, 95(1993)
- [18] K. D. Hensel, C. Styger, W. Jäger, A. J. Merer and M. C. L. Gerry, *J. Mol. Spectrosc.*, **99**, 3320(1993)

Table 1.1 microwave components used in the present study

	4 - 8 GHz	8 - 18 GHz	18 - 26.5 GHz	26.5 - 40 GHz
Directional Coupler	MM 5013-20	MM 5016-20	Merrimac CWM-10R-22G	Merrimac CWK-10R-29G
Mixer	W&J M14	W&J M74C	W&J SMC1630	MITEQ M2640J
Circulator	TM50A6001	TM10B9201(8-12.4GHz) TM10B2201(12-18GHz)	TM 50A8101	
Local Oscillator	AVANTEK AV-7453	AVANTEK AV-78518	AVANTEK AV-718226	AVANTEK AV-26240/W
Low Noise Amp.	MITEQ AFS3-04000800-10-UJLN	MITEQ AFS4-08001800-30-UJLN	MITEQ JS3-18004000-35	
PIN diode Switch	GM F9114 GM F9014			

MM: Midwest Microwave, W&J: Watkins & Johnson, TM: TRAK Microwave, GM: General Microwave

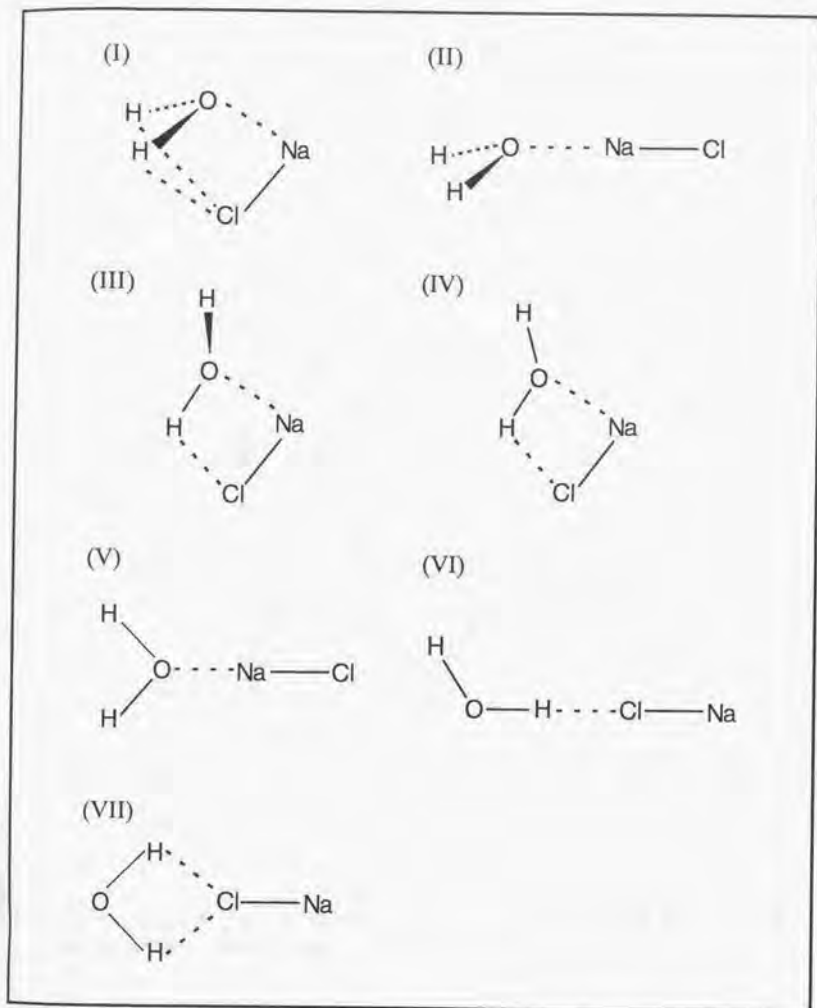


Fig. 1.1 Various possible configurations of the $\text{NaCl-H}_2\text{O}$ structures. Structure (I) has C_s symmetry and a symmetrically hydrogen-bonded structure. Structure (II) has C_s symmetry and has only one interaction point between Na and the lone pair of the O atom. Structure (III) is nonplanar. Only one H atom exist above plane including the Na-Cl-H-O ring. Structures (IV)-(VII) are planar.

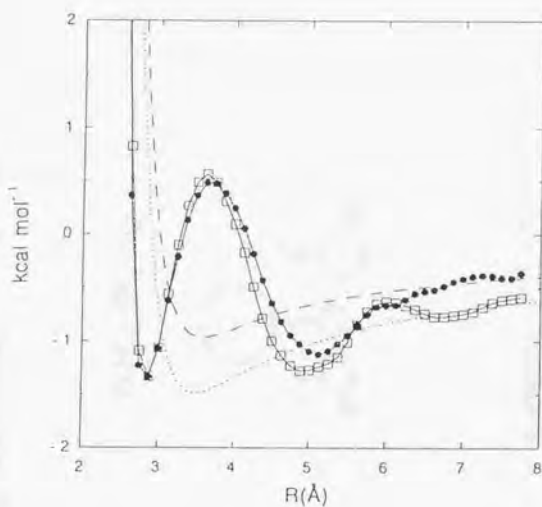
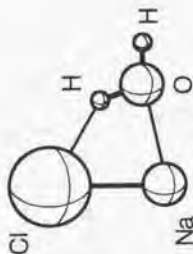


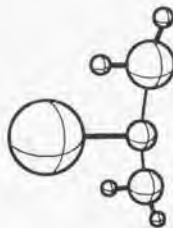
Fig. 1.2 The NaCl potential of mean force in the polarizable water (filled circles) and the single point charge nonpolarizable water (open squares). (*cf.* Smith and Dang, Ref. [4])

The structures of the $\text{NaCl}-(\text{H}_2\text{O})_n$ complexes by *ab initio* calculations

$\text{NaCl}-\text{H}_2\text{O}$



$\text{NaCl}-(\text{H}_2\text{O})_2$



$\text{NaCl}-(\text{H}_2\text{O})_3$

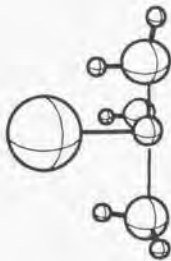


Fig. 1.3 The structures of the $\text{NaCl}-(\text{H}_2\text{O})_n$ complexes. The most stable structures of the $\text{NaCl}-(\text{H}_2\text{O})_n$ ($n = 1, 2$) complexes were optimized by Woon and Dunning, Jr. using the MP2 method in conjunction with *cc-pVDZ* (Na) and *aug-cc-pVDZ* (Cl, O, H). The most stable structures of the $\text{NaCl}-(\text{H}_2\text{O})_3$ complex was predicted from the most stable structures of other $\text{LiX}-(\text{H}_2\text{O})_3$ ($X = \text{F}, \text{Cl}$) complexes. The structures of the $\text{NaCl}-(\text{H}_2\text{O})_n$ ($n = 2, 3$) complexes have C_2 and C_3 symmetry around the NaCl axis, respectively.

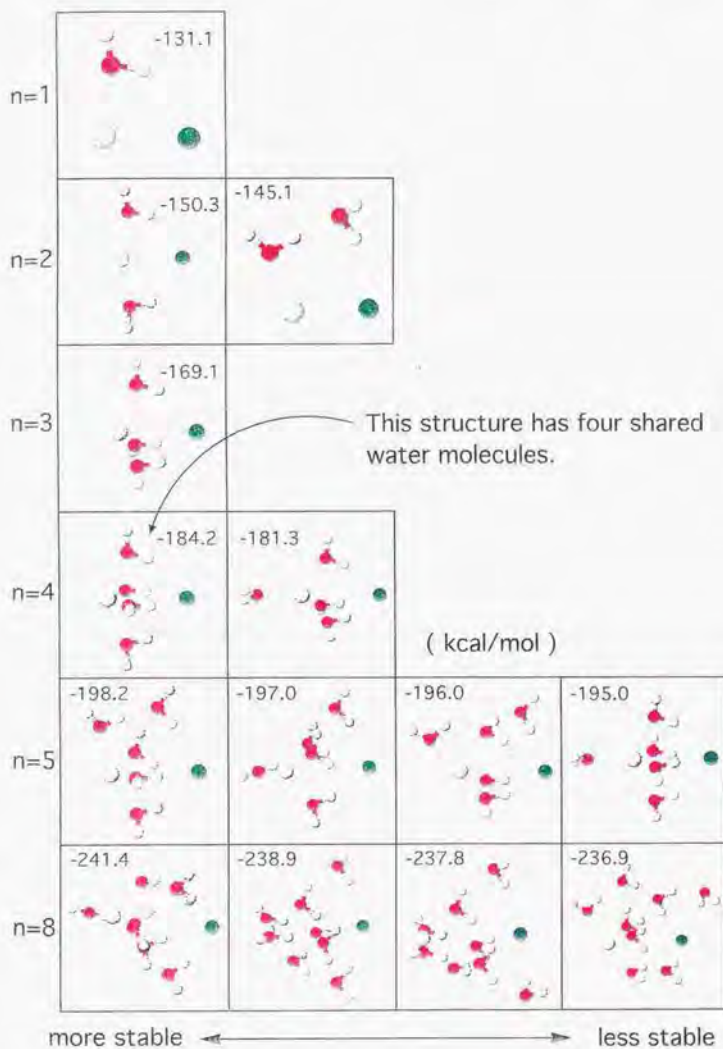


Fig. 1.4 The optimized structures of the $\text{NaCl}-(\text{H}_2\text{O})_n$ ($n = 1 - 5, 8$) complexes. These structures were calculated using their potential functions. (Asada and Nishimoto, Ref [7,8])

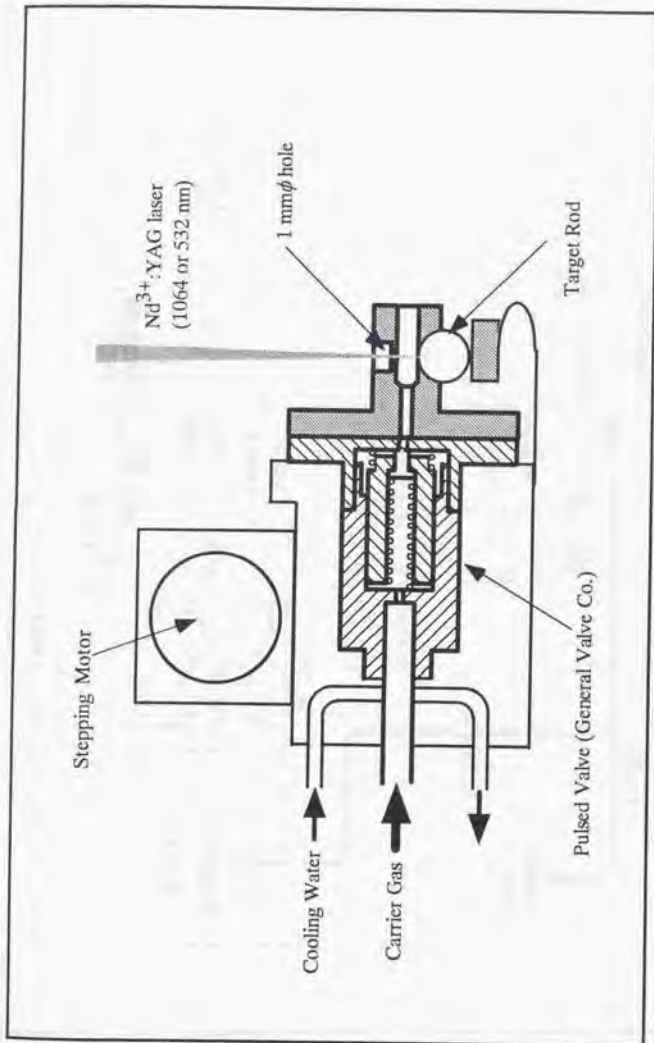


Fig. 1.5 Schematic diagram of the laser ablation nozzle used in the present work. The target rod is connected to a 0.5 mm pitch screw (not shown), which is driven by a stepping motor through a timing belt (not shown).

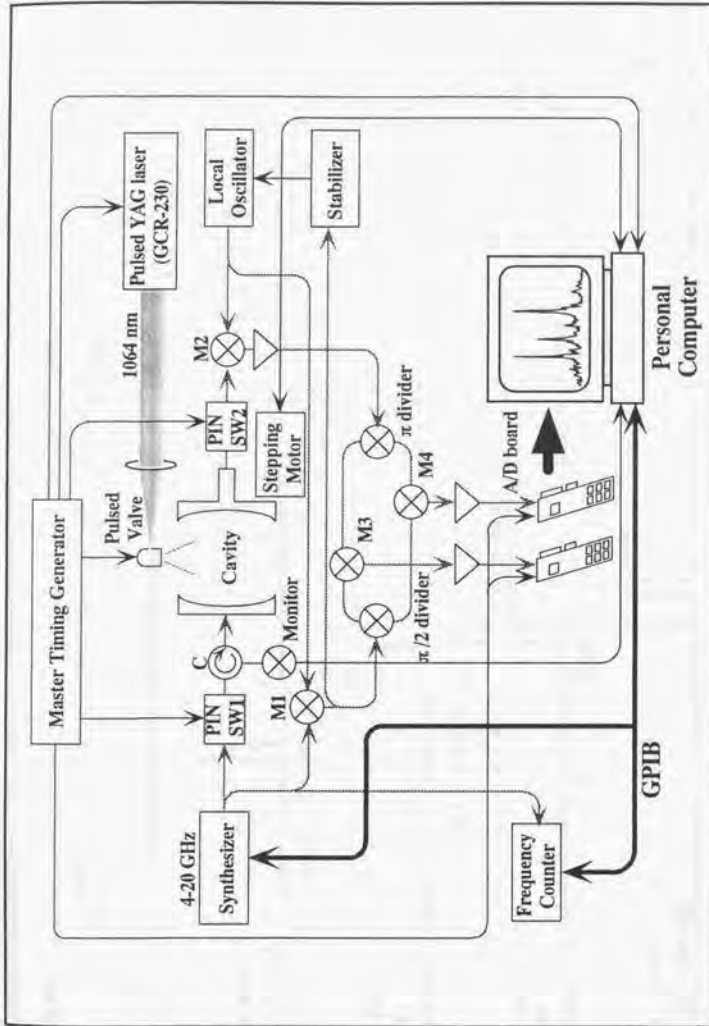


Fig. 1.6 Schematic diagram of the Fourier-transform microwave spectrometer used in the present work

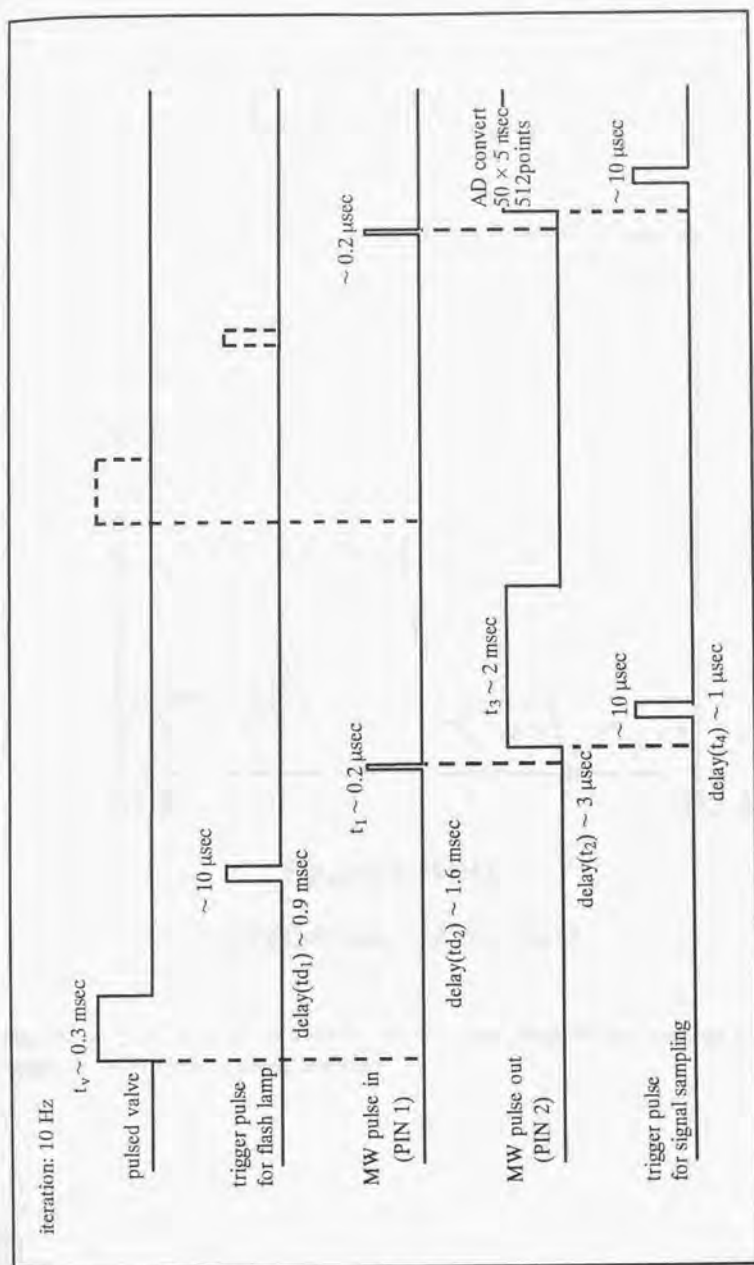


Fig. 1.7 Timing chart showing synchronization of pulsed valve, ablation laser, incident microwave pulse, and signal sampling

Appendix I

The Spectroscopic Studies of the NaCl molecule

The first spectroscopic study of the NaCl monomer itself was reported by Towns and co-worker in 1957 [1]. They observed pure rotational spectra of NaCl with isotopes, ^{35}Cl and ^{37}Cl in the microwave region and determined the rotational constants. Seven years later, Clouser and Gordy observed the pure rotational spectra in the millimeter-wave region and determined the various molecular constants [2]. Hyperfine structure of NaCl was observed by Cederberg *et al.* [3] and Leeuw *et al.* [4] using a molecular-beam electric resonance method. Molecular constants of isolated NaCl so far obtained are shown in Table 1.A1.1.

[1] A. Honig, M. Mandel, M. L. Stich, and C. H. Towns, *Phys. Rev.*, **96**, 629(1954)

[2] P. L. Clouser, and W. Gordy, *Phys. Rev.*, **134**, 864(1964)

[3] J. W. Cederberg, and C. E. Miller, *J. Chem. Phys.*, **50**, 3547(1969)

[4] F. H. de Leeuw, R. van Wachen, and A. Dymanus, *J. Chem. Phys.*, **53**, 981(1970)

Table I.A1.1 The molecular constants of NaCl

		Na ³⁵ Cl	Na ³⁷ Cl	Ref.
ω_e	/cm ⁻¹	364.6880(33) ^a	360.7578(15)	b
B_e	/MHz	6537.406(6)	6397.320(6)	c
D_e	/kHz	9.3540(5)	8.9630(6)	c
$eQq(\text{Na})$	/MHz	-5.6698(60)	-5.6740(9)	d
$eQq(\text{Cl})$	/MHz	-5.6468(60)	-4.4470(13)	d
r_e	/Å		2.360898(46)	e
μ_e	/D		8.97141(7)	d

^a The figures in parentheses are one standard deviation in units of the last significant figure.

^b H. Uehara, K. Horiai, K. Nakagawa, and T. Fujimoto, *J. Mol. Spectrosc.*, 134, 98(1989)

^c P. L. Clouser, and W. Gordy, *Phys. Rev.*, 134, 864(1964)

^d F. H. de Leeuw, R. van Wachen, and A. Dymanus, *J. Chem. Phys.*, 53, 981(1970)



Chapter 2

The Rotational Spectra of the Rg-NaCl (Rg = Ar, Kr) complexes

§ 2.0	Abstract	26
§ 2.1	Experiment	27
§ 2.2	Results and Analysis	29
2.2.1	<i>the Ar-NaCl complex</i>	
2.2.2	<i>the Kr-NaCl complex</i>	
§ 2.3	Discussion	33
2.3.1	<i>the structure of the Rg-NaCl complex</i>	
2.3.2	<i>the induction effect in the Rg-NaCl complex</i>	
2.3.3	<i>the intermolecular potential energy surface of the Rg-NaCl complex</i>	
	References, Tables, Figures	41
	Appendixes	52

§ 2.0 Abstract

Rotational spectra of Rg-NaCl (Rg = Ar, Kr) complexes have been observed for various isotopic species in the 5 - 22 GHz region by using a Fourier-transform microwave spectrometer coupled to a laser ablation source. The rotational constant (B), the centrifugal distortion constants (D , H , and L) and the nuclear quadrupole coupling constants of the Na and Cl atoms have been determined precisely for each isotopic species. We could only observe the transitions with $K = 0$ for the two complexes. Therefore, the structures of the complexes have been determined to be linear molecules with the Rg-Na-Cl configuration. These results were in agreement with those of *ab initio* calculations. But the determined centrifugal distortion constants suggest existence of a large amplitude motion in the complexes. We attempted to estimate the intermolecular potential energy function of Rg-NaCl using the close-coupling method. Furthermore, an induced effect due to complex formation of NaCl has been observed from the determined nuclear quadrupole coupling constant of Na.

§ 2.1 Experiment

We observed Rg-NaCl (Rg = Ar, Kr) complexes using the FTMW spectrometer [1,2] coupled to the laser ablation source [3,4] explained in section 1.2.

In this work, as the type (a) unit gave stronger signals for the same transitions than the other units shown in Fig. 2.1, we always attached the ablation nozzle unit of type (a). The target rod (10 mm ϕ in diameter \times 20 mm in length) was made by compressing commercially available salt (NaCl purity 98 %), which was ground to fine powder before use. On an earlier experimental stage, we tried to use a NaCl crystal rod (JAPAN CRYSATAL OPTICS Co.) as a target rod instead of the compressed NaCl rod. Since the peak intensity for Ar-NaCl was independent on the rods, the compressed NaCl rod was used for most of the experiments. Pure Ar gas and a mixture of 2.5 % Kr diluted in Ar were used as carrier gases for observations of Ar-NaCl and Kr-NaCl, respectively. The vaporized NaCl together with the carrier gas at a stagnation pressure of about 7 atm was expanded as a supersonic jet in the vacuum chamber. The optimized background pressure in the vacuum chamber was typically kept about $3 \sim 4 \times 10^{-6}$ Torr. The complex produced in the supersonic expansion was polarized by an incident microwave pulse with 0.3 μ s duration, and FID signals radiated from the complex were Fourier-transformed to obtain frequency-domain spectra. In order to confirm whether the experimental conditions were kept well during the scan, we monitored the intensity of the rotational transition, $(J, F) = (1, 4) - (0, 3)$ of the NaCl monomer at intervals of 100 MHz scans.

For a measurement of the Stark effect, two electrodes were mounted in the Fabry-Perot cavity (the maximum voltage applied is 20 kV). Each electrode was made of copper wires of 0.3 mm in diameter with 1.5 cm spacings stretched between frames which were made of two 30 cm \times 5 cm plastic plates separated by 30 cm by Al rods. In order to avoid that electrons spattered by the laser ablation affect the

electric field between the two electrodes, we did not use the Q-switched mode but the long pulse mode. However, we were unable to observe any frequency shift due to the Stark effect.

§ 2.2 Results and Analysis

2.2.1 the Ar-NaCl complex

By empirically assuming that the structure of the complex is linear with an Ar-Na-Cl configuration and the distance between Ar and Na is equal to the sum of the van der Waals radius of the Ar atom and ion radius of the Na⁺ ion, its rotational constant was estimated to be about 900 MHz. Based on this prediction, we scanned the predicted region for $J = 5 - 4$, i.e., 8 - 10 GHz. We could observe only two groups of lines with complicated patterns at 9507 MHz and 9770 MHz. These lines disappeared when the ablation laser was turned off or when the pure Ne gas instead of Ar was used as a carrier gas. Therefore, we assigned these spectra as transitions of two isotopic species of Ar-NaCl, i.e., Ar-Na³⁶Cl and Ar-Na³⁷Cl. After measurements for other regions have been performed, we could pick up 9 and 8 groups of lines with nearly same intervals for Ar-Na³⁶Cl and Ar-Na³⁷Cl, respectively. Although we scanned a region as wide as $2B$ continuously, no transitions corresponding to $K = 1$ were observed. Therefore, we concluded that this complex has a linear structure.

The observed spectrum of the $J = 3 - 2$ transition of Ar-Na³⁶Cl has very complicated pattern as shown in Fig. 2.2(a). Similarly, other low- J transitions split into a number of hyperfine components due to the nuclear quadrupole interactions of both Na and Cl. On the other hand, for high- J transitions with J numbers more than $J = 7 - 6$, no splittings due to the hyperfine interaction were observed within the experimental resolution (10 kHz).

The Hamiltonian appropriate for Ar-NaCl may be written as a sum of the rotational term of linear molecule and the two nuclear quadrupole interaction terms, i.e.,

$$H = BJ^2 - DJ^4 + HJ^6 + H_{hb}(\text{Na}) + H_{hb}(\text{Cl}), \quad (2.1)$$

where B , D and H are the rotational constant, fourth-order, and sixth-order centrifugal distortion constants, respectively. The hyperfine interaction term is written as follows [5],

$$H_{hf}(X) = \mathbf{Q}^{(2)} \cdot \mathbf{V}^{(2)}, \quad (2.2)$$

where $\mathbf{Q}^{(2)}$, $\mathbf{V}^{(2)}$ are the nuclear quadrupole moment tensor of rank 2 and electric field gradient tensor of rank 2, respectively, for an atom X . As the nuclear quadrupole coupling constants of Na and Cl are nearly equal in the NaCl monomer, we used the basis functions with a coupling scheme, $\mathbf{I} = \mathbf{I}_{\text{Na}} + \mathbf{I}_{\text{Cl}}$, $\mathbf{F} = \mathbf{I} + \mathbf{J}$, in order to simplify the diagonalization of the Hamiltonian matrix. The matrix elements are shown in Appendix I. As we assume that J is an almost good quantum number, the diagonalization of the matrix was performed for each (J, F) submatrix. As the ratio of the mixing is very large for levels with different quantum numbers of I and same F , we named the diagonalized energies as $n = 0, 1, 2, \dots$ in increasing order of energies for given (J, F) levels. In the fitting procedure, high- J transitions without the hyperfine splittings were simultaneously fitted in a nonlinear least-squares procedure in order to determine the higher-order centrifugal distortion constants precisely. In this work we had to add the sixth-order centrifugal distortion term to the Hamiltonian in order to fit the data within the experimental accuracy. Furthermore, in order to determine hyperfine constants precisely, the transitions that do not overlap with each other were chosen and fitted in the analysis, because the transitions that overlap with each other were affected by the interference effect as will be discussed in Appendix II. The determined molecular constants of Ar-NaCl are shown in Table 2.1, and the observed and calculated frequencies with the calculated relative intensities are listed in Appendix III. Standard deviations of the fittings are 6 and 4 kHz for Ar-Na³⁶Cl and Ar-Na³⁷Cl, respectively. Calculated transitions were drawn as sticks in Fig. 2.2(b). From a comparison between the observed spectrum and the calculated transitions, it was observed that there were

discrepancies for the peak positions.

In order to confirm that the discrepancies between the observed and calculated peak positions are due to an interference effect, we substituted the calculated frequencies and their relative intensities into Eq. (2.A2.1) and assumed appropriate constants for δ and τ in Eq. (2.A2.1). Fourier-transformation of the resultant expression gave a calculated spectrum as shown in Fig. 2.2(b). This calculated spectrum was in good agreement with the observed. Therefore, we concluded that the molecular constants were determined with good accuracy and the observed discrepancies were due to the interference effect.

3.3.2 the Kr-NaCl complex

The rotational constant of Kr-NaCl was predicted using an *ab initio* program package, GAUSSIAN94 [6]. The $^{84}\text{Kr}-^{23}\text{Na}^{36}\text{Cl}$ complex, optimized using the MP4/6-311G* method, was linear and its rotational constant was 640 MHz. According to this prediction, we started to scan in the 5120 – 5290 MHz region. Two transitions at 5242 MHz and 5287 MHz were observed with hyperfine splittings as shown in Fig. 2.3(a). As these transitions showed on the intensity ratio of c.a. 1:3, we assigned the stronger to be $^{84}\text{Kr}-\text{Na}^{36}\text{Cl}$ and the weaker to be $^{86}\text{Kr}-\text{Na}^{36}\text{Cl}$. Finally, 11 rotational transitions were observed for three isotopic species, $^{84}\text{Kr}-\text{Na}^{35}\text{Cl}$, $^{85}\text{Kr}-\text{Na}^{36}\text{Cl}$ and $^{84}\text{Kr}-\text{Na}^{37}\text{Cl}$, and 12 rotational transitions were observed for $^{80}\text{Kr}-\text{Na}^{36}\text{Cl}$.

We used the Hamiltonian that is similar to that of Ar-NaCl except for the eighth-order centrifugal distortion term in the Hamiltonian,

$$H = BJ^2 - DJ^4 + HJ^6 - LJ^8 + H_{hf}(\text{Na}) + H_{hf}(\text{Cl}). \quad (2.3)$$

We used only the transitions that do not overlap with each other in the fitting procedure. Comparison of the calculated spectrum with the observed is shown in

Fig. 2.3(b). The determined molecular constants of Kr-NaCl are given in Table 2.2, and the observed and calculated frequencies with relative intensities are listed in Appendix III. The observed frequencies were fitted within the experimental accuracy.

§ 2.3 Discussion

2.3.1 molecular structures of the Rg-NaCl complexes

The structures of the Rg-NaCl complexes were determined to be linear from the pattern of the observed spectra. Furthermore, we performed *ab initio* calculations using the CCSD(T)/6-311G* method for the two Rg-NaCl complexes and obtained results that their equilibrium structures are linear, supporting the conclusion derived by the present experiments. The moment of inertia of the monomer, I_{NaCl} , and its complex, $I_{\text{Rg-NaCl}}$, are related as follow for X-AB type complexes,

$$I_{\text{Rg-NaCl}} = \mu R^2 + I_{\text{NaCl}} \cdot \left\langle \frac{\cos^2 \theta + 1}{2} \right\rangle_{av} \quad (2.4)$$

where μ , R are the reduced mass, and the distance between Rg and the center of mass of NaCl, respectively. θ is an angle from 0 up to π in the Jacobi coordinate system shown in Fig. 2.4. If we assume that $\langle \cos^2 \theta \rangle$ is nearly equal to 1 in Eq.(2.4), which corresponds to the limit that the complex is linear and the constituent molecules do not vibrate with each other, we can estimate the lower limit of the distance, R_{min} . The R_{min} distances are 4.3107 and 4.3423 Å for Ar-Na³⁵Cl and Ar-Na³⁷Cl, respectively. If the configuration of the complex is Ar-Cl-Na, R_{min} must shrink by the isotopic substitution from ³⁵Cl to ³⁷Cl. Therefore, the Ar atom is located on the Na-side in the complex observed. Furthermore, the difference, 0.0316 Å, between two R_{min} distances is nearly equal to the variation of the center of mass due to the isotopic substitution in NaCl, i.e., 0.0312 Å. It means that the assumption that θ is nearly equal to 0 is reasonable, that is, $R_{\text{min}} = R$, because the difference between two distances shows projection of the NaCl distance on the principle *a*-axis. Similarly, we derived R to be 4.4772, 4.4774, 4.4770, and 4.5090 Å for ⁸⁴Kr-Na³⁵Cl, ⁸⁶Kr-Na³⁵Cl, ⁸²Kr-Na³⁶Cl and ⁸⁴Kr-Na³⁷Cl, respectively. We

showed the r_0 -structures of the Rg-NaCl complexes in Fig. 2.5.

For Kr-NaCl, since plural substituted species for Kr and Cl were observed, we could determine the r_e -coordinates for both the Kr and Cl atoms using Kraitchman's equation [7] for a linear molecule. In addition, we determined the r_e -coordinates for the Na atom using the first-moment equation. We showed the r_e -structure of the Kr-NaCl complex in Fig. 2.5.

Comparison between the r_0 -structure and the r_e -structure of Kr-NaCl shows that these two structures are nearly equal within accuracy, $\pm 0.01 \text{ \AA}$. This result also implies that, since vibrational effects are partially removed in the r_e -structure, the error due to the vibrational effects in Eq. (2.4) is small enough in the determined r_0 -structure. In Fig. 2.5 ion radii (Na⁺: 1.16 Å, Cl⁻: 1.67 Å) for NaCl and the vdW radii (Ar: 1.91 Å, Kr: 2.01 Å) for Rg atoms are given. Although it can be concluded that the bond is essentially the van der Waals bonding, the variation of R is slightly smaller than the difference of the vdW radii between Ar and Kr.

2.3.2 induction effect in the Rg-NaCl complex

Nuclear quadrupole coupling constants are affected by the existence of bending motions in the complexes formed by a diatomic molecule and a rare-gas atom. The effect of vibrational averaging for the nuclear quadrupole coupling constant has been reported for weakly bound complexes, such as Ar-HCl [8]. This vibrational effect is related to the nuclear quadrupole coupling constants of the monomer, $(eQq)_{\text{mono}}$, and its complex, $(eQq)_{\text{comp}}$, by a following equation,

$$(eQq)_{\text{comp}} = \left\langle \frac{3\cos^2\theta - 1}{2} \right\rangle_{\text{av}} \cdot (eQq)_{\text{mono}}, \quad (2.5)$$

where θ is the angle shown in Fig. 2.4. In the present work, as both the Na and Cl nuclei are subjected to the same effect due to the bending motion, the ratio of $(eQq)_{\text{comp}}$ to $(eQq)_{\text{mono}}$ must be equal for both Na and Cl. We show the ratios for the

Rg-NaCl systems in Table 2.3. It shows that the coupling constant of the Na atom is not only affected by the vibrational effect, but are also affected by other effects, such as the induction effect or the dispersion effect because the vibrationally averaged term in Eq. (2.5) should be less than one.

We consider the induction effect due to the induced dipole moment of Rg. In order to estimate the induction effect arising from the induced dipole moment at Rg, we performed a simple calculation based on electrostatic interactions. The Na and Cl nuclei are assumed to have point charges of $+C$, $-C$, respectively. The electric field gradient, $q_{\text{Cl} \rightarrow \text{Na}}$, at the Na atom due to the charge on the Cl atom can be written as

$$q_{\text{Cl} \rightarrow \text{Na}} = -\frac{2 \times (-C)}{r_{\text{NaCl}}^3} = \frac{2C}{r_{\text{NaCl}}^3}, \quad (2.6)$$

where r represents the distance between the atoms designed by the subscripts. Similarly, the electric field gradient, $q_{\text{Na} \rightarrow \text{Cl}}$ at Cl arising from Na is written by

$$q_{\text{Na} \rightarrow \text{Cl}} = -\frac{2C}{r_{\text{NaCl}}^3}. \quad (2.7)$$

Since the electric field at the position separated by a distance r from a point charge, C , is given by C/r^2 , the induced dipole moment at Rg is written as follows,

$$\mu_{\text{ind}} = \alpha_{\text{Rg}} \left\{ \frac{+C}{r_{\text{RgNa}}^2} + \frac{-C}{r_{\text{RgCl}}^2} \right\}, \quad (2.8)$$

where α_{Rg} is the polarizability of the Rg atom. The electric field gradient, $q_{\text{Ar} \rightarrow \text{Na}}$, at the Na atom contributed by this induced dipole moment is written as follows,

$$q_{\text{Ar} \rightarrow \text{Na}} = \frac{6 \cdot \mu_{\text{ind}}}{r_{\text{ArNa}}^4}. \quad (2.9)$$

The electric field gradient, $q_{\text{Ar} \rightarrow \text{Cl}}$, at the Cl atom due to the induced dipole moment is also written by a similar equation to Eq. (2.9). If the vibrational effect due to Eq. (2.5), is ignored, a relation between the nuclear quadrupole coupling constants of the Na atom of the NaCl monomer and its complex, Rg-NaCl, can be obtained as

follows,

$$(eQq)_{\text{comp}} = \frac{q_{\text{Ar} \rightarrow \text{Na}} + q_{\text{Cl} \rightarrow \text{Na}}}{q_{\text{Cl} \rightarrow \text{Na}}} (eQq)_{\text{monom.}} \quad (2.10)$$

where it should be noted that the value $(eQq)_{\text{comp}}$ is independent on the charge of Na and Cl.

We estimate the induction effect for the nuclear quadrupole coupling constant of the Ar-Na³⁵Cl complex using Eqs. (2.6) – (2.10). If the charge, C assumed to be 1.0 e , we obtain the electric field gradients, $q_{\text{Cl} \rightarrow \text{Na}}$ and $q_{\text{Na} \rightarrow \text{Cl}}$, to be $+0.1520 \text{ e/\AA}^3$, -0.1520 e/\AA^3 , respectively. As the induced dipole moment of the Ar atom is 0.656 D, the electric field gradients, $q_{\text{Ar} \rightarrow \text{Na}}$ and $q_{\text{Ar} \rightarrow \text{Cl}}$ are $1.17 \times 10^{-2} \text{ e/\AA}^3$ and $1.07 \times 10^{-3} \text{ e/\AA}^3$, respectively. The contribution of $q_{\text{Ar} \rightarrow \text{Cl}}$ to $q_{\text{Na} \rightarrow \text{Cl}}$ is so small that we can neglect the induction effect on the Cl atom due to the induced dipole moment of the Ar atom. According to Eq. (2.10), the nuclear quadrupole coupling constant of the Na atom is calculated to be -6.1055 MHz. For the Na atom, the calculated value shows that the coupling constant on the Na atom in the Ar-Na³⁵Cl complex will be induced by -0.4357 MHz compared with the coupling constant of the Na³⁵Cl monomer. If the nuclear quadrupole coupling constant of the Cl atom is affected by only the vibrational effect given in Eq. (2.5), we can estimate the magnitude of the root mean square amplitude for the bending motion to be 18.44° in the Ar-Na³⁵Cl complex. Therefore, considering the vibrational effect of NaCl in the complex, the nuclear quadrupole coupling constant of Na is calculated to be -5.1891 MHz in the Ar-Na³⁵Cl complex. Although this result reproduces only

$$\begin{aligned} & \frac{(eQq)_{\text{comp.}}(\text{calc.}) - (eQq)_{\text{monom.}} \cdot \langle (3 \cos^2 \theta - 1) / 2 \rangle}{(eQq)_{\text{comp.}}(\text{obs.}) - (eQq)_{\text{monom.}} \cdot \langle (3 \cos^2 \theta - 1) / 2 \rangle} \times 100 \\ &= \frac{-5.1891 - (-5.6698) \times 0.8499}{-5.7805 - (-5.6698) \times 0.8499} \times 100 = 38.5 \% \end{aligned}$$

of the observed coupling constant quantitatively, the change of the nuclear quadrupole coupling constants due to the complex formation can be concluded by

showing substantial induction effect due to the induced dipole moment of Ar. The discrepancy between the observed and calculated coupling constants can be ascribed to the fact that the adopted model is too simple; for example, the distance between the Ar and Na atoms is so small that we can not express the interaction between the particles using the lower-order multipole expansion. Furthermore, we must consider that charge transfer from Ar to NaCl occurs by the complex formation. Thus, we performed an *ab initio* calculation for the Ar-Na³⁵Cl complex using the MP2/6-311G(2d) method. According to the *ab initio* calculation, atomic charges are changed significantly by the complex formation, as shown in Table 2.4. In general, contribution to the coupling constant due to the charge transfer tends to increase the absolute value of the coupling constant of the Na atom, while it decreases the value of the Cl atom. By considering this effect for the coupling constants, the root mean square amplitude should be estimated to be smaller than before, and the coupling constant of Na will become larger.

2.3.3 the intermolecular potential energy surface of the Rg-NaCl complex

Since the determined centrifugal distortion constants are very large, it suggests that there exist a large amplitude motions in the complexes. However, as we have discussed before for the structures and the nuclear quadrupole coupling constants of the complexes, there is little possibility of existence of large amplitude motions of the Rg atoms. We compared the stretching and bending frequencies derived in the present work with those calculated by the *ab initio* calculation, where the intermolecular stretching and bending force constants, k_s and k_b , have been determined from the centrifugal distortion constants and the averaged bending amplitude, based on an assumption that the two motions are uncoupled harmonic oscillations [9], namely,

$$k_s = \frac{(4\pi)^4 \mu^2 R^2 B^4}{2hD}, \quad (2.11)$$

and

$$k_b = \frac{\hbar^2}{4\pi^2 \mu' \langle \theta^2 \rangle^2}, \quad (2.12)$$

where θ is the angle defined in Eq.(2.5), and μ' is the reduced mass of the bending motion,

$$\mu' = \frac{\mu R^2 \cdot I_{\text{NaCl}}}{(\mu R^2 + I_{\text{NaCl}})}. \quad (2.13)$$

We show the determined intermolecular stretching and bending force constants in Table 2.5. The calculated vibrational frequencies for normal species of the Rg-NaCl complexes using the CCSD(T)/6-311G* method are also shown in Table 2.5. There exist large discrepancies between the observed and calculated.

In order to examine the discrepancy, we used the close-coupling method to calculate the transition frequencies undergoing large amplitude motions on the intermolecular potential energy surface derived by considering following interaction terms. As discussed in Appendix IV, we can construct a potential function as a sum of interaction terms, i.e.,

$$V(R, \theta) = V_{rep.}(R, \theta) + V_{elec.}(R, \theta) + V_{ind.}(R, \theta) + V_{disp.}(R, \theta), \quad (2.14)$$

where first, second, third, and fourth terms are the repulsion term, the electrostatic term, the induction term, and the dispersion term, respectively. We referred the potential function used by Rogowska, who computed the potential energies of rare gases on the surfaces of alkali halide crystals [10]. The repulsion term can be written using the Born-Mayer expression as follows,

$$V_{rep.}(R, \theta) = \sum_i A_i \exp(-\beta_i r_i), \quad (2.15)$$

where A_i and β_i are positive constants, which represent the magnitude of the interaction at distance, r between Ar and Na/Cl. The index i in the sum runs over Na and Cl. The electrostatic term, $V_{elec.}(R, \theta)$ is zero, because the Ar atom has no

charge, no dipole moment, and so on. The induction term can be written as follows,

$$V_{ind}(R, \theta) = -\frac{1}{2} \alpha_{Ar} \left(\frac{+C}{r_{ArNa}^2} + \frac{-C}{r_{ArCl}^2} \right)^2, \quad (2.16)$$

where the definitions of the parameters follow the definitions used in Eq. (2.8).

The dispersion term between instantaneous multipole moments of Ar and Na/Cl can be written as follows,

$$V_{disp}(R, \theta) = \sum_i \left(-\frac{C_1^i}{r_1^6} - \frac{C_2^i}{r_1^8} - \frac{C_3^i}{r_1^{10}} \right), \quad (2.17)$$

where C_1 , C_2 , and C_3 are positive constants for each atom. The index i in the sum runs over Na and Cl. We listed the parameters of the potential energy surface in Table 2.6.

The vibration-rotation Hamiltonian [11] for the Ar-NaCl complex may be given by the following equation in the coordinate system as shown in Fig. 2.4,

$$H_{vib-rot} = \frac{\hbar^2}{2\mu} \nabla_R^2 + H_{NaCl} + V(R, \theta). \quad (2.18)$$

We considered only the rotational term ignoring the hyperfine interaction term in H_{NaCl} . If NaCl is rigid, the total vibration-rotation wavefunction, $\Psi(R, r)$ can be written as follows,

$$\begin{aligned} \Psi_{JK}^{JM_s}(R, r) &= R^{-1} \sum_I \Phi_{JK}^{JM_s}(\hat{R}, \hat{r}) \cdot \chi_{JK}^{JM_s}(R) \\ \Phi_{JK}^{JM_s}(\hat{R}, \hat{r}) &= \frac{1}{\sqrt{2}} \left\{ \Phi_{JK}^{JM}(\hat{R}, \hat{r}) + (-1)^s \Phi_{J-K}^{JM}(\hat{R}, \hat{r}) \right\} \quad (K \neq 0), \\ \Phi_{JK}^{JM_s}(\hat{R}, \hat{r}) &= \Phi_{j0}^{JM}(\hat{R}, \hat{r}) \quad (K = 0) \end{aligned} \quad (2.19)$$

where the function, $\Phi(\hat{R}, \hat{r})$ and $\chi(R)$ are the angular and the radial wavefunctions, respectively, and J, K, M, j , and s denote the quantum numbers of the total angular momentum of the system, the projection of J along the molecule-fixed z -axis, the projection of J along the space-fixed Z -axis, the quantum number of the angular motion of NaCl in the complex, and the parity of the total wavefunction,

respectively. The quantum number j in the sum runs from 0 up to 50 in this work. We confirmed that the term energy converged less than 0.03 kHz by the truncation of j . The function, $\Phi(\hat{R}, \hat{r})$ is written in the molecule-fixed coordinate system as follows,

$$\Phi_{JK}^{JM}(\hat{R}, \hat{r}) = [(2J+1)/4\pi]^{1/2} D_{M,K}^{J*}(\alpha, \beta, 0) \times Y_{j,K}(\theta, \varphi), \quad (2.20)$$

where $D_{M,K}^{J*}(\alpha, \beta, 0)$ is a rotation matrix describing the orientation of the vector connecting the atom and the diatom in space and $Y_{j,K}(\theta, \varphi)$ is a spherical harmonic describing the orientation of the NaCl in the molecule-fixed coordinate system, which is obtained from the space-fixed system by rotating through angles α and β .

In the close-coupling calculation using Eqs. (2.14) – (2.20), the potential parameter, A_{Na} in Eq. (2.15) was varied to reproduce the determined hyperfine-free transition frequencies of $J = 1 - 0$ and $J = 2 - 1$. When $A_{Na} = 742.27$ eV, the difference between the observed and calculated frequencies was minimized as shown in Table 2.7. The optimized potential energy surface is shown in Fig. 2.6. The determined potential surface could reproduce the observed rotational constant well, as shown in Table 2.7. Although the calculated centrifugal distortion constant could not reproduce the observed constant, it was closer to the observed constant than that obtained from the *ab initio* calculation. Difference between the observed and calculated constants is still large, and we are unable to find origin of the large centrifugal distortion constant.

References

- [1] T. J. Balle and W. H. Flygare, *Rev. Sci. Instrum.*, **52**, 33 (1981)
- [2] Y. Ohshima, M. Iida, and Y. Endo, *J. Chem. Phys.*, **95**, 7001(1991)
- [3] T. G. Dietz, M. A. Duncan, D. E. Powers, and R. E. Smalley, *J. Chem. Phys.*, **74**, 6511(1981)
- [4] D. E. Powers, S. G. Hansen, M. E. Geusic, A. C. Pulu, J. B. Hopkins, T. G. Dietz, M. A. Duncan, P. R. R. Langridge-Smith, and R. E. Smalley, *J. Phys. Chem.*, **86**, 2556(1982)
- [5] A. R. Edmonds, *Angular Momentum in Quantum Mechanics*, Princeton University, Princeton New Jersey(1960)
- [6] M. J. Frisch, G. W. Trucks, H. B. Schlegel, P. M. W. Gill, B. G. Johnson, M. A. Robb, J. R. Cheeseman, T. Keith, G. A. Petersson, J. A. Montgomery, K. Raghavachari, M. A. Al-Laham, V. G. Zakrzewski, J. V. Ortiz, J. B. Foresman, J. Cioslowski, B. B. Stefanov, A. Nanayakkara, M. Challacombe, C. Y. Peng, P. Y. Ayala, W. Chen, M. W. Wong, J. L. Andres, E. S. Replogle, R. Gomperts, R. L. Martin, D. J. Fox, J. S. Binkley, D. J. Defrees, J. Baker, J. P. Stewart, M. Head-Gordon, C. Gonzalez, and J. A. Pople, *Gaussian 94 (Revision D.4)*, Gaussian, Pittsburgh(1994)
- [7] W. Gordy and R. L. Cook, *Microwave Molecular Spectra*, Interscience Publishers, Inc. New York(1970)
- [8] S. E. Novick, P. Davies, S. J. Harris and W. Klemperer, *J. Chem. Phys.*, **59**, 2273(1973)
- [9] K. R. Leopold, G. T. Fraser, F. J. Lin, D. D. Nelson, Jr., and W. Klemperer, *J. Chem. Phys.*, **81**, 4922(1984)
- [10] J. M. Rogowska, *J. Chem. Phys.*, **68**, 3910(1978)
- [11] J. M. Hutson, *J. Chem. Phys.*, **92**, 157(1990)

Table 2.1 The determined molecular constants of Ar-NaCl

		Ar-Na ³⁵ Cl		Ar-Na ³⁷ Cl
		Obs.	Calc. ^a	Obs.
<i>B</i>	/MHz	977.5083(3) ^b	966.4637	951.2264(3)
<i>D</i>	/kHz	9.0897(63)		8.3699(61)
<i>H</i>	/ Hz	4.178(32)		3.802(36)
<i>eQq</i> (Na)	/MHz	-5.781(22)	-6.770	-5.7499(198)
<i>eQq</i> (Cl)	/MHz	-4.799(29)	-3.855	-3.8324(194)
<i>C</i> ₆₆	/kHz	6.0		3.5

^a We optimized the structure of Ar-Na³⁵Cl with the CCSD(T)/6-311G* method using the GAUSSIAN94 package.

^b The figures in parentheses are one standard deviation in units of the last significant figure.

Table 2.2 The determined molecular constants of Kr-NaCl

	$^{84}\text{Kr-Na}^{35}\text{Cl}$ (42.75%) ^a	$^{84}\text{Kr-Na}^{37}\text{Cl}$ (14.25%) ^a	$^{86}\text{Kr-Na}^{35}\text{Cl}$ (12.75%) ^a	$^{82}\text{Kr-Na}^{35}\text{Cl}$ (9.00%) ^a
B	/MHz	639.7265(4)	655.3508(9)	667.0262(6)
D	/kHz	4.1488(158)	3.4865(120)	4.3039(186)
H	/Hz	4.8122(1361)	3.6406(991)	5.1037(1769)
L	/mHz	5.3352(3592)	3.9975(2549)	5.7767(5321)
$eQq(\text{Na})$	/MHz	-6.0738(961)	-5.6629(981)	-6.0920(1379)
$eQq(\text{Cl})$	/MHz	-4.7312(465)	-3.8673(284)	-4.5851(713)
σ_{Rg}	/kHz	5.36	3.09	5.57
				3.84

^a The figures in parentheses are natural abundance of its isotopic species.

^b The figures in parentheses are one standard deviation in units of the last significant figure.

Table 2.3 The ratios of $(eQq)_{\text{comp}}$ to $(eQq)_{\text{mono}}$ in the Rg-NaCl complexes

	Na	Cl
Ar-Na ³⁶ Cl	1.020(5) ^a	0.8499(60)
Ar-Na ³⁷ Cl	1.013(4)	0.8618(46)
-----	-----	-----
⁸⁴ Kr-Na ³⁶ Cl	1.071(18)	0.8379(91)
⁸⁰ Kr-Na ³⁶ Cl	1.062(25)	0.8474(110)
⁸² Kr-Na ³⁶ Cl	1.074(25)	0.8120(135)
⁸⁴ Kr-Na ³⁷ Cl	0.9980(175)	0.8696(67)

^a The figures in parentheses are one standard deviation in units of the last significant figure

Table 2.4 The charge distribution in the Ar-Na³⁶Cl complexes^a

	Ar	Na	Cl
Na ³⁶ Cl		0.7495	-0.7495
Ar-Na ³⁶ Cl	0.0391	0.7087	-0.7478

^a This charge distribution was calculated by the CCSD(T)/6-311G* method using the GAUSSIAN94 package.

Table 2.5 The intermolecular vibrational force constants and its vibrational frequencies for the normal species of the Rg-NaCl complexes

	Ar-Na ³⁶ Cl		⁸⁴ Kr-Na ³⁶ Cl	
	obs. ^a	calc. ^b	obs. ^a	calc. ^b
k_x / mdyn Å ⁻¹	0.00547	0.120	0.00563	0.0819
ω_x / cm ⁻¹	19.81	76.32	16.69	59.00
k_z / mdyn Å	0.000948	0.0106	0.000765	0.0086
ω_z / cm ⁻¹	4.94	26.69	4.10	25.18

^a This work

^b from *ab initio* calculations using the CCSD(T)/6-311G* method

Table 2.6 The initial potential parameters used in present work^a

	Na	Cl
A_1 / eV	1204.4304	6856.7088
$\beta_1 / \text{\AA}^{-1}$	3.2555	3.2555
$C_1^1 / \text{eV}\cdot\text{\AA}^6$	13.2791	122.2990
$C_2^1 / \text{eV}\cdot\text{\AA}^8$	9.4181	150.0754
$C_3^1 / \text{eV}\cdot\text{\AA}^{10}$	16.5409	13.0586

^a These values were calculated according to Ref. [19].

Table 2.7 The comparison of observed constants and calculated molecular constants using close-coupling method.

		obs.	calc.	
			close-coupling method	<i>ab initio</i> ^a
$\nu_{J=1-0}$	/MHz	1954.980 ^b	1954.967 (0.013) ^c	
$\nu_{J=2-1}$	/MHz	3909.888 ^b	3909.895 (-0.007) ^c	
B	/MHz	977.5083(3) ^d	977.4865	966.4637
D	/kHz	9.0897(63) ^d	1.608	0.6897

^a the *ab initio* calculation using the CCSD(T)/6-311G* method.

^b The hyperfine-free frequency was calculated from the determined constants.

^c The figures in parentheses are differences between the observed and calculated frequencies.

^d The figures in parentheses are one standard deviation in units of the last significant figure.

The nozzle units of the laser ablation source



Fig. 2.1 The nozzle units of the laser ablation source. (a) This unit has the conical channel with expansion from 1 mm ϕ to 5 mm ϕ hole between the separation of 7 mm, which is the distance from focal point of laser to the edge of exit channel. We used this unit in the present work. (b) This unit has a straight channel of 3 mm ϕ hole, 17 mm in length. (c) This slit nozzle has square focal region of 12 mm \times 1 mm and its exit channel has the 12 mm \times 3 mm in square, and 7 mm in length

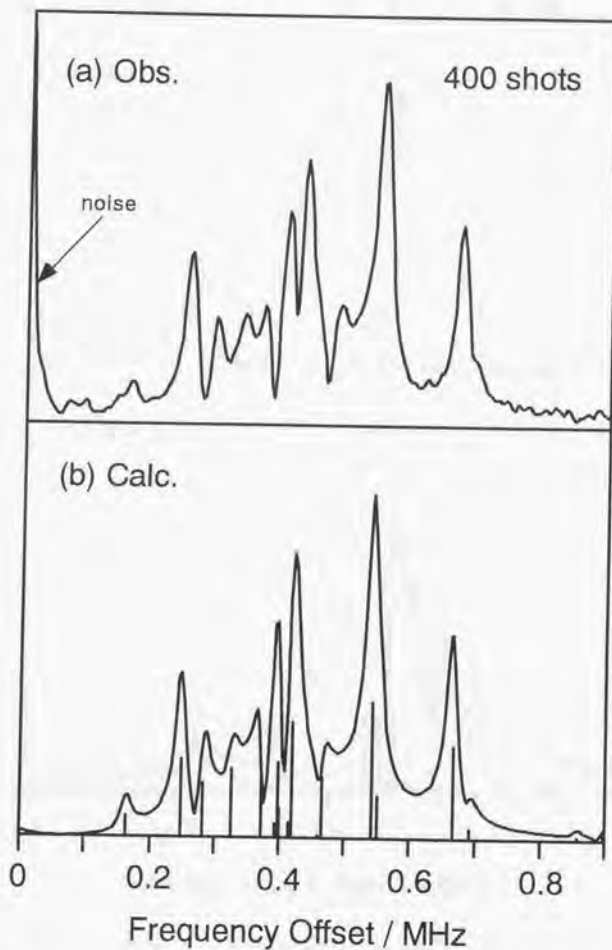
Spectrum of Ar-Na³⁵Cl $J = 3 - 2$ 

Fig. 2.2 The spectrum of $J = 3 - 2$ transition in Ar-Na³⁵Cl. Frequencies are offsets from 5863.656 MHz. (a) observed spectrum (b) calculated spectrum; Sticks represent the calculated transition frequencies and their relative intensities. The simulated spectrum was obtained by Fourier-transforming the synthesized time domain signal given by Eq. (2.A2.1).

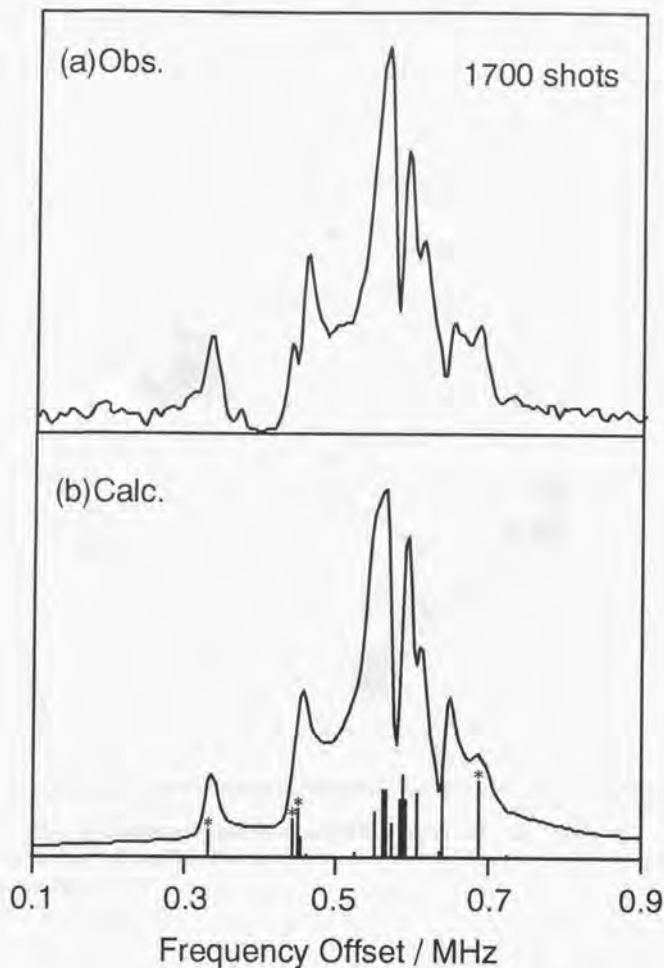
Spectrum of $^{84}\text{Kr-Na}^{35}\text{Cl}$ $J = 5 - 4$ 

Fig. 2.3 The spectrum of $J = 5 - 4$ transition in $^{84}\text{Kr-Na}^{35}\text{Cl}$. Frequency is offset from 6608.000 MHz. (a) observed spectrum. (b) calculated spectrum; Sticks represent the calculated transition frequencies and their relative intensities. The asterisks(*) represent that these lines were used in the fitting procedure. The simulated spectrum was obtained by Fourier-transforming the signal given by Eq. (2.A2.1).

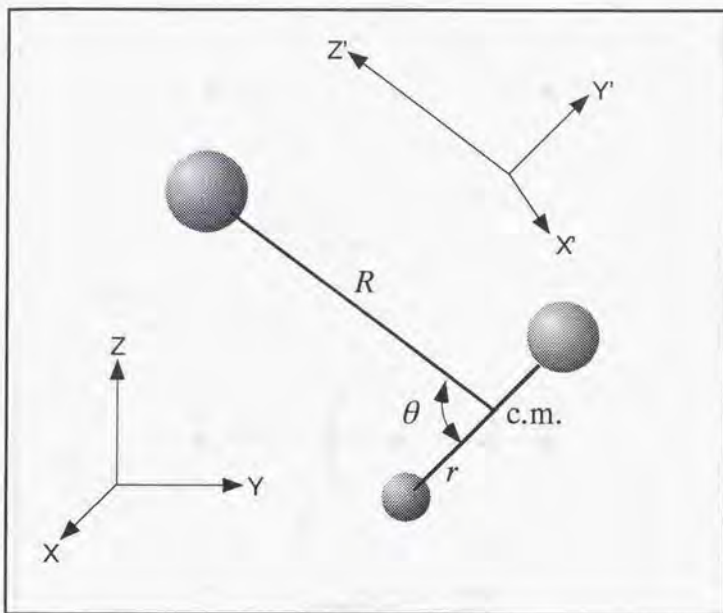


Fig. 2.4 Jacobi coordinate system for an atom-diatom van der Waals molecule. Unprimed axes refer to the space-fixed axes, while primed axes refer to the body-fixed (molecule-fixed) axes.

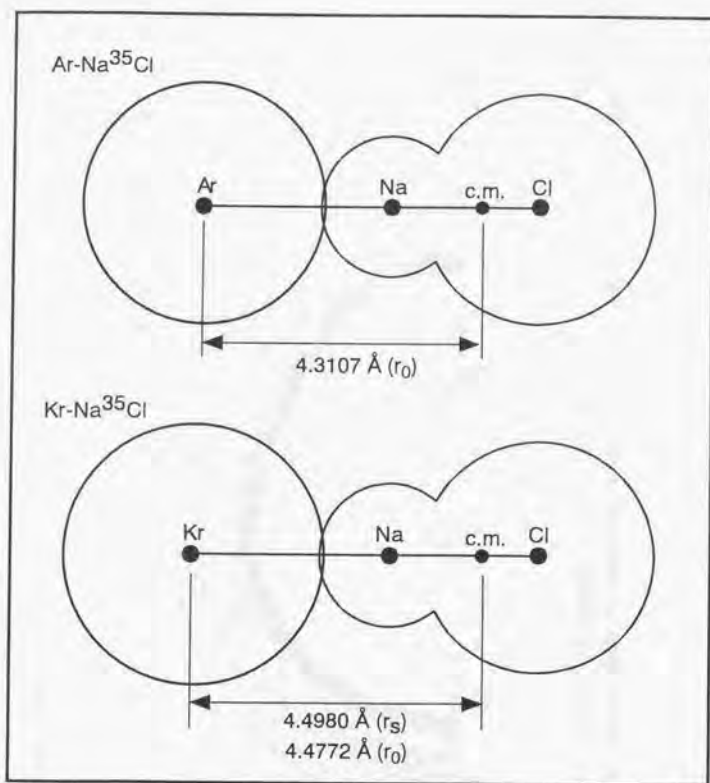


Fig. 2.5 The structures of the Rg-NaCl complexes. The circles represent ion radii (Na^+ : 1.16 Å, Cl^- : 1.67 Å) and van der Waals radii (Ar: 1.91 Å, Kr: 2.01 Å) for each atom. The distance between Na and c.m., the center of mass of Na^{35}Cl , is 1.4244 Å.

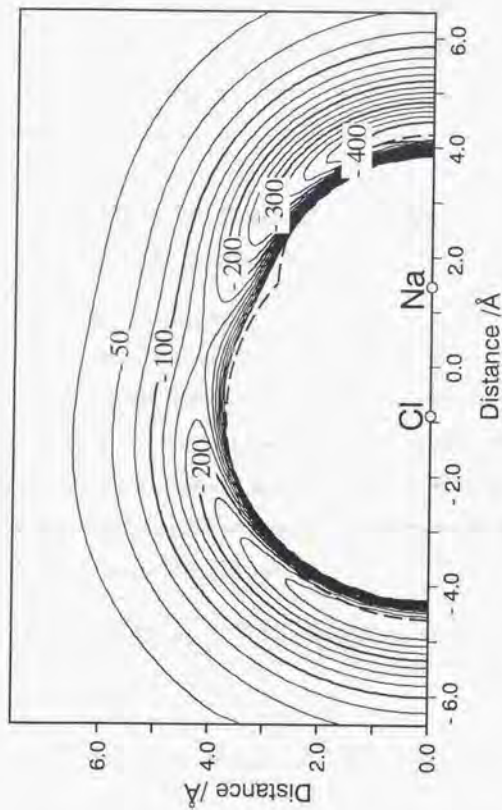


FIG. 2.6 The optimized intermolecular potential energy surface around NaCl estimated by the close-coupling method in this work. The dashed line represents the position of center of mass of Ar with vdW radius contacted with ion radius of NaCl.

Appendix I.

Matrix elements of the nuclear quadrupole interaction due to two nuclei

For molecules with the ${}^1\Sigma$ ground state the magnetic field due to various electrons almost completely cancels. However, the electric quadrupole interaction in molecules is still sizable and it becomes the dominating source of the hyperfine structure. The nuclear quadrupole hyperfine interaction arises from the interaction between a nuclear electric quadrupole moment and a surrounding charge distribution.

The electrostatic interaction between a nucleus and all the electrons and other nuclei in the molecule is given by

$$H_{el} = + \sum_{i,p} \frac{e_i e_p}{|\mathbf{r}_i - \mathbf{r}_p|} = + \sum_{i,p,l} e_i e_p \frac{r_p^l}{r_i^{l+1}} P_l(\cos \theta_{ip}), \quad (2.A1.1)$$

where e_p is the charge of the p -th nucleus with position vector \mathbf{r}_p in the nucleus in question and e_i is the charge of the i -th electron or proton with position vector \mathbf{r}_i in the remainder of the molecule. θ_{ip} is the angle between the vector \mathbf{r}_i and \mathbf{r}_p . We consider only the quadrupole term in the multipole expansion (2.A1.1), that is $l = 2$. Eq. (2.A1.1) can be transformed into

$$H_Q = + \sum_{i,p,q} (-1)^q e_i e_p \frac{r_p^2}{r_i^3} C_q^{(2)}(\theta_i, \varphi_i) C_{-q}^{(2)}(\theta_p, \varphi_p) = (\mathbf{V} \cdot \mathbf{Q}), \quad (2.A1.2)$$

where

$$\mathbf{V} = \sum_i \frac{e_i}{r_i^3} \mathbf{C}^{(2)}(\theta_i, \varphi_i), \quad \mathbf{Q} = \sum_p e_p r_p^2 \mathbf{C}^{(2)}(\theta_p, \varphi_p). \quad (2.A1.3)$$

by using the spherical harmonic addition theorem. $\mathbf{C}^{(2)}$ is the reduced spherical harmonics.

The wavefunction, $|JK_e K_c M_J\rangle$ of an asymmetric top molecule can be expressed in terms of a symmetric top wavefunction, $|JKM_J\rangle$, that is

$$|JK_a K_c M\rangle = \sum_K a_{JKM} |JKM\rangle. \quad (2.A1.4)$$

Therefore, we can use only the symmetric top wavefunctions as basis sets. Now we discuss the matrix elements of the nuclear quadrupole coupling constants due to a nucleus with the nuclear spin, I ($I \geq 1$). Using the basis set functions as $|JKIFM_F\rangle$. The matrix elements of the nuclear quadrupole interaction are

$$\begin{aligned} & \langle \alpha J' K', \beta I, F' M'_F | H_{\text{nb}} | \alpha J K, \beta I, F M_F \rangle \\ & = \delta_{FF'} \delta_{M'_F M_F} (-1)^{J'+I+F} \begin{Bmatrix} F & I' & J' \\ 2 & J & I \end{Bmatrix} \langle \alpha J' K' || V^{(2)} || \alpha J K \rangle \langle \beta I || Q^{(2)} || \beta I \rangle, \end{aligned} \quad (2.A1.5)$$

where α, β represent all the relevant quantum numbers not related to the angular momentum. The reduced matrix element of the quadrupole moment term is written as follows,

$$\begin{aligned} \langle \beta I || Q^{(2)} || \beta I \rangle & = (-1)^{2I} \begin{pmatrix} I & 2 & I \\ -I & 0 & I \end{pmatrix}^{-1} \sum_p e_p \langle \beta I | r_p^2 C_0^{(2)}(\theta_p, \varphi_p) | \beta I \rangle \\ & = (-1)^{2I} \begin{pmatrix} I & 2 & I \\ -I & 0 & I \end{pmatrix}^{-1} \frac{e}{2} \sum_p e_p \langle \beta I | r_p^2 (3 \cos^2 \theta_p - 1) | \beta I \rangle, \quad (2.A1.6) \\ & = (-1)^{2I} \begin{pmatrix} I & 2 & I \\ -I & 0 & I \end{pmatrix}^{-1} \frac{eQ}{2} \end{aligned}$$

where we used the relation between the reduced spherical harmonics and the spherical harmonics,

$$C_q^{(k)}(\theta, \varphi) = \left(\frac{4\pi}{2k+1} \right)^{\frac{1}{2}} Y_{kq}(\theta, \varphi). \quad (2.A1.7)$$

The reduced matrix element of the electric field gradient term in (2.A1.5) is written as follows,

$$\langle \alpha J' K' || V_0^{(2)} || \alpha J K \rangle = (-1)^{-J'+M'} \begin{pmatrix} J' & 2 & J \\ -M' & 0 & M \end{pmatrix}^{-1} \langle \alpha J' K' M' | V_0^{(2)} | \alpha J K M \rangle. \quad (2.A1.8)$$

The element, $V_0^{(2)}$ can be rewritten using the spherical harmonics addition theorem

as follows,

$$V_0^{(2)} = \sum_q (-1)^q C_q^{(2)}(\theta, \varphi) \sum_i \frac{e_i}{r_i^3} C_{-q}^{(2)}(\theta_i, \varphi_i), \quad (2.A1.9)$$

where θ , φ , θ_i , φ_i are the angles of the space-fixed z-axis and the position vector of the i -th electron respectively with respect to the molecule-fixed axes. Substituting Eq. (2.A1.9) for the matrix element of $V_0^{(2)}$,

$$\begin{aligned} & \langle \alpha J' K' M' | V_0^{(2)} | \alpha J K M \rangle \\ &= \sum_q (-1)^q \langle J' K' M' | C_q^{(2)}(\theta, \varphi) | J K M \rangle \left\langle \alpha \left| \sum_i \frac{e_i}{r_i^3} C_{-q}^{(2)}(\theta_i, \varphi_i) \right| \alpha \right\rangle \\ &= (-1)^{-M'+K'} \sum_q (-1)^q [(2J'+1)(2J+1)]^{\frac{1}{2}} \\ & \quad \times \begin{pmatrix} J' & 2 & J \\ -M' & 0 & M \end{pmatrix} \begin{pmatrix} J' & 2 & J \\ -K' & -q & K \end{pmatrix} \left\langle \alpha \left| \sum_i \frac{e_i}{r_i^3} C_{-q}^{(2)}(\theta_i, \varphi_i) \right| \alpha \right\rangle \end{aligned} \quad (2.A1.10)$$

where the last term represents the electric field gradient for each q -value as follows,

$$\begin{aligned} q=0 \quad \left\langle \alpha \left| \sum_i \frac{e_i}{r_i^3} C_0^{(2)}(\theta_i, \varphi_i) \right| \alpha \right\rangle &= \frac{1}{2} \left\langle \alpha \left| \sum_i \frac{e_i}{r_i^3} (3\cos^2\theta_i - 1) \right| \alpha \right\rangle \\ &= \frac{1}{2} \left\langle \frac{\partial^2 V}{\partial z^2} \right\rangle, \end{aligned} \quad (2.A1.11)$$

because

$$V = \sum_i \frac{e_i}{r_i} \quad (2.A1.12)$$

Similarly,

$$\begin{aligned} q=\pm 1 \quad \left\langle \alpha \left| \sum_i \frac{e_i}{r_i^3} C_{\pm 1}^{(2)}(\theta_i, \varphi_i) \right| \alpha \right\rangle &= \mp \sqrt{\frac{3}{2}} \left\langle \alpha \left| \sum_i \frac{e_i}{r_i^3} \cos\theta_i \sin\theta_i e^{\pm i\varphi_i} \right| \alpha \right\rangle \\ &= \mp \frac{1}{\sqrt{6}} \left\{ \left\langle \frac{\partial^2 V}{\partial x \partial z} \right\rangle - i \left\langle \frac{\partial^2 V}{\partial y \partial z} \right\rangle \right\}, \end{aligned} \quad (2.A1.13)$$

$$\begin{aligned} q=\pm 2 \quad \left\langle \alpha \left| \sum_i \frac{e_i}{r_i^3} C_{\pm 2}^{(2)}(\theta_i, \varphi_i) \right| \alpha \right\rangle &= \mp \sqrt{\frac{3}{8}} \left\langle \alpha \left| \sum_i \frac{e_i}{r_i^3} \sin^2\theta_i e^{\pm 2i\varphi_i} \right| \alpha \right\rangle \\ &= \frac{1}{2\sqrt{6}} \left\{ \left\langle \frac{\partial^2 V}{\partial x^2} \right\rangle + \left\langle \frac{\partial^2 V}{\partial y^2} \right\rangle \pm 2i \left\langle \frac{\partial^2 V}{\partial x \partial y} \right\rangle \right\}, \end{aligned} \quad (2.A1.14)$$

Therefore, we can obtain the expression of the matrix elements of the nuclear quadrupole interaction as follows,

$$\begin{aligned}
 & \langle \alpha J' K', \beta I, F' M'_F | H_{qF} | \alpha J K, \beta I, F M_F \rangle \\
 &= \delta_{FF'} \delta_{M'_F M_F} (-1)^{J'-J+K'-I+F} \begin{Bmatrix} F & I' & J' \\ 2 & J & I \end{Bmatrix} \frac{eQ}{2} \begin{pmatrix} I & 2 & I \\ -I & 0 & I \end{pmatrix}^{-1} \\
 & \times [(2J'+1)(2J+1)]^{\frac{1}{2}} \sum_q (-1)^q \begin{pmatrix} J' & 2 & J \\ -K' & -q & K \end{pmatrix} \left\langle \alpha \sum_{\tau} \frac{e_{\tau}}{I_{\tau}^3} C_{-q}^{(2)}(\theta_{\tau}, \varphi_{\tau}) \right\rangle \alpha
 \end{aligned} \tag{2.A1.15}$$

Now we consider the case that the hyperfine interaction is resulted from the nuclear quadrupole moments of two nuclei in the molecule. It is possible to consider two coupling schemes in this case, they are scheme (I), $\mathbf{J} + \mathbf{I}_1 = \mathbf{F}_1$, $\mathbf{F}_1 + \mathbf{I}_2 = \mathbf{F}$ and scheme (II), $\mathbf{I}_1 + \mathbf{I}_2 = \mathbf{I}$, $\mathbf{J} + \mathbf{I} = \mathbf{F}$. In scheme (I), the matrix element of the interaction can be written as follows,

$$\begin{aligned}
 & \langle (J' I_1) F_1' I_2' F' M'_F | H_{qF}(1) + H_{qF}(2) | (J I_1) F_1 I_2 F M_F \rangle \\
 &= \langle (J' I_1) F_1' I_2' F' M'_F | H_{qF}(1) | (J I_1) F_1 I_2 F M_F \rangle \\
 &+ \sum_{F_2', I_2'} (-1)^{J'-J'+F-F'} [(2F_1'+1)(2F_2'+1)(2F_1+1)(2F_2+1)]^{\frac{1}{2}} \\
 & \times \begin{Bmatrix} I_1 & J' & F_1' \\ I_2 & F' & F_2' \end{Bmatrix} \begin{Bmatrix} I_1 & J & F_1 \\ I_2 & F & F_2 \end{Bmatrix} \langle I_1 (J' I_2) F_2' F' M'_F | H_{qF}(2) | I_1 (J I_2) F_2 F M_F \rangle \\
 &= \delta_{FF'} \delta_{M'_F M_F} (-1)^{F_1'+I_2'+F} (2F+1)^{\frac{1}{2}} \begin{Bmatrix} F_1' & F & I_2 \\ F & F_1 & 2 \end{Bmatrix} \langle (J' I_1) F_1' | H_{qF}(1) | (J I_1) F_1 \rangle \\
 &+ \delta_{FF'} \delta_{M'_F M_F} \sum_{F_2', I_2'} (-1)^{J'-J'+I_1'+F_1'+F} [(2F_1'+1)(2F_2'+1)(2F_1+1)(2F_2+1)(2F+1)]^{\frac{1}{2}} \\
 & \times \begin{Bmatrix} I_1 & J' & F_1' \\ I_2 & F' & F_2' \end{Bmatrix} \begin{Bmatrix} I_1 & J & F_1 \\ I_2 & F & F_2 \end{Bmatrix} \begin{Bmatrix} F_2' & F & I_1 \\ F & F_2 & 2 \end{Bmatrix} \langle (J' I_2) F_2' | H_{qF}(2) | (J I_2) F_2 \rangle.
 \end{aligned} \tag{2.A1.16}$$

The matrix element in the last term can be immediately evaluated by referring to Eq. (2.A1.15). In scheme (II), the matrix element of $H_{qF}(1)$ can be written as follows,

$$\begin{aligned}
& \langle JK', (I_1 I_2) I', FM'_F | H_{hb}(1) JK, (I_1 I_2) I, FM_F \rangle \\
&= \delta_{FF} \delta_{M'_F M_F} (-1)^{J+I'+F} \begin{Bmatrix} F & I' & J' \\ 2 & J & I \end{Bmatrix} \langle JK' \| \mathbf{V}^{(2)} \| JK \rangle \langle (I_1 I_2) I' \| \mathbf{Q}^{(2)} \| (I_1 I_2) I \rangle \\
&= \delta_{FF} \delta_{M'_F M_F} (-1)^{J+I_1+I_2+I'+F} [(2I'+1)(2I+1)]^{\frac{1}{2}} \begin{Bmatrix} F & I' & J' \\ 2 & J & I \end{Bmatrix} \begin{Bmatrix} I_1 & I' & I_2 \\ I & I_1 & 2 \end{Bmatrix} \\
&\quad \times \langle JK' \| \mathbf{V}^{(2)} \| JK \rangle \langle I_1 \| \mathbf{Q}^{(2)} \| I_1 \rangle
\end{aligned} \tag{2.A1.17}$$

The reduced matrix elements in the last term of Eq. (2.A1.17) can be evaluated by using Eqs. (2.A1.6), (2.A1.8), and (2.A1.10). Similarly, we can obtain the matrix element of $H_{hb}(2)$. Therefore, the total matrix element of coupling scheme (II) can be written as follows,

$$\begin{aligned}
& \langle JK', (I_1 I_2) I', FM'_F | H_{hb}(1) + H_{hb}(2) JK, (I_1 I_2) I, FM_F \rangle \\
&= \delta_{FF} \delta_{M'_F M_F} (-1)^{J+K'+I_1+I_2+I'+F} \\
&\quad \times \frac{[(2J'+1)(2J+1)(2I'+1)(2I+1)]^{\frac{1}{2}}}{2} \begin{Bmatrix} F & I' & J' \\ 2 & J & I \end{Bmatrix} \\
&\quad \times \left[(-1)^{I'} \begin{Bmatrix} I_1 & I' & I_2 \\ I & I_1 & 2 \end{Bmatrix} \begin{Bmatrix} I_1 & 2 & I_1 \\ -I_1 & 0 & I_1 \end{Bmatrix}^{-1} \sum_q (-1)^q \begin{Bmatrix} J' & 2 & J \\ -K' & -q & K \end{Bmatrix} eQ(1) T_q^{(2)}(\nabla E_1) \right. \\
&\quad \left. + (-1)^{I'} \begin{Bmatrix} I_2 & I' & I_1 \\ I & I_2 & 2 \end{Bmatrix} \begin{Bmatrix} I_2 & 2 & I_2 \\ -I_2 & 0 & I_2 \end{Bmatrix}^{-1} \sum_q (-1)^q \begin{Bmatrix} J' & 2 & J \\ -K' & -q & K \end{Bmatrix} eQ(2) T_q^{(2)}(\nabla E_2) \right]
\end{aligned} \tag{2.A1.18}$$

where

$$T_q^{(2)}(\nabla E) = \left\langle \alpha \left| \sum_I \frac{e_I}{I^3} C_{-q}^{(2)}(\theta_i, \varphi_i) \right| \alpha \right\rangle. \tag{2.A1.19}$$

If the two nuclear spins are equal, that is, $I_1 = I_2 = I_n$, Eq. (2.A1.18) is simplified as follows,

$$\begin{aligned}
& \langle J'K', (I_1 I_2) I', F' M_F' | H_{\text{hfs}}(1) + H_{\text{hfs}}(2) | JK, (I_1 I_2) I, F M_F \rangle \\
&= \delta_{FF'} \delta_{M_F M_F'} (-1)^{J-J'+K'+I_1+I_2+2I'+F} \frac{[(2J'+1)(2J+1)(2I'+1)(2I+1)]^{\frac{1}{2}}}{2} \\
&\times \begin{Bmatrix} F & I' & J' \\ 2 & J & I \end{Bmatrix} \begin{Bmatrix} I_s & I' & I_s \\ I & I_s & 2 \end{Bmatrix} \begin{Bmatrix} I_s & 2 & I_s \\ -I_s & 0 & I_s \end{Bmatrix}^{-1} \\
&\times \sum_q (-1)^q \begin{pmatrix} J' & 2 & J \\ -K' & -q & K \end{pmatrix} \left[(-1)^{I-I'} eQ(1) T_q^{(2)}(\nabla E_1) + eQ(2) T_q^{(2)}(\nabla E_2) \right]
\end{aligned} \tag{2.A1.20}$$

References

- A. R. Edmonds, *Angular momentum in Quantum mechanics*, Princeton, New Jersey(1960)
- R. N. Zare, *Angular momentum*, A Wiley-Interscience Publishers, New York(1988)
- W. Gordy and R. L. Cook, *Microwave Molecular Spectra*, Wiley, New York(1984)

Appendix II.

The interference effect due to our Fourier-transform microwave spectrometer

An observed FID signal may be written as follows,

$$F(t) = \sum_i S_i \cos\{2\pi\omega_i(t - \delta)\} \cdot e^{-\tau(t-\delta)^2}, \quad (2.A2.1)$$

where S_i , ω_i are the relative intensity and the frequency difference between the resonance frequency and incident microwave frequency, respectively, for a transition i . The constant δ is the delay between the turning off of the incident microwave and the start of the A/D conversion, i.e., $(t_2 + t_d)$ shown in Fig. 1.7. The constant τ is a suitable decay constant of the FID signal.

We confirmed to reproduce the observed spectrum as shown in Fig. 2.2 by a Fourier-transformation of Eq. (2.A2.1). This result proves that the existence of the interference effect on the observed spectra are due to Eq. (2.A2.1).

Appendix III.

The observed and calculated transitions of Rg-NaCl complexes

Only the transitions used in the fitting procedures were listed as the observed lines in the following tables. Substituting the calculated frequencies and its intensities listed in the following tables into Eq. (2.A2.1), we confirmed that the observed spectrum was reproduced accurately, as exemplified in Figs. 2.2 and 2.3.

Ar-Na ³⁵ Cl	Table 2.A3.1
Ar-Na ³⁷ Cl	2.A3.2
⁸⁴ Kr-Na ³⁵ Cl	2.A3.3
⁸⁴ Kr-Na ³⁷ Cl	2.A3.4
⁸⁶ Kr-Na ³⁵ Cl	2.A3.5
⁸² Kr-Na ³⁶ Cl	2.A3.6

Table 2.A3.1 The principal observed and calculated transition frequencies of Ar-Na³⁵Cl (in MHz)

J' n' F'	J'' n'' F''	Yobs	Ycalc	Mobs - Ycalc	Intensity weight	J' n' F'	J'' n'' F''	Mobs	Ycalc	Mobs - Ycalc	Intensity weight
3.0 3.0 6.0 2.0 3.0 5.0	3.0 3.0 6.0 2.0 3.0 5.0	5864.204	5864.201	0.0031	5.5714	3.0 1.0 2.0 2.0 3.0 1.0	3.0 1.0 2.0 2.0 3.0 1.0	5864.204	5864.207	-0.0031	1.7154
3.0 2.0 5.0 2.0 3.0 5.0	3.0 2.0 5.0 2.0 3.0 5.0	5862.429	5862.423	0.0068	0.9281	3.0 3.0 1.0 2.0 3.0 1.0	3.0 3.0 1.0 2.0 3.0 1.0	5863.818	5863.818	-0.0004	0.8476
3.0 3.0 5.0 2.0 3.0 4.0	3.0 3.0 5.0 2.0 3.0 4.0	5864.087	5864.079	0.0074	4.6980	3.0 2.0 1.0 2.0 2.0 1.0	3.0 2.0 1.0 2.0 2.0 1.0	5864.069	5864.069	0.0000	0.5970
3.0 2.0 5.0 2.0 2.0 4.0	3.0 2.0 5.0 2.0 2.0 4.0	5864.925	5864.923	0.0019	3.7783	3.0 3.0 0.0 2.0 3.0 1.0	3.0 3.0 0.0 2.0 3.0 1.0	5864.942	5864.942	-0.0000	0.4224
3.0 3.0 4.0 2.0 2.0 4.0	3.0 3.0 4.0 2.0 2.0 4.0	5865.434	5865.434	0.0000	0.3522	3.0 2.0 1.0 2.0 2.0 0.0	3.0 2.0 1.0 2.0 2.0 0.0	5864.069	5864.069	0.0000	0.5978
3.0 2.0 4.0 2.0 3.0 4.0	3.0 2.0 4.0 2.0 3.0 4.0	5864.045	5864.045	0.0000	0.5489	4.0 3.0 7.0 3.0 3.0 6.0	4.0 3.0 7.0 3.0 3.0 6.0	7817.840	7817.847	-0.0070	6.8667
3.0 1.0 4.0 2.0 2.0 4.0	3.0 1.0 4.0 2.0 2.0 4.0	5863.614	5863.613	0.0008	0.9697	4.0 2.0 6.0 3.0 6.0 6.0	4.0 2.0 6.0 3.0 6.0 6.0	7816.147	7816.145	0.0022	0.7051
3.0 1.0 3.0 2.0 2.0 4.0	3.0 1.0 3.0 2.0 2.0 4.0	5864.546	5864.546	0.0000	0.1785	4.0 3.0 6.0 3.0 6.0 5.0	4.0 3.0 6.0 3.0 6.0 5.0	7817.771	7817.771	0.0000	5.7585
3.0 3.0 4.0 2.0 3.0 3.0	3.0 3.0 4.0 2.0 3.0 3.0	5863.913	5863.908	0.0044	3.1761	4.0 2.0 6.0 3.0 2.0 5.0	4.0 2.0 6.0 3.0 2.0 5.0	7817.920	7817.924	-0.0054	5.0647
3.0 2.0 4.0 2.0 2.0 3.0	3.0 2.0 4.0 2.0 2.0 3.0	5864.056	5864.056	0.0000	3.0668	4.0 3.0 5.0 3.0 2.0 5.0	4.0 3.0 5.0 3.0 2.0 5.0	7818.826	7818.826	0.0000	0.2214
3.0 1.0 4.0 2.0 1.0 3.0	3.0 1.0 4.0 2.0 1.0 3.0	5863.987	5863.985	0.0027	2.8040	4.0 1.0 6.0 3.0 2.0 5.0	4.0 1.0 6.0 3.0 2.0 5.0	7817.056	7817.061	-0.0045	0.7838
3.0 3.0 3.0 2.0 3.0 3.0	3.0 3.0 3.0 2.0 3.0 3.0	5865.126	5865.126	0.0000	0.2479	4.0 3.0 5.0 3.0 3.0 4.0	4.0 3.0 5.0 3.0 3.0 4.0	7817.705	7817.715	-0.0103	4.4082
3.0 2.0 3.0 2.0 2.0 3.0	3.0 2.0 3.0 2.0 2.0 3.0	5865.394	5865.394	0.0000	0.1986	4.0 2.0 5.0 3.0 2.0 4.0	4.0 2.0 5.0 3.0 2.0 4.0	7817.748	7817.748	0.0000	4.3029
3.0 1.0 3.0 2.0 3.0 3.0	3.0 1.0 3.0 2.0 3.0 3.0	5863.032	5863.019	0.0124	0.2308	4.0 1.0 5.0 3.0 1.0 4.0	4.0 1.0 5.0 3.0 1.0 4.0	7817.771	7817.771	0.0000	4.0494
3.0 1.0 3.0 2.0 1.0 3.0	3.0 1.0 3.0 2.0 1.0 3.0	5864.926	5864.917	0.0083	1.0633	4.0 1.0 4.0 3.0 3.0 4.0	4.0 1.0 4.0 3.0 3.0 4.0	7816.606	7816.614	-0.0082	0.1533
3.0 0.0 3.0 2.0 2.0 3.0	3.0 0.0 3.0 2.0 2.0 3.0	5862.727	5862.704	0.0227	0.4332	4.0 1.0 4.0 3.0 1.0 4.0	4.0 1.0 4.0 3.0 1.0 4.0	7818.434	7818.435	-0.0016	0.9519
3.0 3.0 2.0 2.0 3.0 3.0	3.0 3.0 2.0 2.0 3.0 3.0	5864.500	5864.500	0.0000	0.1193	4.0 0.0 4.0 3.0 2.0 4.0	4.0 0.0 4.0 3.0 2.0 4.0	7816.485	7816.484	0.0011	0.3013
3.0 3.0 2.0 2.0 1.0 3.0	3.0 3.0 2.0 2.0 1.0 3.0	5865.398	5865.398	0.0000	0.1823	4.0 3.0 4.0 3.0 3.0 3.0	4.0 3.0 4.0 3.0 3.0 3.0	7817.729	7817.729	0.0000	3.5758
3.0 3.0 3.0 2.0 3.0 2.0	3.0 3.0 3.0 2.0 3.0 2.0	5863.940	5863.940	0.0006	2.2299	4.0 2.0 4.0 3.0 2.0 3.0	4.0 2.0 4.0 3.0 2.0 3.0	7817.768	7817.768	0.0000	3.6118
3.0 3.0 3.0 2.0 1.0 2.0	3.0 3.0 3.0 2.0 1.0 2.0	5865.507	5865.507	0.0000	0.1244	4.0 1.0 4.0 3.0 1.0 3.0	4.0 1.0 4.0 3.0 1.0 3.0	7817.501	7817.503	-0.0019	2.7679
3.0 2.0 3.0 2.0 2.0 2.0	3.0 2.0 3.0 2.0 2.0 2.0	5864.025	5864.030	-0.0052	2.3891	4.0 0.0 4.0 3.0 0.0 3.0	4.0 0.0 4.0 3.0 0.0 3.0	7817.785	7817.785	0.0000	3.6178
3.0 1.0 3.0 2.0 1.0 2.0	3.0 1.0 3.0 2.0 1.0 2.0	5863.405	5863.401	0.0035	1.5046	4.0 3.0 3.0 3.0 3.0 3.0	4.0 3.0 3.0 3.0 3.0 3.0	7816.785	7816.790	-0.0050	0.3048
3.0 0.0 3.0 2.0 0.0 2.0	3.0 0.0 3.0 2.0 0.0 2.0	5864.125	5864.123	0.0022	2.4988	4.0 3.0 3.0 3.0 1.0 3.0	4.0 3.0 3.0 3.0 1.0 3.0	7818.905	7818.895	0.0097	0.6692
3.0 3.0 2.0 2.0 3.0 2.0	3.0 3.0 2.0 2.0 3.0 2.0	5863.324	5863.315	0.0095	0.4750	4.0 2.0 3.0 3.0 2.0 3.0	4.0 2.0 3.0 3.0 2.0 3.0	7816.398	7816.403	-0.0058	0.2682
3.0 3.0 2.0 2.0 1.0 2.0	3.0 3.0 2.0 2.0 1.0 2.0	5864.881	5864.882	-0.0015	0.6731	4.0 2.0 3.0 3.0 0.0 3.0	4.0 2.0 3.0 3.0 0.0 3.0	7819.092	7819.092	0.0000	0.3384
3.0 2.0 2.0 2.0 2.0 2.0	3.0 2.0 2.0 2.0 2.0 2.0	5862.727	5862.690	0.0366	0.3497	4.0 1.0 2.0 3.0 1.0 3.0	4.0 1.0 2.0 3.0 1.0 3.0	7817.481	7817.481	0.0000	0.3217
3.0 2.0 2.0 2.0 0.0 2.0	3.0 2.0 2.0 2.0 0.0 2.0	5865.473	5865.473	0.0000	0.4251	4.0 3.0 3.0 3.0 1.0 3.0	4.0 3.0 3.0 3.0 1.0 3.0	7819.585	7819.585	0.0000	0.1322
3.0 1.0 2.0 2.0 1.0 2.0	3.0 1.0 2.0 2.0 1.0 2.0	5863.113	5863.113	0.0000	0.2891	4.0 3.0 3.0 3.0 3.0 2.0	4.0 3.0 3.0 3.0 3.0 2.0	7817.410	7817.415	-0.0055	1.8091
3.0 3.0 1.0 2.0 3.0 2.0	3.0 3.0 1.0 2.0 3.0 2.0	5864.102	5864.102	0.0000	0.1046	4.0 2.0 3.0 3.0 2.0 2.0	4.0 2.0 3.0 3.0 2.0 2.0	7817.743	7817.743	0.0000	2.2848
3.0 3.0 1.0 2.0 1.0 2.0	3.0 3.0 1.0 2.0 1.0 2.0	5865.659	5865.659	0.0000	0.2983	4.0 1.0 3.0 3.0 1.0 2.0	4.0 1.0 3.0 3.0 1.0 2.0	7817.769	7817.769	0.0000	2.6853
3.0 3.0 2.0 2.0 3.0 1.0	3.0 3.0 2.0 2.0 3.0 1.0	5863.032	5863.031	0.0006	0.5238	4.0 3.0 2.0 3.0 3.0 2.0	4.0 3.0 2.0 3.0 3.0 2.0	7818.112	7818.105	0.0069	0.9104
3.0 2.0 2.0 2.0 2.0 1.0	3.0 2.0 2.0 2.0 2.0 1.0	5864.056	5864.054	0.0022	1.1700	4.0 2.0 2.0 3.0 2.0 2.0	4.0 2.0 2.0 3.0 2.0 2.0	7817.777	7817.777	0.0000	0.4783

Table 2.A3.1 - Continued

J'	n'	F'	J''	n''	F''	Obs.	Calc.	Obs. - Calc.	Intensity weight
4.0	3.0	1.0	3.0	3.0	2.0	-	7818.850	-	0.1076
4.0	3.0	2.0	3.0	3.0	1.0	7817.317	7817.318	-0.0003	1.0734
4.0	2.0	2.0	3.0	2.0	1.0	-	7817.762	-	1.7082
4.0	3.0	1.0	3.0	3.0	1.0	7818.052	7818.064	-0.0113	0.6405
4.0	3.0	1.0	3.0	3.0	0.0	7817.544	7817.540	0.0040	0.5714
6.0			5.0			11722.463	11722.445	0.0174	0.00
7.0			6.0			13673.061	13673.072	-0.0111	0.00
8.0			7.0			15622.340	15622.346	-0.0055	1.00
9.0			8.0			17570.138	17570.133	0.0053	1.00
10.0			9.0			19516.333	19516.324	0.0088	1.00
11.0			10.0			21460.831	21460.837	-0.0060	1.00

Table 2.A3.2 The principal observed and calculated transition frequencies of Ar-Na³⁷Cl (in MHz)

J' n' F'	J'' n'' F''	MHz	MHz - Calc.	Intensity weight	J' n' F'	J'' n'' F''	MHz	MHz - Calc.	Intensity weight
3.0 3.0 6.0	2.0 3.0 5.0	5706.575	5706.574	0.0005	5.5714	1.00	5706.219	0.0056	0.8420
3.0 2.0 5.0	2.0 3.0 5.0	5704.919	5704.918	0.0016	0.8817	1.00	5706.435	-	0.5860
3.0 3.0 5.0	2.0 3.0 4.0	5706.478	5706.476	0.0021	4.6484	0.00	5706.572	-	0.4146
3.0 2.0 5.0	2.0 2.0 4.0	5706.674	5706.673	0.0011	3.8038	1.00	5706.435	-	0.5859
3.0 3.0 4.0	2.0 2.0 4.0	-	5707.779	-	0.2146	0.00	7607.765	-0.0005	6.6667
3.0 2.0 4.0	2.0 3.0 4.0	-	5706.349	-	0.3777	0.00	7606.167	-	0.6561
3.0 1.0 4.0	2.0 2.0 4.0	5706.074	5706.072	0.0017	0.9175	1.00	7607.707	0.0012	5.7052
3.0 1.0 3.0	2.0 2.0 4.0	-	5706.927	-	0.1711	0.00	7607.824	0.0034	5.0989
3.0 3.0 4.0	2.0 3.0 3.0	5706.348	5706.350	-0.0023	3.0596	0.00	7608.776	-	0.1121
3.0 2.0 4.0	2.0 2.0 3.0	5706.393	5706.393	0.0004	2.9015	0.00	7607.098	-	0.7307
3.0 1.0 4.0	2.0 1.0 3.0	5706.393	5706.387	0.0063	2.8054	0.00	7607.570	-	4.4430
3.0 3.0 3.0	2.0 3.0 3.0	-	5707.464	-	0.1774	0.00	7607.649	-0.0085	4.3417
3.0 2.0 3.0	2.0 2.0 3.0	-	5707.596	-	0.1244	0.00	7607.699	-	4.0525
3.0 1.0 3.0	2.0 3.0 3.0	-	5705.498	-	0.1929	0.00	7608.311	-	0.9084
3.0 1.0 3.0	2.0 1.0 3.0	5707.236	5707.242	-0.0061	1.0202	0.00	7606.522	-	0.2059
3.0 0.0 3.0	2.0 2.0 3.0	-	5705.205	-	0.3742	0.00	7607.641	-	3.5623
3.0 3.0 2.0	2.0 1.0 3.0	-	5708.657	-	0.1540	0.00	7607.698	-	3.6325
3.0 3.0 3.0	2.0 3.0 2.0	5706.306	5706.305	0.0016	2.2711	0.00	7607.456	0.0016	2.7871
3.0 3.0 3.0	2.0 1.0 2.0	-	5707.822	-	0.1311	0.00	7607.509	-	3.5832
3.0 2.0 3.0	2.0 2.0 2.0	-	5705.446	-	2.4509	0.00	7606.864	-	0.3665
3.0 1.0 3.0	2.0 1.0 2.0	5705.851	5705.857	-0.0064	1.5161	1.00	7608.829	-	0.5574
3.0 0.0 3.0	2.0 0.0 2.0	-	5706.504	-	2.4708	0.00	7606.404	-	0.2601
3.0 3.0 2.0	2.0 3.0 2.0	-	5705.755	-	0.5210	0.00	7608.795	-	0.3449
3.0 3.0 2.0	2.0 1.0 2.0	-	5707.272	-	0.5905	0.00	7607.417	-	0.2973
3.0 2.0 2.0	2.0 2.0 2.0	-	5705.229	-	0.3014	0.00	7609.366	-	0.1257
3.0 2.0 2.0	2.0 0.0 2.0	-	5707.678	-	0.4179	0.00	7607.414	0.0024	1.8625
3.0 1.0 2.0	2.0 1.0 2.0	5705.568	5705.570	-0.0018	0.2592	1.00	7607.621	-	2.1562
3.0 3.0 1.0	2.0 3.0 2.0	-	5706.405	-	0.1026	0.00	7607.704	-	2.6917
3.0 3.0 1.0	2.0 1.0 2.0	-	5707.923	-	0.2920	0.00	7607.951	-	0.8600
3.0 3.0 2.0	2.0 3.0 1.0	5705.568	5705.568	0.0005	0.5307	1.00	7607.330	-	0.4889
3.0 2.0 2.0	2.0 2.0 1.0	-	5706.379	-	1.0930	0.00	7607.301	-0.0030	1.0809
3.0 1.0 2.0	2.0 1.0 1.0	-	5706.590	-	1.7146	0.00	7607.674	-	1.6877

Table 2.A3.2 - Continued

J'	n'	F'	J''	n''	F''	Mbs.	Malc.	Mbs - Malc.	Intensity	weight
4.0	3.0	1.0	3.0	3.0	1.0	-	7607.941	+	0.6320	0.00
4.0	3.0	1.0	3.0	3.0	0.0	-	7607.487	-	0.5714	0.00
6.0		5.0				11407.655	11407.664	-0.0095		0.00
7.0		6.0				13306.075	13306.072	0.0028		1.00
8.0		7.0				15203.231	15203.233	-0.0020		1.00
9.0		8.0				17099.024	17099.022	0.0025		1.00
10.0		9.0				18993.337	18993.338	-0.0011		1.00

Table 2.A3.3 The principal observed and calculated transition frequencies of $^{86}\text{Kr-Na}^{26}\text{Cl}$ (in MHz)

$J'' n'' F'' J' n' F'$	ν_{obs}	ν_{calc}	Obs.-Calc.	Intensity weight	$J'' n'' F'' J' n' F'$	ν_{obs}	ν_{calc}	Obs.-Calc.	Intensity weight
3.0 3.0 5.0 2.0 3.0 5.0	3966.0334	3966.0302	0.0032	5.5714	3.0 1.0 2.0 2.0 1.0 1.0	-	3966.0342	-	1.7153
3.0 2.0 5.0 2.0 3.0 5.0	-	3964.2023	-	0.9162	3.0 3.0 1.0 2.0 3.0 1.0	3965.6467	3965.6168	0.0099	0.8463
3.0 3.0 5.0 2.0 3.0 4.0	3965.9124	3965.9090	0.0034	4.6851	3.0 2.0 1.0 2.0 2.0 1.0	-	3965.8905	-	0.5944
3.0 2.0 5.0 2.0 2.0 4.0	3966.1513	3966.1513	-0.0002	3.7843	3.0 3.0 0.0 2.0 3.0 1.0	-	3965.1660	-	0.4206
3.0 3.0 4.0 2.0 2.0 4.0	-	3967.3140	-	0.3954	3.0 2.0 1.0 2.0 2.0 0.0	-	3965.8905	-	0.5950
3.0 2.0 4.0 2.0 3.0 4.0	-	3965.8470	-	0.4929	4.0 3.0 7.0 3.0 3.0 6.0	5287.5058	5287.5058	-0.0060	6.6667
3.0 1.0 4.0 2.0 2.0 4.0	-	3965.4378	-	0.9571	4.0 2.0 6.0 3.0 3.0 6.0	-	5285.7530	-	0.6018
3.0 1.0 3.0 2.0 2.0 4.0	-	3966.3926	-	0.1767	4.0 3.0 6.0 3.0 3.0 5.0	5287.4308	5287.4308	-0.0018	5.7439
3.0 3.0 4.0 2.0 3.0 3.0	3965.7437	3965.7438	-0.0001	3.1185	4.0 2.0 6.0 3.0 2.0 5.0	5287.5801	5287.5801	-0.0007	5.0725
3.0 2.0 4.0 2.0 2.0 3.0	-	3965.8665	-	2.9967	4.0 3.0 5.0 3.0 2.0 5.0	-	5286.5430	-	0.1789
3.0 1.0 4.0 2.0 1.0 3.0	3965.8151	3965.8113	0.0038	2.8045	4.0 1.0 5.0 3.0 2.0 5.0	5286.7100	5286.7154	-0.0054	0.7704
3.0 3.0 3.0 2.0 3.0 3.0	-	3966.3926	-	0.2227	4.0 3.0 5.0 3.0 3.0 4.0	-	5287.3803	-	4.3102
3.0 2.0 3.0 2.0 2.0 3.0	-	3967.2268	-	0.1714	4.0 2.0 5.0 3.0 2.0 4.0	-	5287.3948	-	4.3102
3.0 1.0 3.0 2.0 3.0 3.0	-	3964.8223	-	0.2216	4.0 1.0 5.0 3.0 1.0 4.0	-	5287.4289	-	4.0501
3.0 1.0 3.0 2.0 1.0 3.0	-	3966.7661	-	1.0531	4.0 1.0 4.0 3.0 3.0 4.0	-	5286.2336	-	0.1326
3.0 0.0 3.0 2.0 2.0 3.0	-	3964.4987	-	0.4190	4.0 1.0 4.0 3.0 1.0 4.0	-	5288.1098	-	0.9414
3.0 3.0 2.0 2.0 3.0 3.0	-	3966.3544	-	0.1115	4.0 0.0 4.0 3.0 2.0 4.0	-	5286.0745	-	0.2701
3.0 3.0 2.0 2.0 1.0 3.0	-	3968.2981	-	0.1746	4.0 3.0 4.0 3.0 3.0 3.0	-	5287.3792	-	3.5732
3.0 3.0 3.0 2.0 3.0 2.0	-	3965.7534	-	2.2595	4.0 2.0 4.0 3.0 2.0 3.0	-	5287.4199	-	3.6193
3.0 3.0 3.0 2.0 1.0 2.0	-	3967.3856	-	0.1253	4.0 1.0 4.0 3.0 1.0 3.0	5287.1520	5287.1550	-0.0030	2.7724
3.0 2.0 3.0 2.0 2.0 2.0	-	3965.8636	-	2.4054	4.0 0.0 4.0 3.0 0.0 3.0	-	5287.4423	-	3.6093
3.0 1.0 3.0 2.0 1.0 2.0	-	3965.2154	-	1.5073	4.0 3.0 3.0 3.0 3.0 3.0	-	5286.4410	-	0.3279
3.0 0.0 3.0 2.0 0.0 2.0	3965.9460	3965.9506	-0.0056	2.4922	4.0 3.0 3.0 3.0 1.0 3.0	-	5288.6112	-	0.6300
3.0 3.0 2.0 2.0 3.0 2.0	-	3965.1151	-	0.4837	4.0 2.0 3.0 3.0 2.0 3.0	-	5286.0184	-	0.2706
3.0 3.0 2.0 2.0 1.0 2.0	-	3966.7474	-	0.6504	4.0 2.0 3.0 3.0 0.0 3.0	-	5288.7464	-	0.3370
3.0 2.0 2.0 2.0 2.0 2.0	-	3964.4995	-	0.3332	4.0 1.0 3.0 3.0 1.0 3.0	-	5287.1279	-	0.3162
3.0 2.0 2.0 2.0 0.0 2.0	-	3967.3145	-	0.4227	4.0 3.0 2.0 3.0 1.0 3.0	-	5289.2873	-	0.1909
3.0 1.0 2.0 2.0 1.0 2.0	-	3964.9145	-	0.2822	4.0 3.0 3.0 3.0 3.0 2.0	-	5287.0792	-	1.8169
3.0 3.0 1.0 2.0 3.0 2.0	-	3965.9011	-	0.1018	4.0 2.0 3.0 3.0 2.0 2.0	-	5287.3825	-	2.2372
3.0 3.0 1.0 2.0 1.0 2.0	-	3967.5333	-	0.2968	4.0 1.0 3.0 3.0 1.0 2.0	-	5287.4288	-	2.6867
3.0 3.0 2.0 2.0 3.0 1.0	-	3964.8508	-	0.5247	4.0 3.0 2.0 3.0 3.0 2.0	-	5287.7553	-	0.8963
3.0 2.0 2.0 2.0 2.0 1.0	-	3965.8627	-	1.1478	4.0 2.0 2.0 3.0 2.0 2.0	-	5287.4433	-	0.4813

Table 2.A3.3 - Continued

J' n' F'	J'' n'' F''	Mobs	Mcalc	Mobs - Mcalc	Intensity weight	J' n' F'	J'' n'' F''	Mobs	Mcalc	Mobs - Mcalc	Intensity weight
4.0 3.0 1.0	3.0 3.0 2.0	-	5288.5076	-	0.1046	5.0 3.0 4.0	3.0 3.0 3.0	6608.4574	6608.4462	0.0112	3.1239
4.0 3.0 2.0	3.0 3.0 1.0	5286.9689	5286.9683	-0.0004	1.0761	5.0 2.0 4.0	4.0 2.0 3.0	-	6608.5513	-	3.3351
4.0 2.0 2.0	3.0 2.0 1.0	-	5287.4154	-	1.7022	5.0 1.0 4.0	4.0 1.0 3.0	-	6608.5548	-	3.6674
4.0 3.0 1.0	3.0 3.0 1.0	-	5287.7216	-	0.6385	5.0 3.0 3.0	4.0 3.0 3.0	-	6609.0106	-	0.6792
4.0 3.0 1.0	3.0 3.0 0.0	-	5287.1924	-	0.5714	5.0 3.0 3.0	4.0 1.0 3.0	-	6610.4839	-	0.1247
5.0 3.0 8.0	4.0 3.0 7.0	-	6608.6410	-	7.7273	5.0 2.0 3.0	4.0 2.0 3.0	-	6608.6376	-	0.3924
5.0 2.0 7.0	4.0 3.0 7.0	-	6606.9385	-	0.3510	5.0 3.0 3.0	4.0 3.0 2.0	6608.3288	6608.3345	-0.0057	2.2298
5.0 3.0 7.0	4.0 3.0 6.0	-	6608.5906	-	6.7807	5.0 2.0 3.0	4.0 2.0 2.0	-	6609.5768	-	2.7806
5.0 2.0 7.0	4.0 2.0 6.0	6608.6855	6608.6913	-0.0058	6.2543	5.0 3.0 2.0	4.0 3.0 2.0	-	6609.2079	-	0.5465
5.0 3.0 6.0	4.0 3.0 6.0	-	6608.7263	-	0.1932	5.0 3.0 2.0	4.0 3.0 1.0	-	6608.4557	-	1.6667
5.0 3.0 6.0	4.0 2.0 6.0	-	6609.5297	-	0.1166	7.0	6.0	9249.5265	9249.5696	-0.0341	0.00
5.0 2.0 6.0	4.0 3.0 6.0	-	6608.4654	-	0.1921	8.0	7.0	10569.2737	10569.2766	-0.0029	0.00
5.0 2.0 6.0	4.0 2.0 6.0	-	6609.2697	-	0.1714	9.0	8.0	11888.4367	11888.4347	0.0010	0.30
5.0 1.0 6.0	4.0 2.0 6.0	-	6607.7418	-	0.6271	10.0	9.0	13207.0140	13207.0122	0.0018	0.50
5.0 3.0 6.0	4.0 3.0 5.0	-	6608.5675	-	5.5669	11.0	10.0	14524.9905	14524.9917	-0.0012	0.50
5.0 2.0 6.0	4.0 2.0 5.0	-	6608.5634	-	5.4978	12.0	11.0	15842.3533	15842.3546	-0.0013	0.50
5.0 1.0 6.0	4.0 1.0 5.0	-	6608.6067	-	5.2285	13.0	12.0	17159.0726	17159.0710	0.0007	0.50
5.0 3.0 5.0	4.0 2.0 5.0	-	6610.0655	-	0.2824	-	-	-	-	-	-
5.0 2.0 5.0	4.0 3.0 5.0	-	6609.7149	-	0.2662	-	-	-	-	-	-
5.0 1.0 5.0	4.0 1.0 5.0	-	6609.1336	-	0.7965	-	-	-	-	-	-
5.0 0.0 5.0	4.0 3.0 5.0	-	6607.0171	-	0.1082	-	-	-	-	-	-
5.0 0.0 5.0	4.0 2.0 5.0	-	6607.2729	-	0.1766	-	-	-	-	-	-
5.0 3.0 5.0	4.0 3.0 4.0	-	6608.5620	-	4.6761	-	-	-	-	-	-
5.0 2.0 5.0	4.0 2.0 4.0	-	6608.5853	-	4.7018	-	-	-	-	-	-
5.0 1.0 5.0	4.0 1.0 4.0	6608.4574	6608.4527	0.0047	3.9821	-	-	-	-	-	-
5.0 0.0 5.0	4.0 0.0 4.0	-	6608.5932	-	0.4679	-	-	-	-	-	-
5.0 3.0 4.0	4.0 3.0 4.0	-	6607.5080	-	0.2791	-	-	-	-	-	-
5.0 3.0 4.0	4.0 1.0 4.0	-	6609.9024	-	0.4594	-	-	-	-	-	-
5.0 2.0 4.0	4.0 2.0 4.0	-	6607.1498	-	0.2445	-	-	-	-	-	-
5.0 2.0 4.0	4.0 1.0 4.0	-	6609.4261	-	0.1273	-	-	-	-	-	-
5.0 2.0 4.0	4.0 0.0 4.0	-	6609.8555	-	0.2584	-	-	-	-	-	-
5.0 1.0 4.0	4.0 1.0 4.0	-	6608.5278	-	0.3525	-	-	-	-	-	-

Table 2.A3.4 - Continued

J	n	F	J'	n'	F'	ν_{obs}	ν_{calc}	$\nu_{obs} - \nu_{calc}$	Intensity weight
5.0	2.0	3.0	4.0	2.0	2.0	-	6395.5746	-	2.7425
5.0	3.0	2.0	4.0	3.0	2.0	-	6396.1171	-	0.5359
5.0	3.0	2.0	4.0	3.0	1.0	-	6395.4752	-	1.6667
6.0		5.0				-	7673.8682	-	0.0000
7.0		6.0				-	8951.7307	-	0.0000
8.0		7.0				-	10229.1355	-	0.0000
9.0		8.0				-	11506.0464	-0.0047	0.0000
10.0		9.0				-	12782.4584	12782.4531	0.0053
11.0		10.0				-	14058.3232	14058.3206	0.0026
12.0		11.0				-	15333.6269	15333.6319	-0.0050
13.0		12.0				-	16608.3595	16608.3579	0.0016

Table 2.A3.5 - Continued

J'	n'	F'	J''	n''	F''	ν_{obs}	ν_{calc}	$\nu_{obs} - \nu_{calc}$	Intensity	weight
5.0	2.0	3.0	4.0	2.0	3.0	-	6551.6544	-	0.3910	0.00
5.0	3.0	3.0	4.0	3.0	2.0	-	6551.3567	-	2.2286	0.00
5.0	2.0	3.0	4.0	2.0	2.0	-	6551.6013	-	2.7630	0.00
5.0	3.0	2.0	4.0	3.0	2.0	-	6552.2343	-	0.5478	0.00
5.0	3.0	2.0	4.0	3.0	1.0	-	6551.4790	-	1.6567	0.00
6.0	0.0	0.0	5.0	0.0	0.0	-	7860.9791	-	-	0.00
7.0	0.0	0.0	6.0	0.0	0.0	9169.8663	9169.8785	-0.0122	-	0.00
8.0	0.0	0.0	7.0	0.0	0.0	10478.2553	10478.2621	-0.0068	-	0.50
9.0	0.0	0.0	8.0	0.0	0.0	11786.0976	11786.0983	-0.0007	-	0.50
0.0	0.0	0.0	9.0	0.0	0.0	13083.3716	13083.3671	0.0044	-	0.50
11.0	0.0	0.0	10.0	0.0	0.0	14400.0567	14400.0577	-0.0010	-	0.50
12.0	0.0	0.0	11.0	0.0	0.0	15706.1648	15706.1650	-0.0002	-	0.50

Table 2.A3.6 The principal observed and calculated transition frequencies of $^{82}\text{Kr-Na}^{35}\text{Cl}$ (in MHz)

$J'' n'' F''$	$J' n' F'$	F''	F'	ν_{obs}	ν_{calc}	Mbs - Calc.	Intensity weight	$J'' n'' F''$	$J' n' F'$	F''	F'	ν_{obs}	ν_{calc}	Mbs - Calc.	Intensity weight
4.0 3.0 7.0	3.0 3.0 6.0	5335.2149	5335.2196	-0.0047	6.6667	1.00	5.0 3.0 8.0	4.0 3.0 7.0	6668.2589	-	-	7.7273	0.00	7.7273	0.00
4.0 2.0 6.0	3.0 3.0 6.0	5333.4783	-	0.6844	0.00	0.00	5.0 2.0 7.0	4.0 3.0 7.0	6666.5658	-	-	0.5433	0.00	0.5433	0.00
4.0 3.0 6.0	3.0 3.0 5.0	5335.1462	5335.1472	-0.0010	5.7359	1.00	5.0 3.0 7.0	4.0 3.0 6.0	6668.2107	-	-	6.7724	0.00	6.7724	0.00
4.0 2.0 6.0	3.0 3.0 5.0	5335.2553	5335.2920	0.0033	5.0772	1.00	5.0 2.0 7.0	4.0 2.0 6.0	6668.3078	0.0007	0.0007	6.2597	1.00	6.2597	1.00
4.0 3.0 6.0	3.0 2.0 5.0	5336.2953	-	0.1610	0.00	0.00	5.0 3.0 6.0	4.0 3.0 6.0	6668.3486	-	-	0.2078	0.00	0.2078	0.00
4.0 1.0 5.0	3.0 2.0 5.0	5286.7100	5334.4457	47.7357	0.7625	0.00	5.0 3.0 6.0	4.0 2.0 5.0	6669.1618	-	-	0.1032	0.00	0.1032	0.00
4.0 3.0 5.0	3.0 3.0 4.0	5335.0999	-	4.3170	0.00	0.00	5.0 2.0 6.0	4.0 3.0 6.0	6668.0607	-	-	0.1753	0.00	0.1753	0.00
4.0 2.0 5.0	3.0 2.0 4.0	5335.1052	-	4.3175	0.00	0.00	5.0 2.0 6.0	4.0 2.0 6.0	6668.8740	-	-	0.1873	0.00	0.1873	0.00
4.0 1.0 5.0	3.0 1.0 4.0	5335.1439	-	4.0505	0.00	0.00	5.0 1.0 6.0	4.0 2.0 5.0	6667.3789	-	-	0.6189	0.00	0.6189	0.00
4.0 1.0 4.0	3.0 3.0 4.0	5333.9549	0.1224	0.00	0.1224	0.00	5.0 3.0 6.0	4.0 3.0 5.0	6668.1885	-	-	5.5620	0.00	5.5620	0.00
4.0 1.0 4.0	3.0 1.0 4.0	5335.8186	-	0.9351	0.00	0.00	5.0 2.0 6.0	4.0 2.0 5.0	6668.1798	-	-	5.5045	0.00	5.5045	0.00
4.0 0.0 4.0	3.0 2.0 4.0	5333.8114	-	0.2548	0.00	0.00	5.0 1.0 6.0	4.0 1.0 5.0	6668.2252	-	-	5.2258	0.00	5.2258	0.00
4.0 3.0 4.0	3.0 3.0 3.0	5335.0916	-	3.5711	0.00	0.00	5.0 3.0 5.0	4.0 2.0 5.0	6669.6861	-	-	0.2880	0.00	0.2880	0.00
4.0 2.0 4.0	3.0 2.0 3.0	5335.1371	-	3.6224	0.00	0.00	5.0 2.0 5.0	4.0 3.0 5.0	6669.3006	-	-	0.2687	0.00	0.2687	0.00
4.0 1.0 4.0	3.0 1.0 3.0	5334.8731	5334.8734	-0.0003	2.7751	1.00	5.0 1.0 5.0	4.0 1.0 5.0	6668.7477	-	-	0.7896	0.00	0.7896	0.00
4.0 0.0 4.0	3.0 0.0 3.0	5335.1558	-	3.6043	0.00	0.00	5.0 0.0 5.0	4.0 3.0 5.0	6666.6388	-	-	0.1201	0.00	0.1201	0.00
4.0 3.0 3.0	3.0 3.0 3.0	5334.1766	-	0.8380	0.00	0.00	5.0 3.0 5.0	4.0 3.0 5.0	6666.9179	-	-	4.6745	0.00	4.6745	0.00
4.0 3.0 3.0	3.0 1.0 3.0	5336.3312	-	0.6116	0.00	0.00	5.0 3.0 5.0	4.0 2.0 5.0	6668.1791	-	-	4.7035	0.00	4.7035	0.00
4.0 2.0 3.0	3.0 2.0 3.0	5333.7409	-	0.2699	0.00	0.00	5.0 2.0 5.0	4.0 2.0 4.0	6668.2053	-	-	3.9857	1.00	3.9857	1.00
4.0 2.0 3.0	3.0 0.0 3.0	5336.4290	-	0.3374	0.00	0.00	5.0 1.0 5.0	4.0 1.0 4.0	6668.0748	0.0018	0.0018	4.6731	0.00	4.6731	0.00
4.0 1.0 3.0	3.0 1.0 3.0	5334.8436	-	0.3128	0.00	0.00	5.0 0.0 5.0	4.0 0.0 4.0	6668.2118	-	-	0.2951	0.00	0.2951	0.00
4.0 3.0 2.0	3.0 1.0 3.0	5336.9844	-	0.1301	0.00	0.00	5.0 3.0 4.0	4.0 3.0 4.0	6667.1651	-	-	0.4469	0.00	0.4469	0.00
4.0 3.0 3.0	3.0 2.0 2.0	5334.8052	-	1.8252	0.00	0.00	5.0 3.0 4.0	4.0 1.0 4.0	6666.7696	-	-	0.2442	0.00	0.2442	0.00
4.0 2.0 3.0	3.0 2.0 2.0	5335.0892	-	2.2160	0.00	0.00	5.0 2.0 4.0	4.0 2.0 4.0	6669.0098	-	-	0.1301	0.00	0.1301	0.00
4.0 1.0 3.0	3.0 1.0 2.0	5335.1450	-	2.6876	0.00	0.00	5.0 2.0 4.0	4.0 1.0 4.0	6669.4379	-	-	0.2707	0.00	0.2707	0.00
4.0 3.0 2.0	3.0 3.0 2.0	5335.4584	-	0.8885	0.00	0.00	5.0 1.0 4.0	4.0 0.0 4.0	6668.1447	-	-	3.1896	1.00	3.1896	1.00
4.0 2.0 2.0	3.0 2.0 2.0	5335.1626	-	0.4828	0.00	0.00	5.0 1.0 4.0	4.0 1.0 4.0	6668.0748	0.0047	0.0047	3.3225	0.00	3.3225	0.00
4.0 3.0 1.0	3.0 3.0 2.0	5336.1963	-	0.1030	0.00	0.00	5.0 3.0 4.0	4.0 3.0 3.0	6668.0748	0.0047	0.0047	3.6581	0.00	3.6581	0.00
4.0 3.0 2.0	3.0 3.0 1.0	5334.6940	5334.6918	0.0022	1.0752	1.00	5.0 2.0 4.0	4.0 2.0 3.0	6668.1658	-	-	0.6679	0.00	0.6679	0.00
4.0 2.0 2.0	3.0 2.0 1.0	5335.1280	-	1.7001	0.00	0.00	5.0 1.0 4.0	4.0 1.0 3.0	6668.1745	-	-	0.6679	0.00	0.6679	0.00
4.0 3.0 1.0	3.0 3.0 1.0	5335.4297	-	0.6373	0.00	0.00	5.0 3.0 3.0	4.0 3.0 3.0	6670.6112	-	-	0.1232	0.00	0.1232	0.00
4.0 3.0 1.0	3.0 3.0 0.0	5334.9099	-	0.5714	0.00	0.00	5.0 3.0 3.0	4.0 1.0 3.0	6670.0988	-	-	-	-	-	-

Table 2.A3.6 - Continued

J	n	F	J'	n'	F'	ν_{obs}	ν_{calc}	$\nu_{obs} - \nu_{calc}$	Intensity	weight
5.0	2.0	3.0	4.0	2.0	3.0	-	6668.2659	-	0.3954	0.00
5.0	3.0	3.0	4.0	3.0	2.0	6667.9517	6667.9580	-0.0063	2.2319	1.00
5.0	2.0	3.0	4.0	2.0	2.0	-	6668.1935	-	2.7652	0.00
5.0	3.0	2.0	4.0	3.0	2.0	-	6668.8136	-	0.5440	0.00
5.0	3.0	2.0	4.0	3.0	1.0	-	6668.0758	-	1.6667	0.00
6.0	-	5.0	-	-	-	-	8000.8224	-	-	0.00
7.0	-	6.0	-	-	-	-	9332.9406	-	-	0.00
8.0	-	7.0	-	-	-	-	10664.5112	-	-	0.00
9.0	-	8.0	-	-	-	-	11995.5144	-0.0032	-	0.50
10.0	-	9.0	-	-	-	-	13325.9158	0.0018	-	0.50
11.0	-	10.0	-	-	-	-	14655.6961	0.0025	-	0.50
12.0	-	11.0	-	-	-	-	15984.8500	-0.0027	-	0.50
							15984.8500	0.0007	-	0.50

Appendix IV

The Origin of the Intermolecular Force

It is known that both the attractive and repulsive forces always exist between two particles and the intermolecular potential energy surface is produced by the sum of these two forces. Now, these two terms will be discussed separately

2.A4.1 attractive terms

We consider the case that molecule A and molecule B interact each other in the coordinate system as shown in Fig. 2.A4.1. The total Hamiltonian of the complex A-B is written by the sum of the Hamiltonian H_A of molecule A, H_B of molecule B, and H' of the perturbation, that is,

$$H = H_A + H_B + H',$$

$$H_A = \sum_i \frac{p_i^2}{m_i} + \sum_{i \neq i'} \frac{e_i \cdot e_{i'}}{r_{ii'}}, \quad H_B = \sum_j \frac{p_j^2}{m_j} + \sum_{j \neq j'} \frac{e_j \cdot e_{j'}}{r_{jj'}}, \quad H' = \sum_{i,j} \frac{e_i \cdot e_j}{r_{ij}}, \quad (2.A4.1)$$

where the condition that $H_A, H_B \gg H'$ is assumed. H_A, H_B have wavefunction $|n_A\rangle, |n_B\rangle$ with energy $E_a^{(n)}, E_b^{(n)}$, respectively. Now we can consider the variation of energy due to the interaction between $|n_A = 0\rangle$ of molecule A and $|n_B = 0\rangle$ of B by using the perturbation method. When we use $|n_A\rangle, |n_B\rangle = |n_A, n_B\rangle$ as basis sets, the variation of energy E' is written as follows.

$$E' = E^{(1)} + E^{(2)},$$

$$E^{(1)} = \langle 0,0 | H' | 0,0 \rangle \quad (\text{electrostatic term})$$

$$E^{(2)} = \sum_{\substack{(n_A, n_B) \\ (n_A, n_B) \neq (0,0)}} \frac{|\langle n_A, n_B | H' | 0,0 \rangle|^2}{E_a^{(0)} + E_b^{(0)} - E_a^{(n_A)} - E_b^{(n_B)}} \quad (2.A4.2)$$

$$= \sum_{\substack{n_A=0 \\ n_B=0}} \dots + \sum_{\substack{n_A=0 \\ n_B \neq 0}} \dots \quad (\text{induction term})$$

$$+ \sum_{\substack{n_A \neq 0 \\ n_B=0}} \dots \quad (\text{dispersion term})$$

To proceed with calculation, we must calculate the matrix element $\langle n_A, n_B | H' | n_A, n_B \rangle$. The Hamiltonian H' can expand in terms of multipole moments of each atom as follows,

$$H' = \sum_{i,j} \frac{e_i \cdot e_j}{r_{ij}} \\ = \sum_{l_a=0}^{\infty} \sum_{l_b=0}^{\infty} \sum_{m=-l_a}^{+l_a} \frac{(-1)^{l_a} (l_a + l_b)!}{[(l_a + m)!(l_b + m)!(l_a - m)!(l_b - m)!]^{1/2}} \cdot \frac{Q_a^{(m)} \cdot Q_b^{(m)}}{R_{AB}^{l_a + l_b + 1}} \quad (2.A4.3)$$

where $Q_l^{(m)}$ is expressed by

$$Q_l^{(m)} = \sum_i e_i r_i^l P_l^m(\cos \theta_i) \cdot e^{im\phi_i} \quad (2.A4.4)$$

where $P_l^m(\cos \theta_i)$ is Legendre's function. This expansion become a good approximation for some small l when the condition, $R_{AB} \gg r_i + r_j$, is satisfied. It is worthy of notice that $Q_l^{(m)}$ represents the m component of the total charge, dipole moment, quadrupole moment in spherical tensor notation for $l = 0, 1, 2$, respectively.

Substituted Eq. (2.A4.3) for H' of the electrostatic term in Eq. (2.A4.2), the electrostatic interaction energy is rewritten as follows.

$$E_{elec} = \sum_{l_a, l_b, m} \frac{(-1)^{l_a} (l_a + l_b)!}{[(l_a + m)!(l_b + m)!(l_a - m)!(l_b - m)!]^{1/2}} \cdot \frac{\langle 0 | Q_{l_a}^{(m)} | 0 \rangle \langle 0 | Q_{l_b}^{(m)} | 0 \rangle}{R_{AB}^{l_a + l_b + 1}} \quad (2.A4.5)$$

Now if both constituent molecules of the complex have C_3 or more symmetry axis, the dipole moment and quadrupole moment of each constituent molecule become

$$\mu_z = \mu, \mu_x = \mu_y = 0, \\ Q_{zz} = -2Q_{xx} = -2Q_{yy} = Q, \quad Q_{xy} = Q_{yz} = Q_{zx} = 0, \quad (2.A4.6)$$

in the molecular fixed axis system (xyz). Each interaction term for (l_a, l_b) in the electrostatic term is written as shown in Table 2.A4.1.

Substituted Eq. (2.A4.3) for H' of the induction term in Eq. (2.A4.2), the interaction energy is rewritten as follows.

$$\begin{aligned}
E_{ind} &= E_{ind}^A + E_{ind}^B \\
E_{ind}^A &= \sum_{\substack{n_A=0, \\ n_B=0}} \frac{\langle 0,0|H|0,n_B\rangle \cdot \langle 0,n_B|H'|0,0\rangle}{E_a^{(0)} + E_b^{(0)} - E_a^{(n_A)} - E_b^{(n_B)}} \\
&= - \sum_{\substack{l_a, l_b \\ l_a', l_b' \\ m, m'}} f(l_a, l_b, m) \cdot f(l_a', l_b', m') \langle 0|Q_m^{l_a}|0\rangle \langle 0|Q_m^{l_b}|0\rangle R_{AB}^{-(l_a+l_b+l_a'+l_b'+2)} \quad (2.A4.7) \\
&\quad \times \sum_{n_B} \frac{\langle 0|Q_{-m}^{(l_a)}|n_B\rangle \cdot \langle n_B|Q_{-m}^{(l_b)}|0\rangle}{E_b^{(n_B)} - E_b^{(0)}}
\end{aligned}$$

where

$$f(l_a, l_b, m) = \frac{(-1)^l (l_a + l_b)!}{[(l_a + m)!(l_b + m)!(l_a - m)!(l_b - m)!]^{\frac{1}{2}}} \quad (2.A4.8)$$

The matrix element $\langle 0|Q_{-m}^{(l)}|n\rangle$ vanishes for $l=0$ because $Q_0^{(0)}$ is scalar. Therefore, the term of $l=1$ contributes dominantly for the induced term. The term for $l=1$ can be related to the polarization α as follows

$$(\alpha)_{m,m'} = 2 \cdot \sum_{n_B} \frac{\langle 0|Q_{-m}^{(1)}|n_B\rangle \cdot \langle n_B|Q_{-m'}^{(1)}|0\rangle}{E_b^{(n_B)} - E_b^{(0)}} \quad (2.A4.9)$$

If we consider the intermolecular interaction of complex between atom and the molecule with C_2 or more symmetry, we can estimate the energy of the induced term as shown in Table 2.A4.2

Substituted Eq. (2.A4.3) for H' of the dispersion term in Eq. (2.A4.2), the interaction energy is rewritten as follows.

$$\begin{aligned}
E_{disp} &= \sum_{\substack{n_A=0, \\ n_B=0}} \frac{\langle 0,0|H''|n_A, n_B\rangle \cdot \langle n_A, n_B|H'|0,0\rangle}{E_a^{(0)} + E_b^{(0)} - E_a^{(n_A)} - E_b^{(n_B)}} \\
&= - \sum_{\substack{l_a, l_b \\ l_a', l_b' \\ m, m'}} f(l_a, l_b, m) \cdot f(l_a', l_b', m') R_{AB}^{-(l_a+l_b+l_a'+l_b'+2)} \quad (2.A4.10) \\
&\quad \times \sum_{n_A, n_B} \frac{\langle 0|Q_m^{l_a}|n_A\rangle \langle n_A|Q_m^{l_b}|0\rangle \langle 0|Q_{-m}^{(l_a)}|n_B\rangle \langle n_B|Q_{-m'}^{(l_b)}|0\rangle}{E_a^{(0)} + E_b^{(0)} - E_a^{(n_A)} - E_b^{(n_B)}}
\end{aligned}$$

Using

$$\left[E_a^{(n_A)} - E_a^{(0)} + E_b^{(n_B)} - E_b^{(0)} \right]^{-1} = \frac{U_a U_b}{(U_a + U_b) [E_a^{(n_A)} - E_a^{(0)}] [E_b^{(n_B)} - E_b^{(0)}]} \quad (2.A4.11)$$

and assuming that both A and B have the isotropic polarizability and $l_a = l_a' = l_b = l_b' = 1$, we can obtain the expression of London's formula, i.e.,

$$E_{disp} = -\frac{3}{2} \frac{U_a U_b \alpha_A \alpha_B}{(U_a + U_b) R_{AB}^6}, \quad (2.A4.12)$$

where U_a and U_b are ionization energy for molecule A and B, respectively.

2.A4.2 repulsive terms

We used above that the interaction energy between A and B such as Eqs. (2.A4.5), (2.A4.7), and (2.A4.10) can be expressed by the expansion in series of R^{-n} . The expression become a good approximation for the sum of only small l -value in long distance, but the approximation become worse in short distance such as molecular complexes. Therefore, we always use the semiempirical expression instead of the exact expression in the short distance.

A simple physical picture of the repulsive interaction can be given in terms of the Hellmann-Feynman electrostatic theorem and the Pauli exclusion principle. According to these theorems, the repulsion term is written as following term,

$$V_{rep.}(R, \theta) = \sum A \cdot e^{-\beta R}. \quad (2.A4.13)$$

where the constant, A and β , are determined by fitting as parameters to reproduce the experimental data.

Table 2.A4.1 The electrostatic interactions between molecules with C_3 or more symmetry axis

(l_a, l_b)	interaction energy
(0,0)	$E^{(C,C)} = \frac{C_A C_B}{R_{AB}}$
(0,1)	$E^{(C,\mu)} = -\frac{C_A \mu_B \cos \theta_B}{R_{AB}^2}$
(0,2)	$E^{(C,Q)} = -\frac{C_A Q_B}{2R_{AB}^3} (3 \cos^2 \theta_B - 1)$
(1,1)	$E^{(\mu,\mu)} = -\frac{\mu_A \mu_B}{R_{AB}^3} [2 \cos \theta_A \cos \theta_B - \sin \theta_A \sin \theta_B \cos(\varphi_A - \varphi_B)]$
(1,2)	$E^{(\mu,Q)} = \frac{3\mu_A Q_B}{2R_{AB}^4} [\cos \theta_A (3 \cos^2 \theta_B - 1) - 2 \sin \theta_A \sin \theta_B \cos \theta_B \cos(\varphi_A - \varphi_B)]$
(2,2)	$E^{(Q,Q)} = \frac{3Q_A Q_B}{4R_{AB}^5} [1 - 5 \cos^2 \theta_A - 5 \cos^2 \theta_B + 19 \cos^2 \theta_A \cos^2 \theta_B + 2 \sin^2 \theta_A \sin^2 \theta_B \cos^2(\varphi_A - \varphi_B) - 16 \sin \theta_A \sin \theta_B \cos \theta_A \cos \theta_B \cos(\varphi_A - \varphi_B)]$

Table 2.A4.2 The inductive interactions between an atom and a molecule with C_3 or more symmetry axis

	(l_a, l_b)	interaction energy
charge - charge induced dipole interaction	(0, 0)	$E^{(C, \mu \text{ by } C)} = -\frac{C_A^2 \alpha_B}{2R_{AB}^3}$
dipole - charge induced dipole interaction	(1, 0)	$E^{(l_a, \mu \text{ by } C)} = -\frac{2C_A \mu_A \alpha_B \cos \theta_A}{R_{AB}^5}$
quadrupole - charge induced dipole interaction	(2, 0)	$E^{(Q, \mu \text{ by } C)} = -\frac{3C_A Q_A \alpha_B (3 \cos^2 \theta_A - 1)}{2R_{AB}^6}$
dipole - dipole induced dipole interaction	(1, 1)	$E^{(l_a, \mu \text{ by } \mu)} = -\frac{3\mu_A^2 \alpha_B (3 \cos^2 \theta_A + 1)}{2R_{AB}^6}$

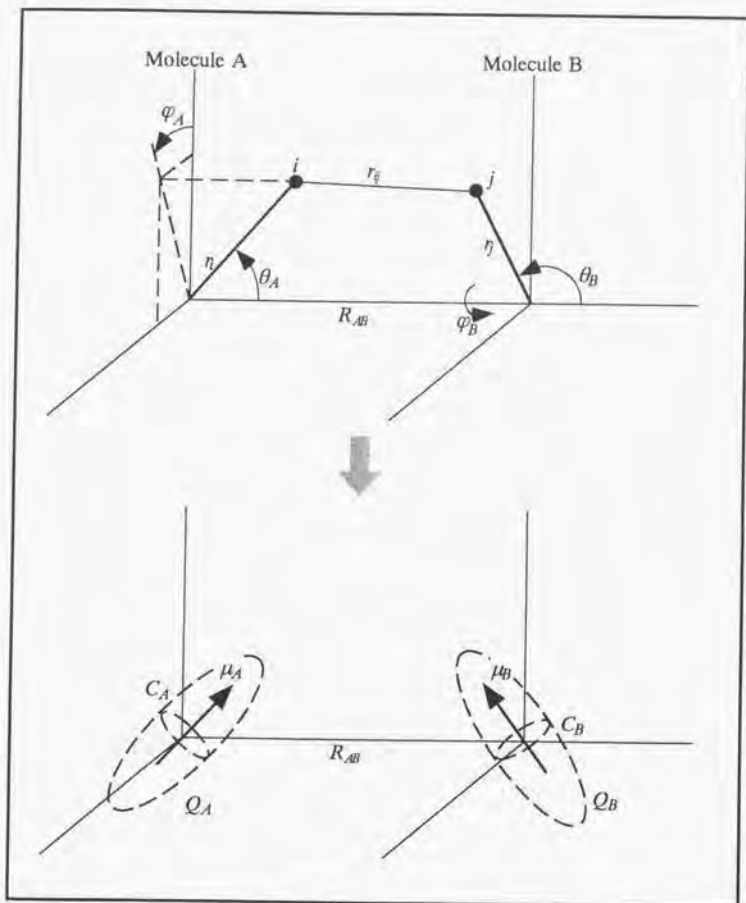


Fig. 3.A4.1 Intermolecular interaction between two molecules. The C , μ , and Q are the charge, the dipole moment, and the quadrupole moment of the constituent molecule in a complex.



Chapter 3

Microwave Spectroscopy of the $\text{NaCl}-(\text{H}_2\text{O})_n$ ($n=1, 2, 3$) Complexes and a Model for Microsolvation Process on NaCl

§ 3.0	Abstract	80
§ 3.1	Experimental	81
§ 3.2	Results and Analysis	82
3.2.1	<i>the $\text{NaCl}-\text{H}_2\text{O}$ complex</i>	
3.2.2	<i>the $\text{NaCl}-(\text{H}_2\text{O})_2$ complex</i>	
3.2.3	<i>the $\text{NaCl}-(\text{H}_2\text{O})_3$ complex</i>	
§ 3.3	Discussion	88
3.3.1	<i>the structures of the $\text{NaCl}-(\text{H}_2\text{O})_n$ complexes</i>	
3.3.2	<i>the intermolecular interaction in the $\text{NaCl}-(\text{H}_2\text{O})_n$ complexes</i>	
3.3.3	<i>the microsolvation process on NaCl</i>	
	References, Tables, Figures	99
	Appendixes	117

§ 3.0 Abstract

The rotational spectra of the $\text{NaCl}-(\text{H}_2\text{O})_n$ ($n=1, 2, 3$) complexes have been observed by a Fourier-transform microwave spectrometer combined with a laser ablation technique for the first time. The 4 isotopic species (normal, ^{37}Cl , two deuterated species) for $\text{NaCl}-\text{H}_2\text{O}$, 2 isotopic species (normal, ^{37}Cl species) for $\text{NaCl}-(\text{H}_2\text{O})_2$, and 2 isotopic species (normal, ^{37}Cl species) for $\text{NaCl}-(\text{H}_2\text{O})_3$ were observed. The molecular constants including the hyperfine coupling constants for each isotopic species have been determined within the experimental accuracy. The r_0 -structures of the $\text{NaCl}-(\text{H}_2\text{O})_n$ were determined using these rotational constants. The determined structures are a nearly planar asymmetric rotor, an asymmetric rotor with C_2 axis, and a symmetric rotor with C_3 axis for $\text{NaCl}-\text{H}_2\text{O}$, $\text{NaCl}-(\text{H}_2\text{O})_2$, and $\text{NaCl}-(\text{H}_2\text{O})_3$, respectively. The determined structures showed that the distance between Na and Cl, $r(\text{NaCl})$, in the $\text{NaCl}-(\text{H}_2\text{O})_n$ becomes longer with the increase of the number of H_2O attached. This tendency is in good agreement with that of a previous *ab initio* calculation. The determined nuclear quadrupole coupling constants of the Na and Cl atoms were perturbed by the complex formation. It is confirmed that the coupling constants for the Na atom are mainly dominated by the effect of the electrostatic interaction of H_2O . On the other hand, the coupling constants for the Cl atom are perturbed by other effects, such as polarization, electron repulsion, and charge transfer in addition to the electrostatic interaction. The possibility of these effects was confirmed by a comparison between the experimental data and results of *ab initio* calculations. We could qualitatively confirm that the charge distributions of both Na and Cl change from the direction along the NaCl axis to the perpendicular direction to the NaCl axis with increase of the number of H_2O .

§ 3.1 Experiment

We used the Fourier-transform microwave spectrometer combined with the laser ablation method discussed in detail in section 1.2.

The same ablation nozzle unit used in the $\text{Rg}-\text{NaCl}$ complex (see Chapter 3.2) was used for the present study. The target rod was made by the same method as explained in section 1.2 (NaCl purity 98%). Although both fundamental and second harmonic of a Nd^{3+} :YAG laser were used to vaporize the NaCl , intensities of the spectrum was not changed significantly. The sample gas was a mixture of 0.2% of H_2O diluted in Ar. When we observe the deuterated species, we used D_2O (Aldrich Co., purity 99.9%) as a precursor instead of H_2O . We scanned a wide range from 6 to 25 GHz in a conditions that the rotational transition, $(J, F) = (1, 4) - (0, 3)$ of the free NaCl monomer are observed with an adequate intensity. In order to check weather the experimental conditions are kept well, we monitored the rotational transition at an intervals of 100 MHz.

We optimized the condition for the observation of the $\text{NaCl}-(\text{H}_2\text{O})_n$ complexes as follows. The stagnation pressure was at 7~10 atm. The optimized background pressure in the vacuum chamber was typically kept about 4×10^{-5} Torr in $\text{NaCl}-\text{H}_2\text{O}$ and $\text{NaCl}-(\text{H}_2\text{O})_2$, but about $6\sim 8 \times 10^{-6}$ Torr in $\text{NaCl}-(\text{H}_2\text{O})_3$. The optimum microwave pulse width, t_p , and attenuator combination was 0.3 μs and 20 dB for *a*-type transitions of $\text{NaCl}-\text{H}_2\text{O}$, while those of other species were 0.4 μs and 16 dB for $\text{NaCl}-(\text{H}_2\text{O})_2$, 0.6 μs and 16 dB for $\text{NaCl}-(\text{H}_2\text{O})_3$. According to Eq. (1.1), this result implies that the dipole moment decreases with the increase of the water molecules, which is in agreement with *ab initio* calculations.

§ 3.2 Results and Analysis

As a result of a scan in a wide region of 6 to 25 GHz, we were able to observe a lot of unassigned lines. The observed lines are shown as a stick diagram in Fig. 3.1. We confirmed that these lines require the vaporization of NaCl by turning off the ablation laser. Furthermore, these lines were not observed when we used the pure Ar gas as a carrier gas. Therefore, we considered that the lines belong to species arising from complexes containing both NaCl and H_2O . Intensities of the observed lines shown in Fig. 3.1 have uncertainty because it is very difficult to keep the best experimental conditions.

3.2.1 the $\text{NaCl}-\text{H}_2\text{O}$ complex

The transitions of $\text{Na}^{35}\text{Cl}-\text{H}_2\text{O}$ and $\text{Na}^{37}\text{Cl}-\text{H}_2\text{O}$ are represented by open and filled circles in Fig. 3.1, respectively. We could observe 9 *a*-type, 2 *b*-type *R*-branch and one *b*-type *Q*-branch transitions for $\text{Na}^{35}\text{Cl}-\text{H}_2\text{O}$ and 9 *a*-type, one *b*-type *R*-branch and one *b*-type *Q*-branch transitions for $\text{Na}^{37}\text{Cl}-\text{H}_2\text{O}$. Therefore, it is concluded that this complex is an asymmetric top molecule. An example of the observed spectra of the $\text{NaCl}-\text{H}_2\text{O}$ complex is shown in Fig. 3.2. The observed spectrum showed a complicated pattern because of the splittings due to the nuclear quadrupole interactions of the Na and Cl atoms. In the present work we could observe only the transitions with $K_a = 0$ and 1.

Transition frequencies observed in the present study were fitted to the following Hamiltonian,

$$H = H_{\text{rot}} + H_{\text{hf}}(\text{Na}) + H_{\text{hf}}(\text{Cl}), \quad (3.1)$$

where the first, second and third terms correspond to the rotation of the molecular frame, the nuclear quadrupole interaction of Na, and the nuclear quadrupole interaction of Cl, respectively. Since $\text{NaCl}-\text{H}_2\text{O}$ is an asymmetric top, the rotational term of the Hamiltonian is expressed as Watson's A-reduced asymmetric

top Hamiltonian [1], that is

$$H_{rot} = AJ_a^2 + BJ_b^2 + CJ_c^2 - \Delta_J J^4 - \Delta_{JK} J^2 J_a^2 - \Delta_K J_a^4 - 2\delta_J J^2 (J_b^2 - J_c^2) - \delta_K [J_a^2 (J_b^2 - J_c^2) - (J_b^2 - J_c^2) J_a^2]. \quad (3.2)$$

Because only the transitions with $K_a = 0$ and 1 were observed, the centrifugal distortion constants of Δ_K , δ_J , and δ_K could not be determined, and these constants were fixed to zero. The nuclear quadrupole interaction term of both atoms is expressed as follows.

$$H_{hfs} = \mathbf{Q}^{(2)} \cdot \mathbf{V}^{(2)}, \quad (3.3)$$

where \mathbf{Q} and \mathbf{V} are the nuclear quadrupole moment tensor and the electric field gradient tensor, respectively, for a nucleus. We used the coupling scheme, $\mathbf{I}_{Na} + \mathbf{I}_{Cl} = \mathbf{I}$ and then $\mathbf{J} + \mathbf{I} = \mathbf{F}$, by the same reason discussed in the Rg-NaCl complex. Although the matrix elements of the hyperfine interaction terms have nonvanishing terms with $\Delta K_a = 0, 1,$ and 2 (see Chapter 2, Appendix I), we assumed that the term with $\Delta K_a = 1$ is so small that they can be neglected. Therefore, the Wang transformation was used to simplify the diagonalization of the Hamiltonian matrix. As each I component is mixed well with the elements with $\Delta I = \pm 2$ in the diagonalization process like the Rg-NaCl complexes, it is impossible to assign the original wavefunctions after the diagonalization. Thus, an index, n , was used in the analysis of the Rg-NaCl complexes to discriminate different levels with same F , and the same method was used for the present case. To avoid the interference effect (see Chapter 2, Appendix II), only the lines that didn't overlap with each other were given non-zero weights in the least-squares fitting procedure. The transition frequencies used in the least-squares fitting are listed with the calculated frequencies in Appendix I. We determined the molecular constants of the NaCl-H₂O precisely as shown in Table 3.1. Standard deviations of the fittings were about 6 and 7 kHz for Na³⁶Cl-H₂O and Na³⁷Cl-H₂O, respectively, both of which are well within the experimental accuracy. Although we tried to observe the splittings

due to the internal rotation of H_2O in the complex, they were not observed in the present work. The determined molecular constants including the nuclear quadrupole coupling constants are in good agreement with those of our *ab initio* calculation (MP2/6-311G(2d,p) method) using GAUSSIAN94 [2].

Furthermore, we searched for the transitions of deuterated species based on a prediction using the result of $\text{Na}^{35}\text{Cl}-\text{H}_2\text{O}$ and $\text{Na}^{37}\text{Cl}-\text{H}_2\text{O}$ together with the *ab initio* calculation [3]. We were able to observe 6 *a*-type and 2 *b*-type *R*-branch transitions for two deuterated species, $\text{Na}^{35}\text{Cl}-\text{DHO}$ and $\text{Na}^{36}\text{Cl}-\text{HDO}$, respectively. (Here the H atom closer to the Cl atom is written first in the chemical formula.) This result confirmed us that the observed transitions are due to $\text{NaCl}-\text{H}_2\text{O}$. But no transition of $\text{Na}^{36}\text{Cl}-\text{D}_2\text{O}$ was observed in the present work. Although the observed spectra will be split by the nuclear quadrupole interactions of the Na, Cl, and D atoms, these spectra were so weak that we couldn't perform the least-squares fitting including the hyperfine interactions as have been done for the $\text{Na}^{35}\text{Cl}-\text{H}_2\text{O}$ complex. The patterns of the observed hyperfine splittings for these deuterated species are similar to those of $\text{Na}^{36}\text{Cl}-\text{H}_2\text{O}$. Therefore, it is understood that the nuclear quadrupole coupling constants of the D atom in the HDO are so small ($\chi_{aa} = 276.45$ kHz, $\chi_{bb} - \chi_{cc} = 54.80$ kHz for HDO molecule) [4] that we could not resolve the hyperfine splittings due to the D atom. We tried to obtain hyperfine-free frequencies by comparisons of the hyperfine patterns of the transitions of deuterated species with those of $\text{Na}^{36}\text{Cl}-\text{H}_2\text{O}$, and then these hyperfine-free frequencies are used to a least-squares fit for Watson's A-reduced asymmetric top Hamiltonian, given by Eq. (3.2). The determined hyperfine-free frequencies are listed in Appendix I and the determined molecular constants are shown in Table 3.1. Standard deviations of the fittings are about 10 and 5 kHz for $\text{Na}^{36}\text{Cl}-\text{DHO}$ and $\text{Na}^{36}\text{Cl}-\text{HDO}$, respectively.

3.2.2 the $\text{NaCl}-(\text{H}_2\text{O})_2$ complex

The observed lines of $\text{Na}^{36}\text{Cl}-(\text{H}_2\text{O})_2$ and $\text{Na}^{37}\text{Cl}-(\text{H}_2\text{O})_2$ are shown as open and filled squares in Fig. 3.1, respectively. According to the *ab initio* calculation [3], it was predicted that the most stable structure of $\text{NaCl}-(\text{H}_2\text{O})_2$ is an almost planar asymmetric top molecule with equivalent H_2O molecules for the C_2 symmetry operation along the NaCl axis (i.e. b -axis) as shown in Fig. 1.3 or 1.4. Therefore, for $\text{NaCl}-(\text{H}_2\text{O})_2$, only the b -type transitions are allowed. This fact is in agreement with our experimental results, in which we could observe only 17 b -type R -branch transitions. If $\text{NaCl}-(\text{H}_2\text{O})_2$ has C_2 symmetry with one set of equivalent O atoms and two sets of equivalent H atoms as shown in Fig. 1.3, the total wavefunction in this system must obey Bose-Einstein statistics [5]. The total spin function is written by the product of the spin functions of these atoms. Since we can neglect the spin functions of the O atom because $I = 0$, the total number of symmetric spin functions becomes

$$n_{\text{sym}} = (2I_1 + 1)(2I_2 + 1)(2I_1I_2 + I_1 + I_2 + 1) = 10 \quad (3.4)$$

and that of anti-symmetric spin functions becomes

$$n_{\text{antisym}} = (2I_1 + 1)(2I_2 + 1)(2I_1I_2 + I_1 + I_2) = 6 \quad (3.5)$$

where I_1 and I_2 represent the nuclear spins of the two different types of nuclei. As the symmetry axis is along the b -axis, the rotational wavefunction can be classified into two; levels with $K_a K_c = ee, oo$ are symmetric and those with eo, oe anti-symmetric. Therefore the intensity ratio of the transitions of the symmetric states and those of the anti-symmetric states is 10 : 6. Although we could not determine accurate intensity ratios because of the complicated hyperfine splittings, transitions between symmetric states were in general observed stronger than those between anti-symmetric states. We could thus confirm that the $\text{NaCl}-(\text{H}_2\text{O})_2$ complex has two sets of equivalent H atoms.

An example of the observed spectra is shown in Fig. 3.3. The observed transitions were fitted to the Hamiltonian given in Eq. (3.1). We used the same method as discussed previously, where non-zero weights were given for only the transitions without the interference effect in the least-squares fitting procedure. The transition frequencies used in the fitting procedure are listed in Appendix I. The determined molecular constants are shown in Table 3.2. Standard deviations of the fittings were about 6 kHz for both $\text{Na}^{36}\text{Cl}-(\text{H}_2\text{O})_2$ and $\text{Na}^{37}\text{Cl}-(\text{H}_2\text{O})_2$. The determined molecular constants are in good agreement with those of our *ab initio* calculation (MP2/6-311G(2d,p) method) using GAUSSIAN94 [2].

We did not try to observe transitions of the deuterated species for $\text{NaCl}-(\text{H}_2\text{O})_2$ in the present work.

3.2.3 the $\text{NaCl}-(\text{H}_2\text{O})_3$ complex

The observed lines of $\text{Na}^{36}\text{Cl}-(\text{H}_2\text{O})_3$ and $\text{Na}^{37}\text{Cl}-(\text{H}_2\text{O})_3$ are shown as open and filled triangles in Fig. 3.1, respectively. The patterns of the observed spectra clearly show that this species is a symmetric top.

The observed transitions were fitted to the Hamiltonian given in Eq. (3.1). As the molecule is a symmetric top, the rotational term is expressed by the following equation,

$$H_{\text{rot}} = BJ^2 + A_1 J_{\perp}^2 - D_J J^4 - D_{JK} J^2 J_{\perp}^2 - D_K J_{\perp}^4 \quad (3.6)$$

where A_1 is $(A - B)$ for prolate symmetric top and is $(C - B)$ the oblate symmetric top molecules and J_{\perp} is the projection of J along the symmetry axis. As the selection rule of a symmetric top is $\Delta K = 0$ for pure rotational transitions, it is impossible to determine the constants, A and D_K in the least-squares fitting procedure and, therefore, these constants were fixed. We used the same method discussed above, where non-zero weights were given for only the transitions without the interference effect in the least-squares fitting. The transition frequencies used

in the fitting are listed in Appendix I. The determined molecular constants are shown in Table 3.3. Standard deviations of the fit were about 7 and 4 kHz for $\text{Na}^{36}\text{Cl}-(\text{H}_2\text{O})_3$ and $\text{Na}^{37}\text{Cl}-(\text{H}_2\text{O})_3$, respectively, both of which are well within the experimental accuracy.

The fact that the observed species is a symmetric top is in agreement with the result of an *ab initio* calculation for $\text{NaCl}-(\text{H}_2\text{O})_3$ [6]. However, according to the *ab initio* calculation, the most stable structure of the $\text{NaCl}-(\text{H}_2\text{O})_4$ is also a symmetric top molecule with four equivalent H_2O molecules with a C_4 symmetry axis, as shown in Fig. 1.4. Therefore, we performed *ab initio* calculations for $\text{NaCl}-(\text{H}_2\text{O})_3$ and $\text{NaCl}-(\text{H}_2\text{O})_4$ using GAUSSIAN 94 [6]. The rotational constants calculated with the MP2/6-311G(2d,p) method are 1839 MHz and 1469 MHz for the $\text{NaCl}-(\text{H}_2\text{O})_3$ and the $\text{NaCl}-(\text{H}_2\text{O})_4$, respectively. As the observed rotational constant, 1878 MHz, is in good agreement with the former, the observed transitions are assigned as those of $\text{NaCl}-(\text{H}_2\text{O})_3$.

An example of the observed spectra is shown in Fig. 3.4(a). The observed spectrum shows a very complicated pattern due to the hyperfine splittings of the Na and Cl atoms together with the overlap of different K -components. As we can not obtain the information on the ratio of the populations between different K -components experimentally, it is very difficult to reproduce the observed spectrum accurately. Because this complex is predicted to be almost spherical (*cf.* $A = 1858$ MHz, $B = 1839$ MHz) from our *ab initio* calculation, we supposed that the difference of the population between different K -components is so small that we can neglect the effect to reproduce the observed spectrum using Eq. (2.A2.1). A simulated spectrum obtained by Fourier-transforming Eq. (2.A2.1) is shown in Fig. 3.4(b). It is seen that the simulated spectrum well reproduces the observed spectrum.

We did not try to observe transitions of the deuterated species of $\text{NaCl}-(\text{H}_2\text{O})_3$ in the present work.

§ 3.3 Discussion

3.3.1 Structures of the $\text{NaCl}-(\text{H}_2\text{O})_n$ ($n = 1, 2, 3$) complexes

From a comparison between the observed rotational constants and the calculated rotational constants of the *ab initio* calculation [3], the structure of $\text{NaCl}-\text{H}_2\text{O}$ has been confirmed to have a ring ($\text{Na}-\text{Cl}-\text{H}-\text{O}$ ring) structure. We calculated the inertia defects Δ ($= I_c - I_a - I_b$) from the determined rotational constants of the isotopomers of the $\text{NaCl}-\text{H}_2\text{O}$ complex, as shown in Table 3.1. All of the inertia defects have small positive values. In general, in addition to the negative contribution due to non-planarity, the inertia defects is contributed by the vibrational Δ_{vib} , centrifugal distortion Δ_{cent} , and electron-rotation Δ_{elec} interaction terms. Thus,

$$\Delta = -2 \sum_i m_i c_i^2 + \Delta_{\text{vib}} + \Delta_{\text{cent}} + \Delta_{\text{elec}}, \quad (3.7)$$

where contribution of Δ_{cent} is usually so small as to be neglected. Contribution of Δ_{elec} to Δ is also negligible because this molecule does not have out-of-plane electrons with low excitation energies such as delocalized π -electrons. The non-planarity term is always negative, while Δ_{vib} has a small positive value when contributions of in-plane vibrations are larger than those of out-of-plane vibrations. Herschbach and Laurie [7] discussed the contribution of the vibration motions to Δ_{vib} , and introduced a following approximation for Δ_{vib} .

$$\Delta_{\text{vib}} \approx \frac{4K}{\omega}, \quad (3.8)$$

where ω is the vibrational frequency of the lowest in-plane motion and $K = 16.863 \text{ amu}^{\text{Å}} \text{ cm}^{-1}$. We have calculated the vibrational frequencies of the $\text{NaCl}-\text{H}_2\text{O}$ complex using the MP2/6-311G(2d,p) method and obtained a result that the lowest vibrational frequency of the in-plane motion is about 163 cm^{-1} . The magnitude of Δ_{vib} is thus estimated to be about $0.4138 \text{ amu}^{\text{Å}} \text{ cm}^{-1}$. This result is in good agreement

with the observed inertia defects. Therefore, we concluded that the $\text{NaCl}-\text{H}_2\text{O}$ complex is a planar or slightly non-planar molecule.

Since the rotational constants of various isotopic species are precisely determined, the r_e -coordinates of the Cl and two H atoms in the molecule-fixed axis system are estimated by using of Kraitchman's equation [1], as listed in Table 3.4. Although the $|z|$ coordinate of the Cl atom is fixed at zero in the calculation, this assumption is reasonable because the observed inertia defects are small. The $|z|$ coordinate of one H atom, which consists a four membered ring, is nearly zero, but that of the other H atom, which is not bonded, is about $0.199(18) \text{ \AA}$. The non-planarity of this H atom is in agreement with the result of the *ab initio* calculations. When the hydrogen atom is substituted by deuterium, it is known that the vibrational effect is not cancelled out perfectly in Kraitchman's equation as a result of large amplitude motions involving hydrogen, producing large isotope effect of the H atom [8]. This means that we cannot neglect a possibility of the planar structure for this complex. Therefore, we may consider two types of structures; (I) a planar molecule and (II) a non-planar molecule that the H atom outside of the ring locates at an out-of-plane position.

We performed a least-squares fitting for the rotational constants of four isotopic species and determined the r_0 -structures of the $\text{NaCl}-\text{H}_2\text{O}$ complex for two types of the structures. The structural parameters of the determined structures are listed in Table 3.5. In type (II) the out-of-plane H atom was rotated by 23° around the axis that connects between the O and in-plane H atoms according to the *ab initio* calculation [3] and was fixed in the fitting procedure. The structural parameters of both (I) and (II) configurations are nearly identical and in fair agreement with that of the *ab initio* calculation within two standard deviations, as shown in Table 3.5. From a comparison between the parameters of the complex and of the monomer, it is seen that the $r(\text{NaCl})$ is increased by $0.06(3) \text{ \AA}$, which is

definitely larger than one standard deviation of the fit. This tendency is in agreement with the result of Woon and Dunning, Jr. We showed the determined structure (I) of this complex in Fig. 3.5, in which circles around the atoms represents the ion radii for NaCl and the vdW radii for H_2O . We can see that there is a large overlap of electron clouds between the Cl and H atoms. Therefore, it is expected that the binding energy is fairly large for the complex, which is consistent with the fact that no splittings due to the internal rotation of H_2O were observed.

In $\text{NaCl}-(\text{H}_2\text{O})_2$, the fact that this complex has C_2 symmetry suggests that all heavy atoms in the complex lie in a plane. But, as shown in Table 3.2, the values of inertia defects imply that this structure is slightly non-planar. Therefore, although it cannot be excluded that non-bonded hydrogen atoms lie slightly out-of-plane, we assumed that this complex is planar because the $|e|$ coordinates of four hydrogen atoms cannot be determined precisely from the determined rotational constants in the present work. Therefore, only seven parameters should be optimized to determine the structure of $\text{NaCl}-(\text{H}_2\text{O})_2$. Now, however, the only three independent rotational constants were obtained because of the planarity and the existence of the Cl atom on the b axis. According to the result of *ab initio* calculations as shown in Table 3.5, only three parameters, $r(\text{NaCl})$, $r(\text{ONa})$, and $\angle \text{ONaCl}$, change significantly with the increase of the number of water. Although it was expected to determine these three parameters as variables among the structural parameters and fix other parameters at the values determined for type (I) of $\text{NaCl}-\text{H}_2\text{O}$, $r(\text{ONa})$ and $\angle \text{ONaCl}$ were not determined simultaneously from the determined rotational constants. Therefore, the two parameters, $r(\text{NaCl})$ and $\angle \text{ONaCl}$, were optimized as variables of the molecular structure of $\text{NaCl}-(\text{H}_2\text{O})_2$, where the other parameters were fixed at the values determined for type (I) of $\text{NaCl}-\text{H}_2\text{O}$. The determined parameters are 2.602 Å and 76.6° for $r(\text{NaCl})$ and $\angle \text{ONaCl}$, respectively. This r_0 -structure was determined by using the three

rotational constants obtained from the two isotope species as shown in Fig. 3.6. From a comparison with the structure of the $\text{NaCl}-\text{H}_2\text{O}$ complex, it is seen that these two structural parameters, $r(\text{NaCl})$ and $\angle\text{ONaCl}$, dramatically change their values. The bond length, $r(\text{NaCl})$, increased from 2.42(3) Å to 2.60(1) Å. This result is in agreement with the *ab initio* calculation [3]. The angle, $\angle\text{ONaCl}$, decreased from 81.1° to 76.6°. When the determined structure is drawn as shown in Fig. 3.6, the overlap between ion radii of Na and Cl becomes nearly zero, and the overlap between the Cl atom and the H_2O molecule is larger than that of $\text{NaCl}-\text{H}_2\text{O}$. In order to check feasibility of the structure determined, we calculated the structure when $r(\text{ONa})$ was changed slightly. Based on a small change of $r(\text{ONa})$ in the *ab initio* calculation, change of the two optimized parameters was examined when $r(\text{ONa})$ was changed by +0.01 Å. The change of $r(\text{ONa})$ by +0.01 Å yielded the parameters 2.619 Å and 75.6° for $r(\text{NaCl})$ and $\angle\text{ONaCl}$, respectively. Thus, possible regions of parameters, $r(\text{NaCl})$ and $\angle\text{ONaCl}$, could be set as 2.60 – 2.62 Å and 76.6 – 75.6°, respectively.

For $\text{NaCl}-(\text{H}_2\text{O})_3$, we observed spectra of only two isotopic species. Since the complex is a symmetric top, there are only two independent rotational constants. Although it was confirmed that only two parameters, $r(\text{NaCl})$ and $\angle\text{ONaCl}$, may change significantly like the case of the $\text{NaCl}-(\text{H}_2\text{O})_2$ complex, it is still not possible to determine these two parameters simultaneously because only the species with substituted atoms lying on the symmetric top axis were observed in the present work. According to our *ab initio* calculation shown in Table 3.5, $\angle\text{ONaCl}$ decrease monotonically with the increase of the number of water. Therefore, we assume the angle $\angle\text{ONaCl}$ of this complex to be 72.0°, which is smaller by the same amount of angle from $\text{NaCl}-\text{H}_2\text{O}$ to $\text{NaCl}-(\text{H}_2\text{O})_2$, and the other parameters fixed at the values for $\text{NaCl}-\text{H}_2\text{O}$. Under this assumption, $r(\text{NaCl})$ was determined to be 2.8350(3) Å. The difference of $r(\text{NaCl})$ from $\text{NaCl}-(\text{H}_2\text{O})_2$ to $\text{NaCl}-(\text{H}_2\text{O})_3$, which is about 0.233 Å,

is in agreement with that of our *ab initio* calculation shown in Table 3.5. A part of the structure is given in Fig. 3.7. In Fig. 3.7 we can see that $r(\text{NaCl})$ is now large enough that charge clouds of Na and Cl do not overlap with each other. As the angle $\angle\text{OHCl}$ is nearly equal to 180° , it is expected that relatively strong bonds between OH-Cl are produced. Based on the results of our *ab initio* calculation, we examined the change of the optimized parameter $r(\text{NaCl})$ when $r(\text{ONa})$ was changed about $+0.03 \text{ \AA}$ and/or when $\angle\text{ONaCl}$ was changed about -4.3° from that of $\text{NaCl}-(\text{H}_2\text{O})_2$. By the changes of these parameters, a possible $r(\text{NaCl})$ region was estimated to be $2.80 \sim 2.84 \text{ \AA}$.

3.3.2 Intermolecular Interaction in the $\text{NaCl}-(\text{H}_2\text{O})_n$ ($n = 1, 2, 3$) complexes

We consider in detail how the nuclear quadrupole coupling constants of the $\text{Na}^{35}\text{Cl}-\text{H}_2\text{O}$ complex change by the complex formation. The determined nuclear quadrupole coupling constants for the Na and Cl atoms are remarkably different from those of the monomer. In the weak coupling limit that the electric field gradients at the Na and Cl nuclei are not perturbed by the complex formation, the observed coupling constants are obtained by rotating the free NaCl coupling constants χ_0 to the principal axes of the complex and averaging over the ground vibrational state. So far, this effect of the complex formation on the coupling constants has been reported for various systems, and are related to the following equation [9],

$$\begin{pmatrix} \chi_{aa}^0 & \chi_{ab}^0 & \chi_{ac}^0 \\ \chi_{ba}^0 & \chi_{bb}^0 & \chi_{bc}^0 \\ \chi_{ca}^0 & \chi_{cb}^0 & \chi_{cc}^0 \end{pmatrix} = \chi_0 \begin{pmatrix} \left\langle 1 - \frac{1}{2} \cos^2 \alpha \right\rangle & \left\langle -\frac{3}{2} \cos \alpha \sin \alpha \right\rangle & 0 \\ \left\langle -\frac{3}{2} \cos \alpha \sin \alpha \right\rangle & \left\langle \frac{3}{2} \cos^2 \alpha - \frac{1}{2} \right\rangle & 0 \\ 0 & 0 & -\frac{1}{2} \end{pmatrix}, \quad (3.9)$$

where α is the angle between the b -axis of the complex and NaCl axis. Since angle

α is determined to be 55.5° from the determined structure of the $\text{NaCl}-\text{H}_2\text{O}$ complex, the zero-order quadrupole coupling constants χ_{xy}^0 ($x, y = a, b, c$) are derived as shown in Table 3.6. Regardless of the fact that χ_{cc} does not depend on the vibrational average, the experimental value is different from the calculated χ_{cc}^0 for both Na and Cl. This result suggests that the electric field gradients of both Na and Cl atoms are perturbed by the complex formation. In the case of $\text{Rg}-\text{NaCl}$, it has been seen that perturbation due to the induced effect plays an important role only for the electric field gradient of the Na atom in Chapter 2. In general, there can be following five effects [10] which can perturb the electric field gradients of the Na and Cl atoms, i.e.,

- (I) gradients induced by the multipole moments of H_2O ,
- (II) gradients induced by the induced dipole moment of H_2O arising from NaCl ,
- (III) polarization of the Na and Cl atoms by the electric field arising from H_2O ,
- (IV) overlap of the electron distributions of NaCl and H_2O ,
- (V) charge transfer between NaCl and H_2O .

At first, the magnitude of the effect (I) is estimated using a simple electrostatic model (see Appendix II) as the first-order correction term, because we can predict empirically that this effect is the most dominant among the five effects. The coordinate system as shown in Fig. 3.8 is used and only the dipole moment μ is used as the contributing term of the multipole moments of the H_2O molecule in the present analysis. In this coordinate system the electric field gradients due to μ along the a - and b -axes at any point (r, θ) , which are symbolised by q_{aa} and q_{bb} , respectively, can be written as follows,

$$q_{aa} = -\frac{3\mu}{r^4} [\cos\theta \{3\sin^2(\theta - \alpha) - 1\} + \sin\theta \sin 2(\theta - \alpha)], \quad (3.10)$$

and

$$q_{bb} = -\frac{3\mu}{r^4} [\cos\theta \{3\cos^2(\theta - \alpha) - 1\} - \sin\theta \sin 2(\theta - \alpha)]. \quad (3.11)$$

Similarly, q_{aa} and q_{bb} due to a charge C at any point (r, θ) in the coordinate system shown in Fig. 3.8 is written as follows,

$$q_{aa} = \frac{C}{r^3} (3\cos^2\theta - 2), \quad (3.12)$$

and

$$q_{bb} = -\frac{C}{r^3} (3\cos^2\theta - 1). \quad (3.13)$$

The dipole moment of H₂O in the complex is assumed to lie at the center of mass along the direction of the O atom and its magnitude is the same as the monomer. The angle α was then estimated to be 19.3° from the determined structure of NaCl-H₂O. Using Eqs. (3.10) and (3.11), the first-order corrections of the electric field gradients due to the dipole moment ($\mu = 1.8546$ D) of H₂O at Na ($r = 2.3123$ Å, $\theta = 224.1^\circ$) and Cl ($r = 3.0388$ Å, $\theta = 275.6^\circ$) are estimated as follows.

$$\text{Na: } q_{aa}^1 = +7.734 \times 10^{-3} e/\text{Å}^3, q_{bb}^1 = +2.136 \times 10^{-2} e/\text{Å}^3,$$

$$\text{Cl: } q_{aa}^1 = +3.793 \times 10^{-3} e/\text{Å}^3, q_{bb}^1 = -5.119 \times 10^{-3} e/\text{Å}^3,$$

where the superscripts represent the first-order correction term of the electric field gradients. Using Eqs. (3.12) and (3.13), the zero-order electric field gradients at Na ($r = 2.4148$ Å, $\theta = -55.5^\circ$) arising from the charge of Cl ($C = -0.750e$) and at Cl ($r = 2.4148$ Å, $\theta = 124.5^\circ$) arising from the charge of Na ($C = +0.750e$), respectively, were estimated as follows.

$$\text{Na: } q_{aa}^0 = +5.522 \times 10^{-2} e/\text{Å}^3, q_{bb}^0 = -1.999 \times 10^{-3} e/\text{Å}^3,$$

$$\text{Cl: } q_{aa}^0 = -5.522 \times 10^{-2} e/\text{Å}^3, q_{bb}^0 = +1.999 \times 10^{-3} e/\text{Å}^3.$$

If we assume that the first-order coupling constants are,

$$\chi_{aa}^1 = \chi_{aa}^0 \frac{q_{aa}^0 + q_{aa}^1}{q_{aa}^0}, \quad (3.14)$$

and so on, the corrected nuclear quadrupole coupling constants to the first order are obtained as shown in Table 3.6. Although the determined coupling constants of Na are rather in good agreement with the observed constants, the calculated coupling

constants of Cl are fairly far from the observed constants. Therefore we must consider the induction effect as discussed in Ar-NaCl. That is, the influence of the induced dipole moment of H₂O on the coupling constants of Na and Cl must be considered as the second-order correction. The induced dipole moment arising from the charges of each Na and Cl is estimated to be about 1.01 D ($\alpha = 6.9^\circ$) using the electrostatic model as discussed above. Using Eqs. (3.10) and (3.11), the second-order corrections of the electric field gradients due to the induced dipole moment ($\mu = 1.0113$ D) of H₂O at Na ($r = 2.3123 \text{ \AA}$, $\theta = 214.0^\circ$) and Cl ($r = 3.0388 \text{ \AA}$, $\theta = 263.7^\circ$) are estimated to be,

$$\begin{aligned} \text{Na: } q_{aa}^2 &= +3.107 \times 10^{-3} e/\text{\AA}^3, q_{bb}^2 = +1.521 \times 10^{-2} e/\text{\AA}^3, \\ \text{Cl: } q_{aa}^2 &= +4.722 \times 10^{-3} e/\text{\AA}^3, q_{bb}^2 = -3.959 \times 10^{-3} e/\text{\AA}^3, \end{aligned}$$

If the corrected coupling constants to the second order are written as,

$$\chi_{aa}^2 = \chi_{aa}^0 \frac{q_{aa}^0 + q_{aa}^1 + q_{aa}^2}{q_{aa}^0}, \quad (3.15)$$

and so on, the nuclear quadrupole coupling constants were obtained as shown in Table 3.6. Although the calculated constants $\chi_{aa}^2(\text{Na})$ and $\chi_{bb}^2(\text{Na})$ are still in agreement with the observed within one error, all the coupling constants of the Na atom slightly go away from the observed constants. Although the calculated coupling constants of the Cl atom come closer to the observed constants, the difference between the observed and calculated is still very large. Therefore, we must consider the other effects, (III) - (V). It is seen that there exists large overlap between the van der Waals radius of H and the ion radius of Cl in the NaCl-H₂O complex as seen in Fig. 3.5. Therefore, sizable contribution of the effect (IV) is suggested. Furthermore, it is considered that charge transfer suggested by Woon and Dunning, Jr. also plays an important role in the intermolecular interaction. Since quantitative estimation of these contributions based on a simple model is not possible to explain the discrepancy of the coupling constant for Cl, we performed *ab*

ab initio calculation to obtain eQq values to compare the experimental values at the MP2 level of calculation. It is expected that at MP2 level all the contribution given above may be taken into account. The calculated values are given in Table 3.1, where good agreements are obtained even for those of the Cl atom.

Estimation of the induced effect are performed similarly for both the $\text{NaCl}-(\text{H}_2\text{O})_2$ and $\text{NaCl}-(\text{H}_2\text{O})_3$ complexes. Although the difference between the observed and calculated values is gradually increases, the calculated coupling constants of Na are quantitatively close to the observed ones by considering only effect (I), while the coupling constants of Cl are relatively far from the observed ones by the simple model calculations. On the other hand, *ab initio* values, given in Tables 3.2 and 3.3, show fair agreement with the observed. In Fig. 3.9 we showed the charge distribution of the $\text{NaCl}-(\text{H}_2\text{O})_n$ complexes calculated by the GAMESS [11] MP2/6-311G** method. It is seen that the charge distribution around the Cl atom is perturbed by the weak bond between the in-plane H atom and the Cl atom for all the $\text{NaCl}-(\text{H}_2\text{O})_n$ ($n = 1, 2, 3$) complexes. On the other hand, the overlap between O and Na is so small that it is understood that the coupling constants of Na are little affected by the complex formation in the $\text{NaCl}-\text{H}_2\text{O}$ complex. As the overlap becomes gradually larger with increase of the number of H_2O , it is possible that differences between the observed coupling constants and the calculated coupling constants, in which we considered only the effect (I) becomes gradually larger. It is also seen that the overlap between Na and Cl almost disappears for the $\text{NaCl}-(\text{H}_2\text{O})_3$ complex. This result is in good agreement with the determined structure in Fig. 3.7.

3.3.3 *Microsolvation Process on NaCl*

In general, we can obtain the information on the distortion of the electric field around a nucleus by using a nuclear quadrupole coupling constant. Now we

examine a relation between the nuclear quadrupole coupling constant of the ^{35}Cl atom and the charge distribution around its nucleus [5]. As shown in Table 3.7, if the coupling constant is smaller, the ionic character of the Cl atom in the molecule is larger. For the NaCl molecule, 6 electrons are almost filled in the $3p$ orbitals of the Cl atom, but not entirely so because of slightly covalent character with the NaCl bond in the $3p_\sigma$ orbital. Therefore electric field gradient at Cl has an intermediate value between the two limits of the perfectly covalent bond and the perfectly ionic bond, and

$$q_{\text{Cl}} = -(1-x)q_{310} + (x)0 = -(1-x)q_{310} \quad (3.16)$$

where q_{310} represents the electric field gradient of Cl in the covalent bond limit that only one electron exists in the $3p_\sigma$ orbital, and x represents the fractional importance of the ionic character. Therefore, when an electron in the $3p_\sigma$ orbital of the Cl atom is drawn towards the Na region by a covalence bond character between Na and Cl, the charge distribution around the Cl nucleus is distorted, and therefore the coupling constant of Cl atom increases to have a non-zero value. By a similar consideration, when one electron is drawn towards the Cl region, the coupling constant of Na approaches to zero inversely.

We showed the variations of the nuclear quadrupole coupling constants of the Na, ^{35}Cl , and ^{37}Cl atoms in Fig. 3.10. As the χ_{Na} constant of the $\text{NaCl}-\text{H}_2\text{O}$ complex could not be determined in the present work, we used a χ_{Na} constant by scaling the parameter [12] calculated by the MP2/6-311G(2d,p) method to estimate the coupling constant χ_{Na} along the NaCl axis. In Fig. 3.10(a) are plotted the components of the coupling constants along the direction of the NaCl axis. We can see in Fig. 3.10(a) that the coupling constants increase almost monotonically with the increase of the number of the H_2O molecules. This tendency means that the charge distributions of the Na and Cl atoms gradually change with the number of H_2O from a distribution along the NaCl bond to a distribution perpendicular to the NaCl axis.

This result is supported by looking at the coupling constants perpendicular to the NaCl axis shown in Fig. 3.10(b). For $\text{NaCl}-(\text{H}_2\text{O})_2$ the determined coupling constants suggest that a charge distribution spreads along the a -axis and shrinks along the c -axis. Similarly, since the coupling constants along the axis perpendicular to the NaCl axis are negative for $\text{NaCl}-(\text{H}_2\text{O})_3$, it is expected that a charge distribution spreads along the axis perpendicular to the NaCl axis.

The dependence of the distance $r(\text{NaCl})$ on the number of H_2O is plotted in Fig. 3.11. It is seen that $r(\text{NaCl})$ becomes substantially longer with the number of H_2O . This dependence of $r(\text{NaCl})$ is qualitatively in good agreement with the dependence predicted by *ab initio* calculations. Although we have to note that the determined $r(\text{NaCl})$ of the $\text{NaCl}-(\text{H}_2\text{O})_2$ complex has uncertainty depending on the value assumed for $\angle\text{ONaCl}$, it is still possible to conclude from Fig. 3.11 that $r(\text{NaCl})$ of the $\text{NaCl}-(\text{H}_2\text{O})_3$ complex exceeds the region of $r(\text{NaCl})$ predicted for the contact ion pair state in the simulations of Smith and Dang [13].

References

- [1] W. Gordy and R. L. Cook, *Microwave Molecular Spectra*, Interscience, New York(1970)
- [2] M. J. Frisch, G. W. Trucks, H. B. Schlegel, P. M. W. Gill, B. G. Johnson, M. A. Robb, J. R. Cheeseman, T. Keith, G. A. Petersson, J. A. Montgomery, K. Raghavachari, M. A. Al-Laham, V. G. Zakrzewski, J. V. Ortiz, J. B. Foresman, J. Cioslowski, B. B. Stefanov, A. Nanayakkara, M. Challacombe, C. Y. Peng, P. Y. Ayala, W. Chen, M. W. Wong, J. L. Andres, E. S. Replogle, R. Gomperts, R. L. Martin, D. J. Fox, J. S. Binkley, D. J. Defrees, J. Baker, J. P. Stewart, M. Head-Gordon, C. Gonzalez, and J. A. Pople, Gaussian 94 (Revision D.4), Gaussian, Pittsburgh(1994)
- [3] D. E. Woon and T. H. Dunning, Jr., *J. Am. Chem. Soc.*, **117**, 1090(1995)
- [4] H. A. Fry and S. G. Kukolich, *J. Chem. Phys.*, **76**, 4387(1982)
- [5] C. H. Towns and A. L. Schawlow, *Microwave Spectroscopy*, Dover, New York(1975)
- [6] T. Asada and K. Nishimoto, *Chem. Phys. Letters*, **232**, 518(1995); T. Asada and K. Nishimoto, *Molecular Simulation*, **16**, 307(1996)
- [7] D. R. Herschbach and V. W. Laurie, *J. Chem. Phys.*, **40**, 3142(1964)
- [8] K. R. Leopold, G. T. Fraser, F. J. Lin, D. D. Nelson, Jr., W. Klemperer, *J. Chem. Phys.*, **81**, 4922(1984)
- [9] M. R. Keenan, D. B. Wozniak, and W. H. Flygare, *J. Chem. Phys.*, **75**, 631(1981)
- [10] M. R. Keenan, L. W. Buxton, E. J. Campbell, T. J. Balle, and W. H. Flygare, *J. Chem. Phys.*, **73**, 3523(1980)
- [11] M. W. Schmidt, K. K. Baldridge, J. A. Boatz, S.T.Elbert, M. S. Gordon, J. H. Jensen, S. Koseki, N. Matsunaga, K. A. Nguyen, S. J. Su, T. L. Windus, M. Dupuis, and J. A. Montgomery, *J. Comput. Chem.*, **14**, 1347(1993)
- [12] K. Yamanouchi, S. Kato, K. Morokuma, M. Sugie, H. Takeo, C. Matsumura and K. Kuchitsu, *J. Phys. Chem.*, **91**, 828(1987)

[13] D. E. Smith and L. X. Dang, *J. Chem. Phys.*, 100, 3757(1994)

Table 3.1 The molecular constants of the $\text{NaCl}-\text{H}_2\text{O}$ complexes

	$\text{Na}^{35}\text{Cl}-\text{H}_2\text{O}$	$\text{Na}^{37}\text{Cl}-\text{H}_2\text{O}$	$\text{Na}^{35}\text{Cl}-\text{DHO}^a$	$\text{Na}^{35}\text{Cl}-\text{HDO}^a$	<i>ab initio</i> ^d
A	/ MHz	10270.4349(23) ^b	10004.6641(137)	9761.7543(72)	10123.1251
B	/ MHz	4212.486(14)	4098.7846(19)	4192.0915(101)	4115.0865
C	/ MHz	2983.5819(10)	2924.3614(15)	2943.0927(65)	2925.7562
Δ_J	/ kHz	3.9657(361)	3.6912(514)	3.481(322)	3.903(167)
Δ_K	/ kHz	8.2303(4817)	7.5995(5647)	8.70(217)	6.35(144)
δ_J	/ kHz	1.3850(450)	1.4492(586)	1.342(402)	2.224(209)
$\chi_{aa}(\text{Na})$	/ MHz	-3.3795(208)	-3.4146(91)		-3.2753
$\chi_{bb}(\text{Na})$	/ MHz	-0.4127(331)	-0.3924(199)		-0.5256
$\chi_c(\text{Na})$	/ MHz	3.7922(331)	3.8070(199)		3.8009
$\chi_{aa}(\text{Cl})$	/ MHz	-1.6335(231)	-1.2373(157)		-1.8577
$\chi_{bb}(\text{Cl})$	/ MHz	-2.2981(329)	-1.8147(195)		-1.2963
$\chi_{cc}(\text{Cl})$	/ MHz	3.9316(329)	3.0520(195)		3.1540
A^c	/ $\text{amu}\text{\AA}^2$	0.3074(1)	0.3099(2)	0.4130(73)	0.2349(41)
r.m.s	/ kHz	6.13	7.22	9.85	5.16

^aThe H atom contacted to the Cl atom is written first in the chemical formula.

^bThe figures in parentheses are one standard deviation in units of the last significant figure.

^c $\Delta = I_c - I_a - I_b$.

^dour *ab initio* calculation using the MP2/6-311G(2d,p) method for $\text{Na}^{35}\text{Cl}-\text{H}_2\text{O}$; $\chi_{aa}(\text{Na}) = 0.9548$ MHz, $\chi_{bb}(\text{Cl}) = -1.4836$ MHz

Table 3.2 The molecular constants of the $\text{NaCl}-(\text{H}_2\text{O})_2$ complexes

		$\text{Na}^{35}\text{Cl}-(\text{H}_2\text{O})_2$	$\text{Na}^{37}\text{Cl}-(\text{H}_2\text{O})_2$	<i>ab initio</i> ^d
<i>A</i>	/ MHz	4316.6230(7) ^a	4178.0294(47)	4224.0346
<i>B</i>	/ MHz	2773.4123(19)	2773.4454(138)	2739.6711
<i>C</i>	/ MHz	1698.8422(9)	1676.9485(66)	1661.8258
Δ_J	/ kHz	2.35(11)	1.59(65)	
Δ_{JK}	/ kHz	-4.88(26)	-2.41(210)	
Δ_K	/ kHz	15.38 (16)	15.38 ^b	
δ_J	/ kHz	0.789(48)	0.445(275)	
δ_K	/ kHz	3.44(43)	3.44 ^b	
$\chi_{aa}(\text{Na})$	/ MHz	-4.346(14)	-4.346(23)	-4.5149
$\chi_{bb}(\text{Na})$	/ MHz	-0.247(16)	-0.243(21)	-0.0090
$\chi_{cc}(\text{Na})$	/ MHz	4.592(16)	4.589(21)	4.5239
$\chi_{aa}(\text{Cl})$	/ MHz	-4.704(14)	-3.738(23)	-3.7799
$\chi_{bb}(\text{Cl})$	/ MHz	-0.0971(183)	-0.0236(268)	-0.1859
$\chi_{cc}(\text{Cl})$	/ MHz	4.801(18)	3.762(27)	3.9658
Δ^c	/ $\text{u}\text{\AA}^2$	-1.8158(3)	-1.8135(22)	
r.m.s	/ kHz	5.58	5.80	

^aThe figures in parentheses are one standard deviation in units of the last significant figure.

^bThis value is fixed.

^c $\Delta = I_c - I_a - I_b$

^dour *ab initio* calculation using the MP2/6-311G(2d,p) method for $\text{Na}^{36}\text{Cl}-(\text{H}_2\text{O})_2$

Table 3.3 The molecular constants of the $\text{NaCl}-(\text{H}_2\text{O})_3$ complexes

		$\text{Na}^{36}\text{Cl}-(\text{H}_2\text{O})_3$	$\text{Na}^{37}\text{Cl}-(\text{H}_2\text{O})_3$	<i>ab initio</i> ^d
<i>B</i>	/ MHz	1878.4716(9) ^a	1845.6714(7)	1838.5796
<i>D_J</i>	/ kHz	3.0303(775)	2.8803(374)	
<i>D_{JK}</i>	/ kHz	-4.1478(2450)	-3.9256(1019)	
<i>eQq</i> (Na)	/ MHz	2.6457(123)	2.6510(172)	3.1724
<i>eQq</i> (Cl)	/ MHz	1.5487(244)	1.2727(367)	1.5218
r.m.s	/ kHz	6.59	6.35	

^aThe figures in parentheses are one standard deviation in units of the last significant figure.

^dour *ab initio* calculation using the MP2/6-311G(2d,p) method for $\text{Na}^{36}\text{Cl}-(\text{H}_2\text{O})_3$

Table 3.4 The r_s -coordinates of each atom in the $\text{NaCl}-\text{H}_2\text{O}$ complexes

	$ a $	$ b $	$ c $
Cl	1.308(7) ^a	0.222(7)	0 ^b
H(in-plane)	0.761(22)	1.189(22)	0.070(22)
H(out-of-plane)	2.132(18)	1.676(18)	0.199(18)

^a The figures in parentheses are one standard deviation in units of the last significant figure.

^b This value is fixed at 0.

Table 3.5 The structure parameters of the $\text{NaCl}-(\text{H}_2\text{O})_n$ ($n = 0, 1, 2, 3$) complexes ^f

	NaCl, H ₂ O		NaCl-H ₂ O		NaCl-(H ₂ O) ₂		NaCl-(H ₂ O) ₃	
	exp. ^a	structure I _{b,c}	structure II ^{b,d}	ab initio ^e	exp. ^b	ab initio ^e	exp. ^b	ab initio ^e
$r(\text{NaCl})$ / Å	2.306(1)	2.420(33)	2.410(50)	2.488	2.602(10)	2.603	2.8350(3)	2.806
$r(\text{ONa})$ / Å		2.268(29)	2.282(54)	2.252	2.268	2.265	2.268	2.291
$r(\text{OH}_1)$ ^b / Å	0.9572(3)	0.901(48)	0.900(85)	0.959	0.901	0.950	0.901	0.950
$r(\text{OH}_2)$ ^b / Å	0.9572(3)	1.03(37)	1.33(103)	0.982	1.03	0.981	1.03	0.980
$\angle \text{ONaCl}$ / °		81.1(12)	81.6(20)	79.9	75.6(5)	77.8	72.0	73.5
$\angle \text{NaOH}_1$ / °		80.5(69)	76(12)	82.2	80.5	83.9	80.5	86.5
$\angle \text{H}_1\text{OH}_2$ / °	104.52(5)	104.5 ^f	104.5	107.2	104.5	106.3	104.5	106.9

^a NaCl: P. L. Clouser, and W. Gordy, *Phys. Rev.*, **134**, 864(1964)^b H₂O: W. S. Benedict, N. Gailar, and E. K. Plyler, *J. Chem. Phys.*, **24**, 1139(1956)^c This work.^d The planarity was assumed in the fitting procedure^e The structure with an out-of-plane H atom was assumed in the fitting procedure^f The parameters were calculated at the MP2 level with 6-311G(2d,p) basis sets.^g The figures in parentheses are one standard deviation in units of the last significant figure.^h The value without error is fixed in the fitting procedure.ⁱ H₁ in $r(\text{OH}_1)$ represents the H atom out of the ring^j The H₂ in $r(\text{OH}_2)$ represents the H atom in the ring

Table 3.6 The observed and calculated nuclear quadrupole coupling constants of Na and Cl in the $\text{Na}^{35}\text{Cl}-\text{H}_2\text{O}$ complexes (in MHz)

	obs.	calc.		
		χ^0	χ^1	χ^2
$\chi_{\text{na}}(\text{Na})$	-3.380(21) ^a	-2.941(100)	-3.353(114)	-3.514(119)
$\chi_{\text{ht}}(\text{Na})$	-0.413(33)	0.107(97)	-1.032(936)	-1.842(1670)
$\chi_{\text{cc}}(\text{Na})$	3.792(33)	2.835(3)	4.385(5)	5.356(6)
$\chi_{\text{na}}(\text{Cl})$	-1.634(23)	-2.929(104)	-2.724(97)	-2.478(88)
$\chi_{\text{ht}}(\text{Cl})$	-2.298(33)	0.106(97)	-0.165(151)	-0.375(343)
$\chi_{\text{cc}}(\text{Cl})$	3.932(33)	2.823(3)	2.889(3)	3.119(3)

^a The figures in parentheses are one standard deviation in units of the last significant figure.

Table 3.7 Nuclear quadrupole coupling constants of ^{35}Cl in a few typical molecules

Molecule	eQq
Cl	-109.6 ($-eQq_{310}$)
FCI	-146
ICI	-82.5
CH_3Cl	-74.8
CICN	-83.3
HCl	-68.0
TICl	-15.8
NaCl	-5.6
Cl ⁻ (ionic)	0

Stick Diagram of the observed spectra belonging to laser ablation products

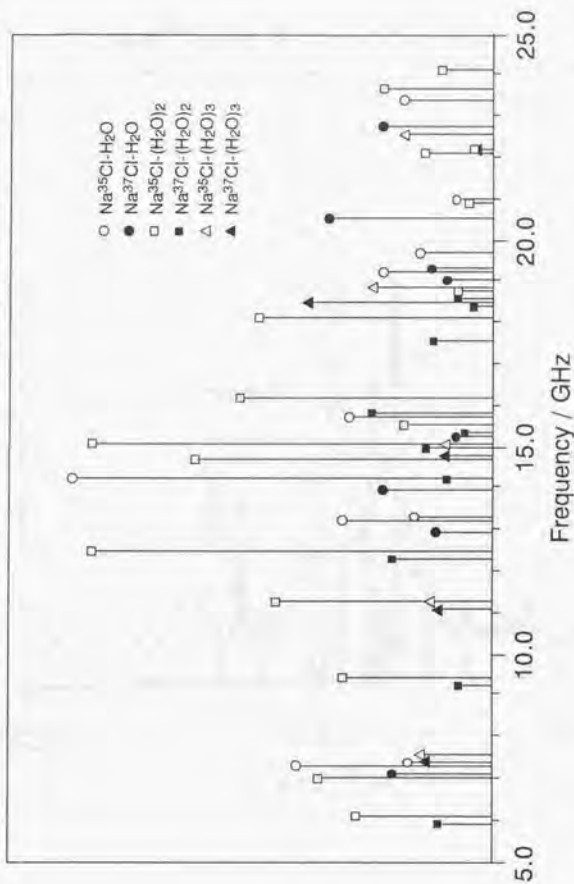


Fig. 3.1 The stick diagram of the observed spectrum of laser ablation products. The circle, square, and triangle symbols represent the transitions of the $\text{NaCl}-\text{H}_2\text{O}$, $\text{NaCl}-(\text{H}_2\text{O})_2$, and $\text{NaCl}-(\text{H}_2\text{O})_3$, respectively. The open and filled mark for each symbol represent the ^{35}Cl and ^{37}Cl isotopic species, respectively.

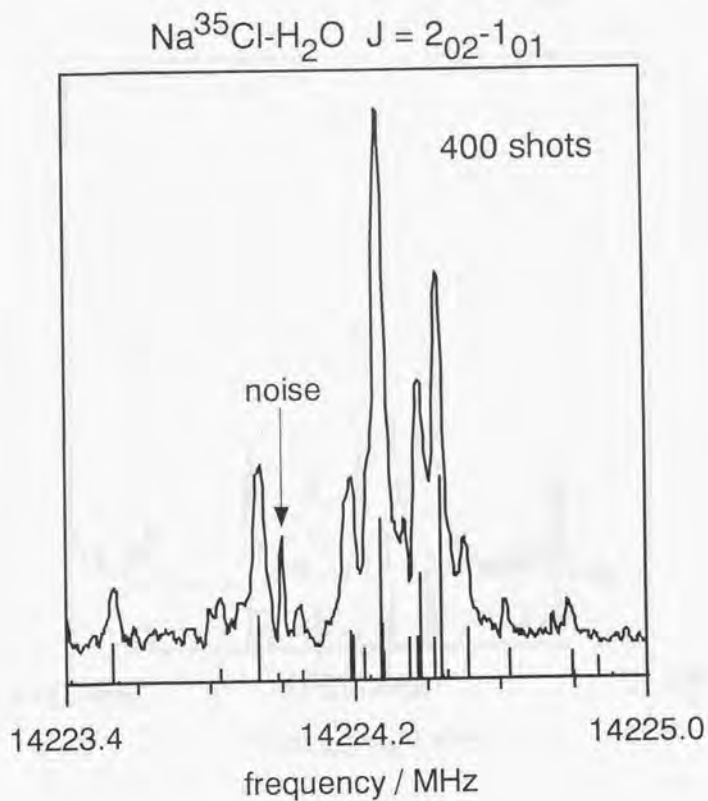


Fig. 3.2 The observed spectrum of $J = 2_{02} - 1_{01}$ of the $\text{Na}^{35}\text{Cl}-\text{H}_2\text{O}$ complex. The sticks represent the hyperfine splitting pattern calculated from the determined molecular constants by the least-squares fitting.

Spectrum of $\text{Na}^{35}\text{Cl}-(\text{H}_2\text{O})_2$ $J = 3_{03} - 2_{12}$

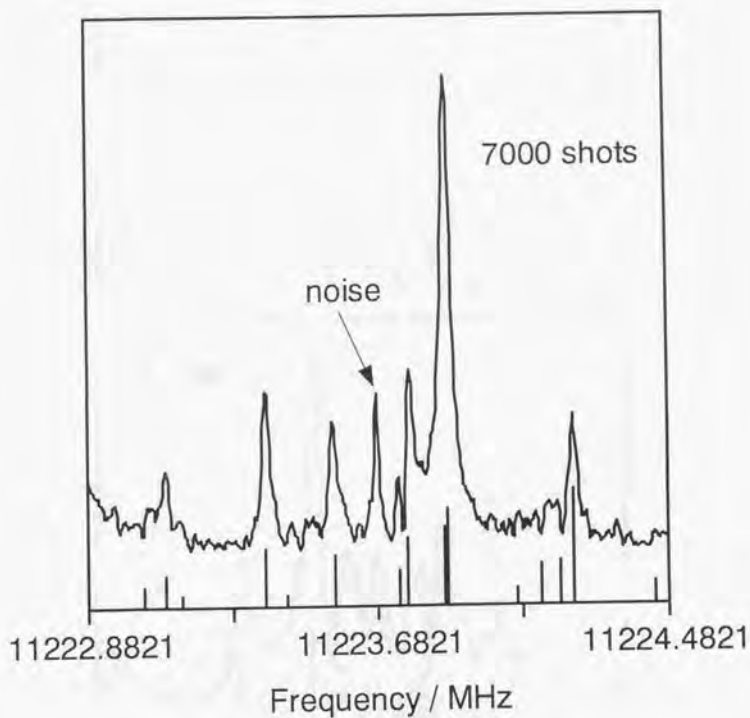


Fig. 3.3 The observed spectrum of $J = 3_{03} - 2_{12}$ of the $\text{Na}^{35}\text{Cl}-(\text{H}_2\text{O})_2$ complex. The sticks represent the calculated frequencies.

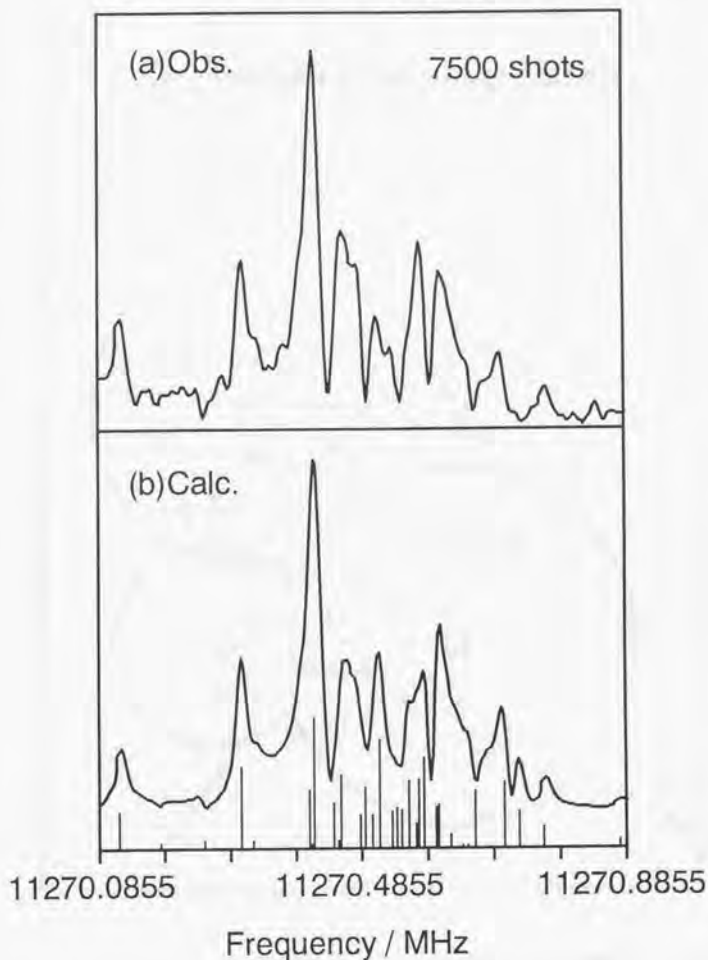
Spectrum of $\text{Na}^{35}\text{Cl}-(\text{H}_2\text{O})_3$ $J = 3 - 2$ 

Fig. 3.4 The observed spectrum of $J = 3 - 2$ of the $\text{Na}^{35}\text{Cl}-(\text{H}_2\text{O})_3$ complex. (a) observed spectrum. (b) calculated spectrum; sticks represent the calculated transition frequencies and its intensity without considering the nuclear spin statistical weight. The simulated spectrum was obtained by Fourier-transforming the synthesized time domain signal by using Eq. (2.A2.1).

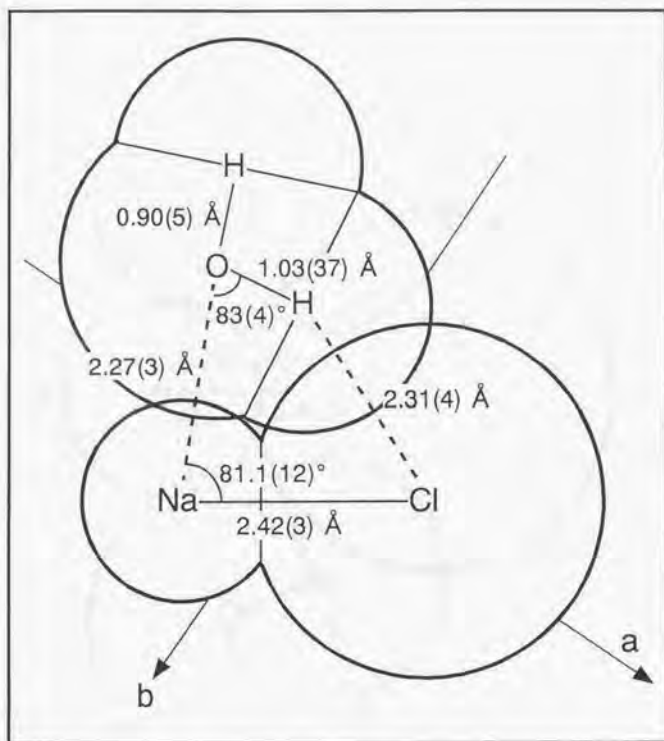
The Structure of the $\text{NaCl}-\text{H}_2\text{O}$ Complex

Fig. 3.5 The structure of the $\text{NaCl}-\text{H}_2\text{O}$ complex (structure I), assuming the planarity. Circles represent the ion radii around the NaCl and the vdW radii of the H_2O molecule.

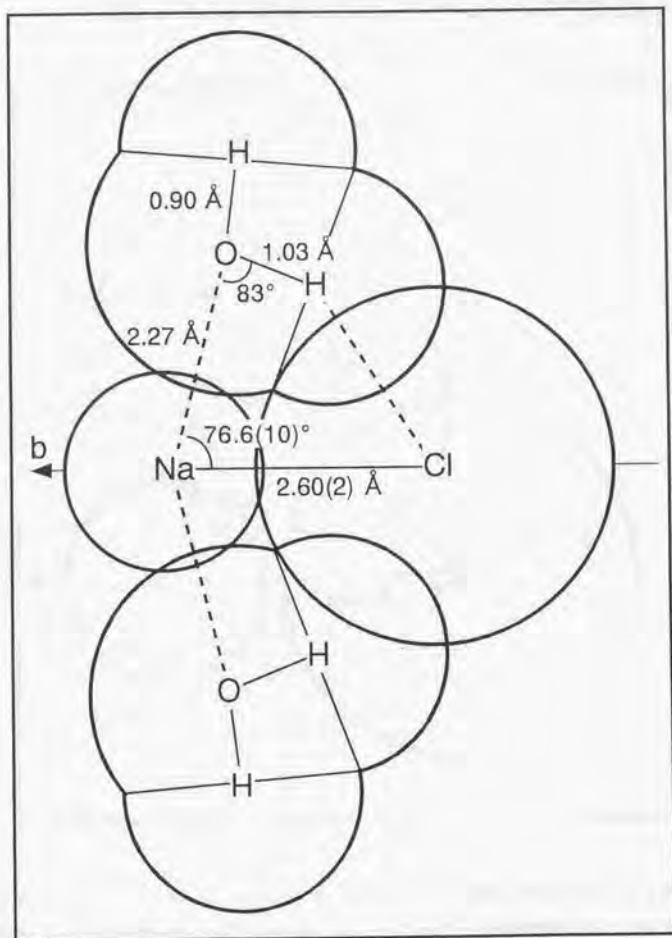
The Structure of the $\text{NaCl}-(\text{H}_2\text{O})_2$ Complex

Fig. 3.6 The structure of the $\text{NaCl}-(\text{H}_2\text{O})_2$ complex. The numbers without errors were fixed at the values of the $\text{NaCl}-\text{H}_2\text{O}$ complex in the fitting procedure.

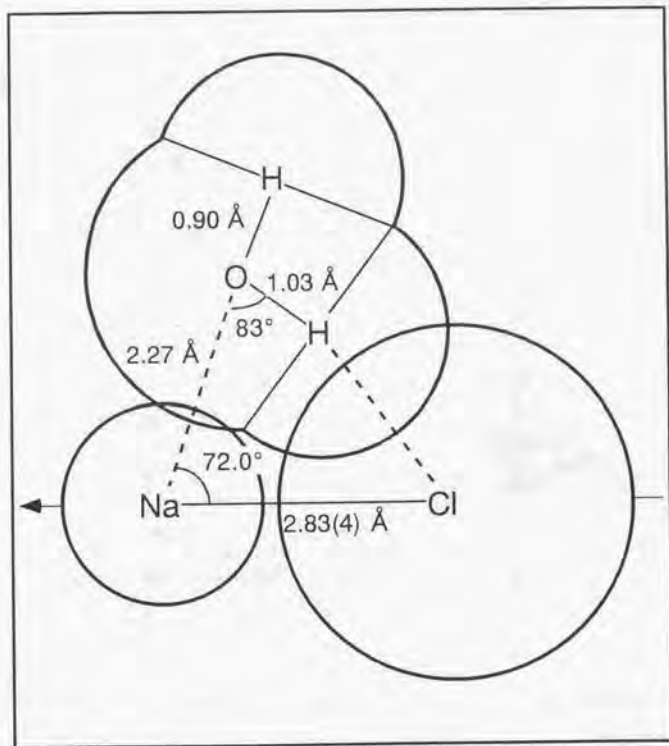
The Structure of the $\text{NaCl}-(\text{H}_2\text{O})_3$ Complex

Fig. 3.7 A part of the structure of the $\text{NaCl}-(\text{H}_2\text{O})_3$ complex. The remaining H_2O molecules attach symmetrically around NaCl . The arrow represents one of the principal axes of the complex. All parameters except for $r(\text{NaCl})$ are fixed in the fitting procedure.

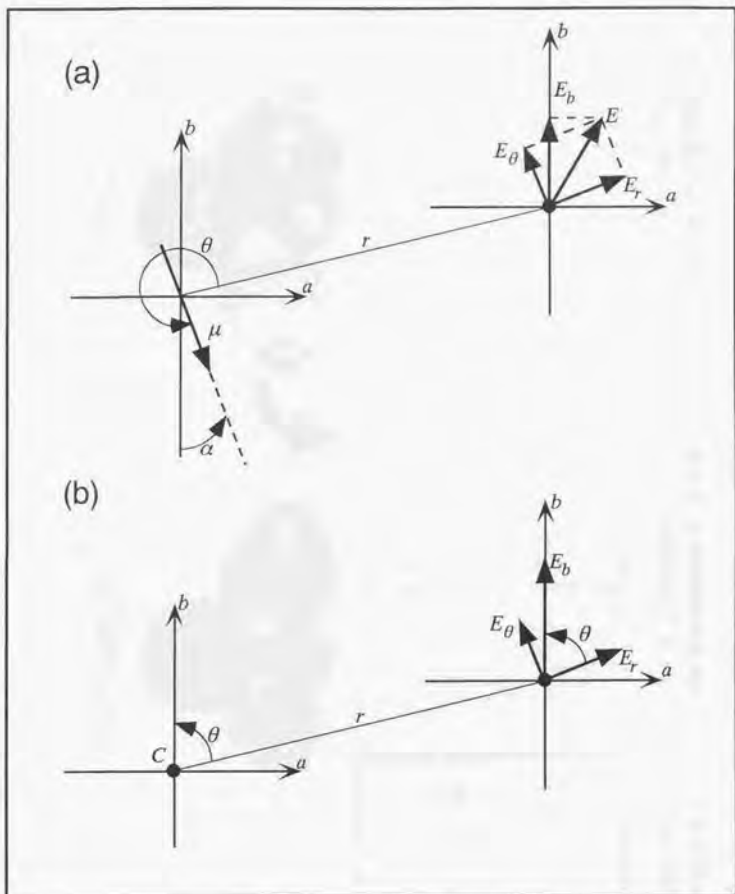


Fig. 3.8 Coordinate systems used in the electrostatic interaction model. The C , μ are the charge, and the dipole moment of the constituent molecule in the complex.

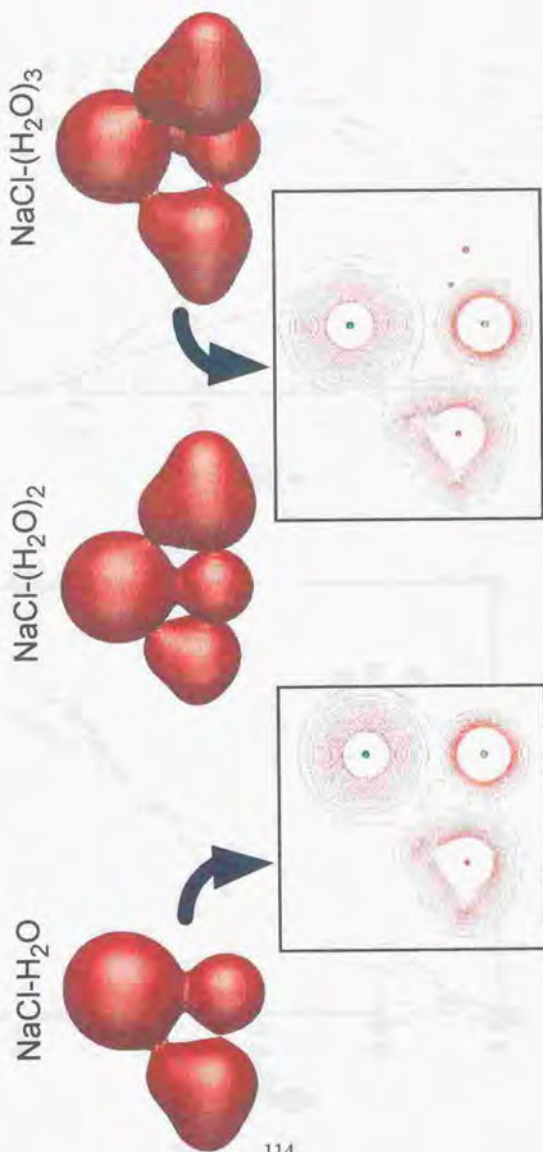
The calculated charge distributions in the $\text{NaCl}-(\text{H}_2\text{O})_n$ complexes

Fig. 3.9 The charge distributions in the $\text{NaCl}-(\text{H}_2\text{O})_n$ ($n = 1, 2, 3$) complexes. These distributions were calculated by GAMESS MP2/6-311G** method. Contour plots represent the electron densities in the planes containing NaCl and one H_2O for $\text{NaCl}-\text{H}_2\text{O}$ and $\text{NaCl}-(\text{H}_2\text{O})_3$, respectively.

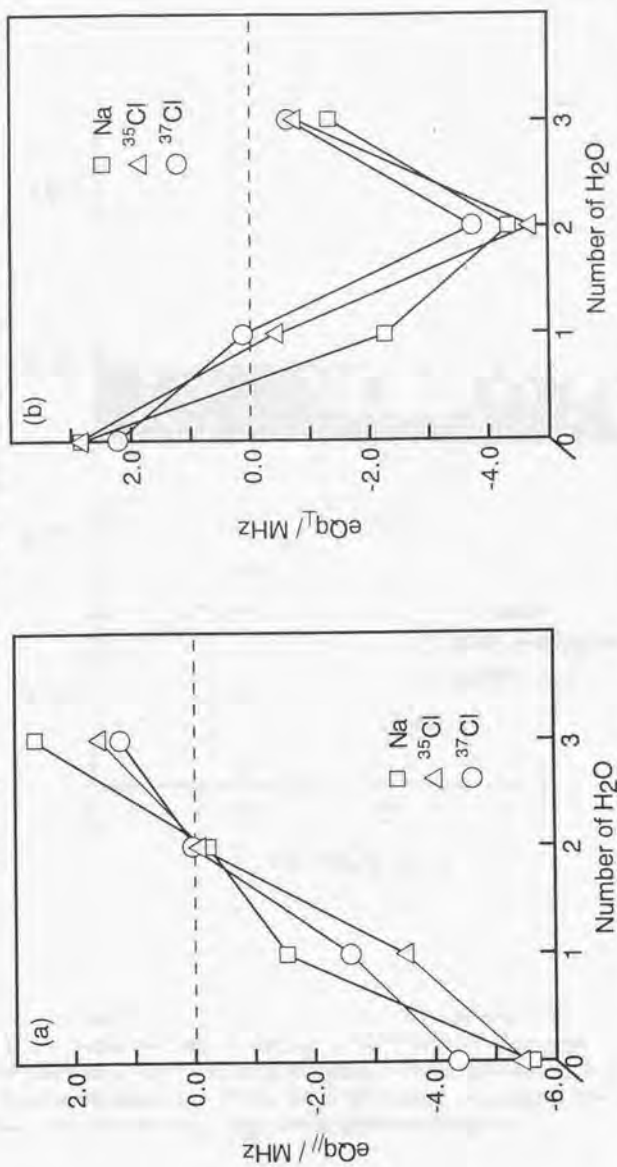
The dependence of eQq on the number of H_2O 

Fig. 3.10 The dependence of the nuclear quadrupole coupling constants on the number of H_2O . The ordinate represents the nuclear quadrupole coupling constant along the NaCl axis of each nucleus for figure (a) and along the axis perpendicular to the NaCl axis and containing H_2O for figure (b). The abscissa represents the coordinate number of H_2O in the $\text{NaCl}-(\text{H}_2\text{O})_n$ complexes. The square, triangle, and circle represent the coupling constants of Na, ^{35}Cl , and ^{37}Cl , respectively.

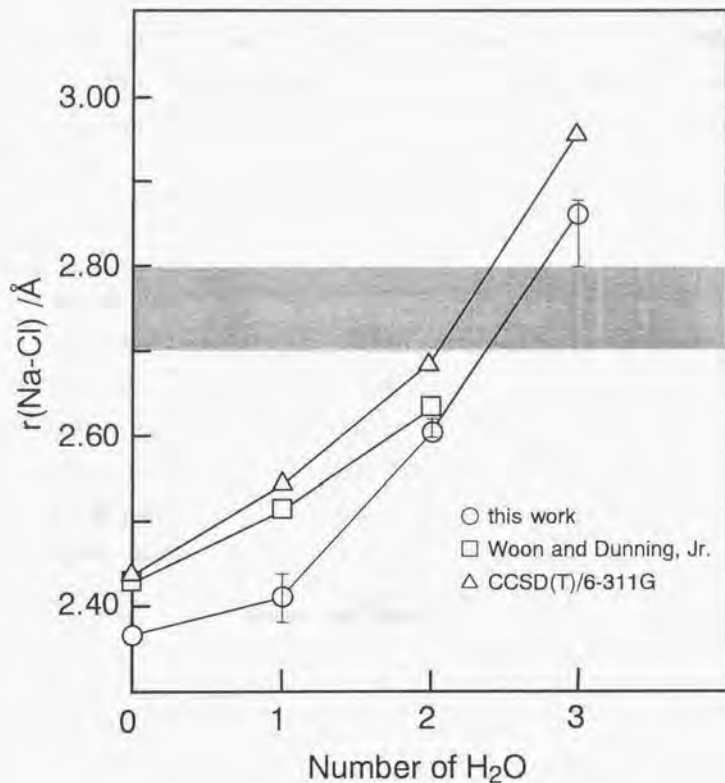
The dependence of $r(\text{NaCl})$ on number of H_2O 

Fig. 3.11 The dependence of the distance $r(\text{NaCl})$ on the number of H_2O . The circle, square, and triangle represent the distance between Na and Cl determined by the microwave experiments (this work), the ab initio calculation of Woon and Dunning, Jr. (Ref. [3]), and our ab initio calculation using CCSD(T)/6-311G method, respectively. The shaded region represents the distance of CIP suggested by Smith and Dang (Ref. [13]).

Appendix I.

The observed and calculated transitions of the $\text{NaCl}-(\text{H}_2\text{O})_n$ complexes

The transitions used in the fitting procedures are listed in the following tables. The transitions affected by the interference effect discussed in Chapter 2 are not listed in the tables. Therefore some lines, especially those for high- J transitions, with relatively strong intensities, which lie close to their center frequencies, are not listed.

$\text{Na}^{35}\text{Cl}-\text{H}_2\text{O}$	Table 3.A1.1
$\text{Na}^{37}\text{Cl}-\text{H}_2\text{O}$	3.A1.2
$\text{Na}^{35}\text{Cl}-\text{DHO}$	3.A1.3
$\text{Na}^{35}\text{Cl}-\text{HDO}$	3.A1.4
$\text{Na}^{35}\text{Cl}-(\text{H}_2\text{O})_2$	3.A1.5
$\text{Na}^{37}\text{Cl}-(\text{H}_2\text{O})_2$	3.A1.6
$\text{Na}^{35}\text{Cl}-(\text{H}_2\text{O})_3$	3.A1.7
$\text{Na}^{37}\text{Cl}-(\text{H}_2\text{O})_3$	3.A1.8

Table 3.A1.1. The observed frequencies of the $\text{Na}^{35}\text{Cl}-\text{H}_2\text{O}$ complex (in MHz)

$J^a_{\text{K}^b_{\text{K}^c}}$	$J^a_{\text{K}^b_{\text{K}^c}}$	$n^d F^e$	$n^d F^e$	obs.	calc.	obs.-calc.	$J^a_{\text{K}^b_{\text{K}^c}}$	$J^a_{\text{K}^b_{\text{K}^c}}$	$n^d F^e$	$n^d F^e$	obs.	calc.	obs.-calc.
1 0 1	0 0 0	3 4	3 3	7196.565	7196.5653	-0.0007	2 1 1	1 1 0	2 4	2 3	15621.512	15621.5112	0.0019
1 0 1	0 0 0	2 3	3 3	7195.522	7195.5241	-0.0020	2 1 1	1 1 0	2 3	3 3	15620.468	15620.4649	0.0028
1 0 1	0 0 0	3 2	3 3	7197.269	7197.2716	-0.0030	2 1 1	1 1 0	2 3	2 3	15621.620	15621.6238	-0.0035
1 0 1	0 0 0	3 3	2 2	7196.356	7196.3532	0.0028	2 1 1	1 1 0	2 2	3 3	15620.468	15620.4649	0.0028
1 0 1	0 0 0	2 2	2 2	7196.376	7196.3898	-0.0136	2 1 1	1 1 0	3 3	3 2	15621.427	15621.4255	0.0016
1 0 1	0 0 0	2 1	2 2	7197.201	7197.2012	0.0001	2 1 1	1 1 0	2 3	2 2	15621.628	15621.6240	0.0035
1 0 1	0 0 0	1 2	1 1	7195.787	7195.7837	0.0030	2 1 1	1 1 0	2 2	3 2	15620.991	15620.9874	0.0033
1 0 1	0 0 0	2 1	1 1	7197.201	7197.2012	0.0001	3 0 3	2 0 2	3 6	3 5	20935.607	20935.6008	0.0058
1 0 1	0 0 0	1 1	1 1	7196.744	7196.7483	-0.0046	3 0 3	2 0 2	2 5	3 5	20934.381	20934.3783	0.0026
2 0 2	1 0 1	2 1	0 0	7197.201	7197.2012	0.0001	3 0 3	2 0 2	1 4	1 3	20935.207	20935.2040	0.0028
2 0 2	1 0 1	3 5	3 4	14224.434	14224.4314	0.0027	3 0 3	2 0 2	0 3	0 2	20935.311	20935.3052	0.0058
2 0 2	1 0 1	3 4	3 3	14224.269	14224.2670	0.0016	3 1 3	2 1 2	3 6	3 5	19646.306	19646.2941	0.0121
2 0 2	1 0 1	2 4	2 3	14224.377	14224.3747	0.0023	3 1 2	2 1 1	3 6	3 5	23318.819	23318.8145	0.0043
2 0 2	1 0 1	3 3	3 2	14223.533	14223.5314	0.0018	3 1 2	2 1 1	0 3	0 2	23318.962	23318.9689	-0.0074
2 0 2	1 0 1	1 2	1 2	14224.795	14224.7917	0.0030	4 0 4	3 0 3	3 7	3 6	27262.845	27262.8501	-0.0050
2 0 2	1 0 1	2 2	1 1	14224.503	14224.5064	-0.0032	4 0 4	3 0 3	1 5	1 4	27262.483	27262.4727	0.0107
2 0 2	1 0 1	1 1	1 0	14224.615	14224.6202	-0.0053	4 0 4	3 0 3	2 4	2 3	27262.845	27262.8607	-0.0156
2 1 2	1 1 1	3 5	3 4	13163.792	13163.7948	-0.0026	1 1 0	1 0 1	3 3	3 4	7307.013	7307.0046	0.0082
2 1 2	1 1 1	2 4	3 4	13162.408	13162.4153	-0.0074	1 1 0	1 0 1	3 4	2 3	7306.505	7306.5008	0.0043
2 1 2	1 1 1	3 4	3 3	13163.316	13163.3050	0.0112	1 1 0	1 0 1	2 3	3 3	7306.052	7306.0578	-0.0061
2 1 2	1 1 1	1 3	2 3	13162.762	13162.7558	0.0062	1 1 1	0 0 0	3 4	3 3	13273.383	13273.3909	-0.0078
2 1 2	1 1 1	1 2	2 3	13163.857	13163.8593	-0.0028	1 1 1	0 0 0	2 3	3 3	13272.772	13272.7748	-0.0030
2 1 2	1 1 1	3 3	2 2	13163.553	13163.5554	-0.0024	1 1 1	0 0 0	3 2	3 3	13273.845	13273.8415	0.0033
2 1 2	1 1 1	1 3	1 2	13162.683	13162.6894	-0.0067	1 1 1	0 0 0	3 3	2 2	13273.326	13273.3294	-0.0029
2 1 2	1 1 1	2 2	2 2	13164.306	13164.3094	-0.0036	1 1 1	0 0 0	1 2	1 1	13272.841	13272.8411	-0.0000
2 1 2	1 1 1	3 1	3 2	13164.136	13164.1370	-0.0015	2 1 2	1 0 1	3 5	3 4	19240.627	19240.6205	0.0068
2 1 2	1 1 1	3 2	1 1	13164.306	13164.3068	-0.0010	2 1 2	1 0 1	3 4	3 3	19240.287	19240.2812	0.0062
2 1 2	1 1 1	2 2	1 1	13164.234	13164.2309	0.0026	2 1 2	1 0 1	2 4	2 3	19240.287	19240.2821	0.0053
2 1 2	1 1 1	2 1	0 1	13163.857	13163.8635	-0.0070	2 1 2	1 0 1	1 3	1 2	19239.741	19239.7469	-0.0061
2 1 1	1 1 0	3 5	3 4	15621.814	15621.8162	-0.0021	2 1 2	1 0 1	3 2	3 2	19240.462	19240.4682	-0.0067
2 1 1	1 1 0	3 4	3 3	15620.873	15620.8678	0.0050	2 1 2	1 0 1	2 2	2 1	19240.462	19240.4628	-0.0013
2 1 1	1 1 0	2 4	3 3	15620.340	15620.3523	-0.0122							

Table 3.A1.2 The observed frequencies of the $\text{Na}^{23}\text{Cl}-\text{H}_2\text{O}$ complex (in MHz)

J^{obs}	J^{calc}	n^{obs}	n^{calc}	obs.-calc.	J^{obs}	J^{calc}	n^{obs}	n^{calc}	obs.-calc.				
1 0 1	0 0 0	3 4	3 3	7023.366	7023.364	0.0025	3 0 3	2 0 2	2 4	2 3	20476.472	20476.476	-0.0039
1 0 1	0 0 0	2 3	3 3	7022.382	7022.371	0.0111	3 0 3	2 0 2	1 4	1 3	20476.385	20476.384	0.0006
1 0 1	0 0 0	3 2	3 3	7024.056	7024.051	0.0047	3 0 3	2 0 2	0 3	0 2	20476.472	20476.464	0.0078
1 0 1	0 0 0	1 2	3 3	7022.569	7022.570	-0.0006	3 1 3	2 1 2	3 6	3 5	19218.048	19218.054	-0.0067
1 0 1	0 0 0	3 3	2 2	7023.193	7023.194	-0.0007	3 1 3	2 1 2	1 4	1 3	19217.587	19217.591	-0.0042
1 0 1	0 0 0	2 2	2 2	7023.233	7023.238	-0.0045	3 1 3	2 1 2	3 3	3 2	19217.583	19217.577	0.0052
1 0 1	0 0 0	1 2	2 2	7022.569	7022.570	-0.0006	3 1 3	2 1 2	0 3	0 2	19217.983	19217.981	0.0017
1 0 1	0 0 0	2 1	2 2	7024.004	7024.008	-0.0039	3 1 3	2 1 2	0 3	0 2	19217.704	19217.707	-0.0037
1 0 1	0 0 0	3 2	1 1	7024.056	7024.051	0.0047	3 1 2	2 1 1	3 6	3 5	22728.462	22728.456	0.0057
1 0 1	0 0 0	2 2	1 1	7023.233	7023.238	-0.0045	3 1 2	2 1 1	0 3	0 3	22728.102	22728.104	-0.0028
1 0 1	0 0 0	1 2	1 1	7022.569	7022.570	-0.0006	1 1 0	1 0 1	3 4	3 4	7345.488	7345.477	0.0113
1 0 1	0 0 0	2 1	1 1	7024.004	7024.008	-0.0039	1 1 0	1 0 1	3 4	2 3	7346.465	7346.470	-0.0050
1 0 1	0 0 0	1 1	1 1	7023.508	7023.499	0.0089	1 1 0	1 0 1	2 3	3 3	7345.972	7345.985	-0.0127
1 0 1	0 0 0	2 1	0 0	7024.004	7024.008	-0.0039	1 1 0	1 0 1	3 3	3 2	7346.179	7346.167	0.0125
2 0 2	1 0 1	3 5	3 4	13894.147	13894.138	0.0078	1 1 0	1 0 1	1 2	1 2	7345.366	7345.358	0.0079
2 0 2	1 0 1	3 4	3 3	13894.016	13894.009	0.0060	1 1 1	0 0 0	3 4	3 3	13194.879	13194.882	-0.0040
2 0 2	1 0 1	1 3	1 2	13893.734	13893.746	-0.0127	1 1 1	0 0 0	2 3	3 3	13194.384	13194.388	-0.0047
2 0 2	1 0 1	1 2	1 2	13894.553	13894.548	0.0037	1 1 1	0 0 0	3 2	3 3	13195.232	13195.239	-0.0071
2 1 2	1 1 1	3 5	3 4	12872.148	12872.146	0.0021	1 1 1	0 0 0	1 2	3 3	13194.450	13194.451	-0.0019
2 1 2	1 1 1	2 4	3 4	12870.912	12870.911	0.0002	1 1 1	0 0 0	2 3	2 2	13194.384	13194.388	-0.0047
2 1 2	1 1 1	3 4	3 3	12871.732	12871.723	0.0088	1 1 1	0 0 0	1 2	2 2	13195.232	13195.239	-0.0071
2 1 2	1 1 1	2 4	2 3	12871.407	12871.405	0.0013	1 1 1	0 0 0	2 1	2 2	13195.232	13195.230	0.0019
2 1 2	1 1 1	3 3	2 2	12871.958	12871.940	0.0177	1 1 1	0 0 0	1 2	1 1	13194.450	13194.451	-0.0019
2 1 2	1 1 1	2 3	2 2	12871.681	12871.692	-0.0115	1 1 1	0 0 0	2 1	1 1	13195.232	13195.230	0.0019
2 1 2	1 1 1	1 2	1 1	12871.619	12871.615	0.0040	1 1 1	0 0 0	2 1	0 0	13195.232	13195.230	0.0019
2 1 1	1 1 0	3 5	3 4	15220.695	15220.705	-0.0108	2 1 2	1 0 1	3 5	3 4	19043.668	19043.664	0.0029
2 1 1	1 1 0	3 4	3 3	15219.816	15219.803	0.0125	2 1 2	1 0 1	3 4	3 3	19043.352	19043.354	-0.0030
2 1 1	1 1 0	2 4	2 3	15220.441	15220.444	-0.0033	2 1 2	1 0 1	2 4	2 3	19043.424	19043.423	0.0011
2 1 1	1 1 0	3 3	3 2	15220.273	15220.287	-0.0149							
3 0 3	2 0 2	3 6	3 5	20476.716	20476.709	0.0062							
3 0 3	2 0 2	2 5	3 5	20475.546	20475.555	-0.0097							

Table 3.A1.3 The observed frequencies of the $\text{Na}^{36}\text{Cl}\text{-HDO}$ complex used in the fitting procedure (in MHz)

J'	K_3'	K_c'	$-J''$	K_3''	K_c''	obs. ^a	calc.	obs.- calc.
1	0	1	0	0	0	6913.1360	6913.1323	.0037
2	0	2	1	0	1	13658.0356	13658.0406	-.0050
2	1	2	1	1	1	12633.3245	12633.3221	.0024
2	1	1	1	1	0	15018.9692	15018.9692	.0000
3	0	3	2	0	2	20087.6012	20087.5993	.0019
3	1	3	2	1	2	18851.2949	18851.2958	-.0009
1	1	1	0	0	0	12621.8630	12621.8616	.0014
2	1	2	1	0	1	18342.0499	18342.0513	-.0014

^a These frequencies were obtained by a comparison with the hyperfine pattern of the $\text{Na}^{36}\text{Cl}\text{-H}_2\text{O}$ complex

Table 3.A1.4 The observed frequencies of the $\text{Na}^{36}\text{Cl}\text{-DHO}$ complex used in the fitting procedure (in MHz)

J'	K_3'	K_c'	$-J''$	K_3''	K_c''	obs. ^a	calc.	obs.- calc.
1	0	1	0	0	0	7141.1703	7141.1650	-.0053
2	0	2	1	0	1	14103.4066	14103.4159	.0093
2	1	2	1	1	1	13039.2665	13039.2607	-.0058
2	1	1	1	1	0	15525.1782	15525.1781	-.0001
3	0	3	2	0	2	20731.0745	20731.0709	-.0036
3	1	3	2	1	2	19454.0197	19454.0214	.0017
1	1	1	0	0	0	12953.7309	12953.7270	-.0039
2	1	2	1	0	1	18851.8270	18851.8310	.0040

^a These frequencies were obtained by a comparison with the hyperfine pattern of the $\text{Na}^{36}\text{Cl}\text{-H}_2\text{O}$ complex

Table 3.A1.5 The observed frequencies of the $\text{Na}^{35}\text{Cl}-(\text{H}_2\text{O})_6$ complex (in MHz)

$J''_k a'' c''$	$J''_k a'' c''$	$n'' F''$	$n'' F''$	$J''_k a'' c''$	obs.	calc.	obs.-calc.	$J''_k a'' c''$	$n'' F''$	$n'' F''$	obs.	calc.	obs.-calc.
1 1 1	0 0 0	3 4	3 3	6015.4812	6015.4772	0.0040	2 2 1	1 1 0	1 1	1 2	14648.6545	14648.6582	-0.0037
1 1 1	0 0 0	2 3	3 3	6015.4033	6015.4051	-0.0018	2 2 1	1 1 0	3 2	2 1	14648.2559	14648.2475	0.0084
1 1 1	0 0 0	3 2	3 3	6015.5293	6015.5268	0.0025	2 2 1	1 1 0	1 2	0 1	14648.8134	14648.8102	0.0032
1 1 1	0 0 0	3 3	2 2	6015.4624	6015.4641	-0.0017	2 2 1	1 1 0	0 2	1 1	14648.1508	14648.1560	-0.0052
1 1 1	0 0 0	1 2	1 1	6015.4251	6015.4207	0.0044	2 2 1	1 1 0	3 1	1 0	14647.5757	14647.5743	0.0014
2 2 0	1 1 1	3 5	3 4	16119.5679	16119.5668	0.0011	2 1 2	1 0 1	3 5	3 4	9413.3580	9413.3556	0.0024
2 2 0	1 1 1	3 4	3 4	16121.4541	16121.4529	0.0012	2 1 2	1 0 1	2 4	3 4	9411.6760	9411.6782	-0.0022
2 2 0	1 1 1	3 4	3 3	16121.5319	16121.5249	0.0070	2 1 2	1 0 1	3 4	3 3	9413.1382	9413.1369	0.0013
2 2 0	1 1 1	2 4	3 3	16120.3908	16120.3925	-0.0017	2 1 2	1 0 1	2 4	2 3	9413.4847	9413.4890	-0.0043
2 2 0	1 1 1	1 3	3 2	16119.8949	16119.8937	0.0012	2 1 2	1 0 1	1 2	2 3	9414.4923	9414.4956	-0.0033
2 2 0	1 1 1	1 1	3 2	16118.4343	16118.4333	0.0010	2 1 2	1 0 1	3 3	3 2	9411.8218	9411.8223	-0.0005
2 2 0	1 1 1	1 2	2 1	16118.8679	16118.8737	-0.0058	2 1 2	1 0 1	3 3	1 2	9414.2247	9414.2209	0.0038
2 0 2	1 1 1	3 5	3 4	7004.6911	7004.6903	0.0008	2 1 2	1 0 1	1 3	1 2	9412.5467	9412.5437	0.0030
2 0 2	1 1 1	2 4	3 4	7002.8027	7002.8043	-0.0016	2 1 2	1 0 1	3 2	3 2	9412.8309	9412.8326	-0.0017
2 0 2	1 1 1	3 4	3 3	7003.9528	7003.9509	0.0019	2 1 2	1 0 1	2 2	2 2	9414.3877	9414.3856	0.0021
2 0 2	1 1 1	2 4	2 3	7002.8752	7002.8764	-0.0012	2 1 2	1 0 1	1 2	3 2	9411.4850	9411.4867	-0.0017
2 0 2	1 1 1	3 3	3 2	7004.2667	7004.2643	0.0024	2 1 2	1 0 1	1 2	1 2	9413.8951	9413.8853	0.0098
2 0 2	1 1 1	3 3	1 2	7004.3642	7004.3704	-0.0062	2 1 2	1 0 1	0 2	2 2	9411.8848	9411.8799	0.0049
2 0 2	1 1 1	3 2	3 2	7005.4062	7005.4044	0.0018	2 1 2	1 0 1	3 2	1 1	9413.5840	9413.5803	0.0037
2 0 2	1 1 1	3 1	3 2	7005.7235	7005.7248	-0.0013	2 1 2	1 0 1	2 2	2 1	9412.9526	9412.9544	-0.0018
2 0 2	1 1 1	3 2	1 1	7005.4453	7005.4432	0.0021	2 1 2	1 0 1	1 2	1 1	9412.2381	9412.2345	0.0036
2 0 2	1 1 1	2 2	2 1	7005.2878	7005.2917	-0.0039	2 1 2	1 0 1	0 2	0 1	9413.3139	9413.3137	0.0002
2 0 2	1 1 1	0 2	0 1	7002.5995	7002.5992	0.0003	2 1 2	1 0 1	2 1	0 1	9414.5739	9414.5687	0.0052
2 0 2	1 1 1	1 1	1 0	7002.9441	7002.9376	0.0065	2 1 2	1 0 1	1 1	1 1	9411.2757	9411.2706	0.0051
2 2 1	1 1 0	3 5	3 4	14648.3417	14648.3456	-0.0039	2 1 2	1 0 1	1 1	1 0	9413.9815	9413.9832	-0.0017
2 2 1	1 1 0	3 4	3 3	14648.0844	14648.0849	-0.0005	3 0 3	2 1 2	3 6	3 5	11224.2227	11224.2215	0.0012
2 2 1	1 1 0	2 4	2 3	14648.5197	14648.5211	-0.0014	3 0 3	2 1 2	3 5	3 4	11223.8742	11223.8794	-0.0052
2 2 1	1 1 0	3 3	3 3	14648.4098	14648.4070	0.0028	3 0 3	2 1 2	2 5	2 4	11223.8742	11223.8697	0.0045
2 2 1	1 1 0	3 3	3 2	14649.0433	14649.0420	0.0013	3 0 3	2 1 2	1 4	2 4	11223.0403	11223.0400	0.0003
2 2 1	1 1 0	2 3	2 2	14648.5197	14648.5232	-0.0035	3 0 3	2 1 2	3 4	3 3	11223.7744	11223.7681	0.0063
2 2 1	1 1 0	1 3	3 2	14647.4269	14647.4248	0.0021	3 0 3	2 1 2	1 4	1 3	11223.3761	11223.3750	0.0011
2 2 1	1 1 0	0 2	1 2	14648.9276	14648.9297	-0.0021	3 0 3	2 1 2	1 3	1 2	11223.0978	11223.1019	-0.0041

Table 3.A1.5 -Continued

$J''_K a''$	$J''_K b''$	$n'' F''$	$n'' F''$	obs.	calc.	obs.-calc.	$J''_K a''$	$J''_K b''$	$n'' F''$	$n'' F''$	obs.	calc.	obs.-calc.
3 0 3	2 1 2	0 3	0 2	11223.5623	11223.5624	-0.0001	4 0 4	3 1 3	2 6	2 5	15031.0751	15031.0749	0.0002
3 0 3	2 1 2	2 2	2 2	11222.6275	11222.6255	0.0020	4 0 4	3 1 3	3 5	3 4	15030.9280	15030.9252	0.0028
3 0 3	2 1 2	3 2	3 1	11223.1377	11223.1437	-0.0060	4 0 4	3 1 3	2 5	2 4	15030.9821	15030.9828	-0.0007
3 0 3	2 1 2	1 2	1 1	11223.7384	11223.7420	-0.0036	4 0 4	3 1 3	1 5	1 4	15030.7838	15030.7836	0.0002
3 2 2	2 1 1	2 5	3 4	18046.1194	18046.1220	-0.0026	4 0 4	3 1 3	3 4	3 3	15031.1326	15031.1294	0.0032
3 2 2	2 1 1	3 4	3 4	18046.1194	18046.1220	-0.0026	4 0 4	3 1 3	2 4	2 3	15031.1326	15031.1379	-0.0053
3 2 2	2 1 1	3 4	1 3	18046.1659	18046.1797	-0.0138	4 0 4	3 1 3	1 4	1 3	15030.5708	15030.5630	0.0078
3 3 0	2 2 1	3 6	3 5	24133.2524	24133.2522	0.0002	4 0 4	3 1 3	0 4	0 3	15030.8277	15030.8324	-0.0047
3 3 0	2 2 1	2 5	2 4	24133.6106	24133.6002	0.0104	4 0 4	3 1 3	3 4	3 3	15030.6047	15030.6163	-0.0116
3 3 1	2 2 0	3 6	3 5	23636.4835	23636.4866	-0.0031	4 0 4	3 1 3	1 3	1 2	15030.8685	15030.8626	0.0059
3 3 1	2 2 0	3 5	3 4	23636.5500	23636.5553	-0.0053	4 2 3	3 1 2	3 7	3 6	20902.2332	20902.2244	0.0088
3 3 1	2 2 0	2 5	2 4	23636.7033	23636.7072	0.0021	4 2 3	3 1 2	3 6	3 5	20902.0759	20902.0725	0.0034
3 3 1	2 2 0	3 4	3 3	23636.9756	23636.9767	-0.0011	4 2 3	3 1 2	3 5	3 4	20902.0759	20902.0725	0.0034
3 3 1	2 2 0	2 4	2 3	23636.7033	23636.7128	-0.0035	4 1 4	3 0 3	3 7	3 6	15523.6560	15523.6575	-0.0015
3 3 1	2 2 0	1 4	1 3	23636.8712	23636.8672	0.0040	4 1 4	3 0 3	3 6	3 5	15523.4492	15523.4514	-0.0022
3 1 3	2 0 2	3 6	3 5	12455.4858	12455.4331	0.0027	4 1 4	3 0 3	2 6	2 5	15523.5435	15523.5497	-0.0062
3 1 3	2 0 2	2 5	2 4	12453.4266	12453.4232	0.0034	4 1 4	3 0 3	3 5	3 4	15523.3694	15523.3877	-0.0183
3 1 3	2 0 2	3 5	3 4	12455.1835	12455.1825	0.0010	4 1 4	3 0 3	2 5	2 4	15523.4492	15523.4488	0.0004
3 1 3	2 0 2	2 5	2 4	12455.3085	12455.3092	-0.0007	4 1 4	3 0 3	1 5	1 4	15523.2589	15523.2653	-0.0054
3 1 3	2 0 2	1 4	1 3	12454.4852	12454.4869	-0.0017	4 1 4	3 0 3	3 4	3 3	15523.5934	15523.5782	0.0152
3 1 3	2 0 2	3 4	3 3	12455.0337	12455.0279	0.0058	4 1 4	3 0 3	2 4	2 3	15523.0743	15523.0725	0.0018
3 1 3	2 0 2	1 4	1 3	12454.8679	12454.8630	0.0049	4 1 4	3 0 3	1 4	1 3	15523.0326	15523.0350	-0.0024
3 1 3	2 0 2	1 3	1 3	12455.9202	12455.9215	-0.0013	4 1 4	3 0 3	3 3	3 2	18590.0179	18590.0177	0.0002
3 1 3	2 0 2	0 3	0 2	12453.6259	12453.6263	-0.0004	5 0 5	4 0 4	2 6	2 5	18590.0179	18590.0138	0.0041
3 1 3	2 0 2	1 3	1 2	12454.4166	12454.4133	0.0033	5 0 5	4 0 4	3 7	3 6	18756.8825	18756.8797	0.0028
3 1 3	2 0 2	0 3	0 2	12455.0337	12455.0372	-0.0035	5 1 5	4 0 4	3 8	3 7	18756.8215	18756.8240	-0.0025
3 1 3	2 0 2	3 2	3 1	12456.0728	12456.0736	-0.0008	5 1 5	4 0 4	2 7	2 6	18756.8145	18756.8126	0.0019
3 1 3	2 0 2	2 2	2 2	12453.7796	12453.7796	0.0022	5 1 5	4 0 4	2 7	2 6	18756.8145	18756.8126	0.0019
3 1 3	2 0 2	3 2	3 1	12454.2334	12454.2357	-0.0023	5 1 5	4 0 4	2 6	2 5	18756.7215	18756.7206	0.0009
3 1 3	2 0 2	3 0	3 1	12455.7538	12455.7552	-0.0014	5 1 5	4 0 4	1 6	1 5	18756.6286	18756.6179	0.0107
4 0 4	3 1 3	3 7	3 6	15031.1971	15031.2012	-0.0041	5 1 5	4 0 4	3 5	3 4	18756.8145	18756.8209	-0.0064
4 0 4	3 1 3	3 6	3 5	15030.9821	15030.9865	-0.0044	5 1 5	4 0 4	2 5	2 4	18756.8145	18756.8267	-0.0122

Table 3.A1.5 -Continued

$J' k_a' k_c'$	$J'' k_a'' k_c''$	$n' F'$	$n'' F''$	obs.	calc.	obs.-calc.
5 1 5	4 0 4	1 5	1 4	18756.4732	18756.4692	0.0040
5 1 5	4 0 4	0 5	0 4	18756.6286	18756.6218	0.0068
6 0 6	5 1 5	3 8	3 7	22042.1108	22042.1114	-0.0006
6 0 6	5 1 5	2 8	2 7	22042.1820	22042.1891	-0.0071
6 0 6	5 1 5	2 7	2 6	22042.1108	22042.1074	0.0034
6 0 6	5 1 5	3 6	3 5	22042.1820	22042.1816	0.0004
6 0 6	5 1 5	2 6	2 5	22042.1820	22042.1850	-0.0030
6 0 6	5 1 5	1 6	1 5	22041.9626	22041.9441	0.0185
6 1 6	5 0 5	3 9	3 8	22093.3269	22093.3191	0.0078
6 1 6	5 0 5	3 8	3 7	22093.1770	22093.2005	-0.0235
6 1 6	5 0 5	2 8	2 7	22093.2754	22093.2777	-0.0023
6 1 6	5 0 5	3 6	3 5	22093.2754	22093.2718	0.0036
6 1 6	5 0 5	2 6	2 5	22093.2754	22093.2754	-0.0000
6 1 6	5 0 5	1 6	1 5	22093.0342	22093.0322	0.0020

Table 3.A1.6. The observed frequencies of the $\text{Na}^{23}\text{Cl}-(\text{H}_2\text{O})_2$ complex (in MHz)

$J^{\text{K}}_a, J^{\text{K}}_b, J^{\text{K}}_c$	n^{F}	n^{F}	obs.	calc.	obs.-calc.	$J^{\text{K}}_a, J^{\text{K}}_b, J^{\text{K}}_c$	n^{F}	n^{F}	obs.	calc.	obs.-calc.		
1 1 1	0 0 0	3 4	3 3	5854.9808	5854.9828	-0.0020	2 1 2	1 0 1	3 5	3 4	9209.0402	9209.0389	0.0013
1 1 1	0 0 0	3 3	3 3	5854.9093	5854.9170	-0.0077	2 1 2	1 0 1	3 4	3 3	9208.8505	9208.8540	-0.0035
1 1 1	0 0 0	3 3	2 2	5854.9808	5854.9815	-0.0007	2 1 2	1 0 1	1 3	1 2	9208.3146	9208.3251	-0.0105
2 2 0	1 1 1	3 5	3 4	15743.9261	15743.9296	-0.0035	3 0 3	2 1 2	3 6	3 5	11179.2956	11179.2885	0.0071
2 2 0	1 1 1	3 4	3 4	15745.6151	15745.6261	-0.0110	3 0 3	2 1 2	3 5	3 4	11178.9895	11178.9847	0.0048
2 2 0	1 1 1	3 4	2 3	15745.6845	15745.6919	-0.0074	3 0 3	2 1 2	3 5	2 4	11178.9586	11178.9606	-0.0020
2 2 0	1 1 1	2 2	2 3	15744.6009	15744.5946	0.0063	3 0 3	2 1 2	3 4	3 3	11178.8984	11178.9002	-0.0018
2 2 0	1 1 1	2 2	2 3	15744.6718	15744.6684	0.0034	3 0 3	2 1 2	2 4	2 3	11178.9566	11178.9545	0.0021
2 2 0	1 1 1	2 2	3 2	15744.5417	15744.5510	-0.0093	3 0 3	2 1 2	1 4	1 3	11178.5044	11178.5241	-0.0197
2 2 0	1 1 1	1 1	3 2	15742.8967	15742.8861	0.0006	3 0 3	2 1 2	2 3	2 2	11179.2584	11179.2623	-0.0039
2 2 0	1 1 1	1 2	1 1	15743.3758	15743.3832	-0.0074	3 0 3	2 1 2	1 2	1 1	11178.6914	11178.6895	0.0019
2 2 0	1 1 1	3 5	3 4	15743.1593	15743.1489	0.0104	3 2 2	2 1 1	3 6	3 5	11178.8539	11178.8546	-0.0007
2 0 2	1 1 1	2 4	3 4	7059.5533	7059.5539	-0.0006	3 2 2	2 1 1	3 5	2 4	17564.7036	17564.7134	-0.0038
2 0 2	1 1 1	2 4	3 4	7057.8610	7057.8544	0.0066	3 2 2	2 1 1	3 5	2 4	17564.6456	17564.6480	-0.0024
2 0 2	1 1 1	2 4	3 3	7058.8971	7058.8885	0.0086	3 1 3	2 0 2	3 5	3 4	12216.4704	12216.4690	0.0014
2 0 2	1 1 1	2 4	2 3	7057.9108	7057.9201	-0.0093	3 1 3	2 0 2	3 5	3 4	12216.3559	12216.3582	-0.0004
2 0 2	1 1 1	1 3	1 2	7057.5968	7057.5867	0.0101	3 1 3	2 0 2	3 4	3 3	12216.1257	12216.1312	-0.0055
2 0 2	1 1 1	0 2	0 1	7057.6584	7057.6750	-0.0066	3 1 3	2 0 2	2 5	2 4	12216.2158	12216.2235	-0.0077
2 2 1	1 1 0	3 5	3 4	14210.6942	14210.6922	0.0020	3 1 3	2 0 2	2 4	2 3	12215.9663	12215.9718	-0.0055
2 2 1	1 1 0	3 4	3 4	14212.1568	14212.1447	0.0121	3 1 3	2 0 2	1 3	1 2	12215.5610	12215.5647	-0.0037
2 2 1	1 1 0	3 4	3 3	14210.4609	14210.4646	-0.0037	3 1 3	2 0 2	0 3	0 2	12216.1257	12216.1235	0.0022
2 2 1	1 1 0	2 4	2 3	14210.8516	14210.8527	-0.0011	4 0 4	3 1 3	3 7	3 6	14887.9614	14887.9607	0.0007
2 2 1	1 1 0	3 3	3 3	14210.7657	14210.7501	0.0156	4 0 4	3 1 3	3 6	3 5	14887.7844	14887.7798	0.0046
2 2 1	1 1 0	3 3	3 2	14211.2959	14211.3010	-0.0051	4 0 4	3 1 3	3 5	3 4	14887.7344	14887.7371	-0.0027
2 2 1	1 1 0	3 3	3 2	14209.8496	14209.8502	-0.0006	4 0 4	3 1 3	3 5	3 4	14887.5915	14887.5839	0.0076
2 2 1	1 1 0	1 3	1 2	14212.1012	14212.0931	0.0081	4 0 4	3 1 3	1 5	1 4	14887.3884	14887.3889	-0.0005
2 2 1	1 1 0	2 2	3 2	14210.1440	14210.1416	0.0024	4 0 4	3 1 3	0 4	0 3	14887.6421	14887.6267	0.0154
2 2 1	1 1 0	1 1	1 2	14210.9615	14210.9700	-0.0085	4 1 4	3 0 3	3 7	3 6	15273.8632	15273.8625	0.0007
2 2 1	1 1 0	3 2	2 1	14210.6021	14210.6099	-0.0078	4 1 4	3 0 3	3 6	3 5	15273.6919	15273.6902	0.0017
2 2 1	1 1 0	1 2	0 1	14211.1501	14211.1429	0.0072	4 1 4	3 0 3	3 5	3 4	15273.6505	15273.6514	-0.0009
2 2 1	1 1 0	3 1	1 0	14210.0231	14210.0147	0.0084							

Table 3.A1.6 -Continued

$J''_k a'' c''$	$J''_k b'' c''$	$n'' F''$	$n'' F''$	$n'' F''$	obs.	calc.	obs.-calc.
4 1 4	3 0 3	1 5	1 4	1 4	15273.5263	15273.5216	0.0047
4 1 4	3 0 3	1 4	1 3	1 3	15273.3135	15273.3139	-0.0004
4 1 4	3 0 3	3 3	3 2	3 2	15273.3882	15273.3755	0.0127
5 0 5	4 1 4	3 8	3 7	3 7	18371.5135	18371.5164	-0.0029
5 0 5	4 1 4	2 7	2 6	2 6	18371.4440	18371.4504	-0.0064
5 0 5	4 1 4	1 6	1 5	1 5	18371.2893	18371.2845	0.0048
5 0 5	4 1 4	3 5	3 4	3 4	18371.4440	18371.4582	-0.0142
5 0 5	4 1 4	0 5	0 4	0 4	18371.2893	18371.2872	0.0021

Table 3.A1.7 The observed frequencies of the $\text{Na}^{35}\text{Cl}-(\text{H}_2\text{O})_n$ complex used in the fitting procedure (in MHz)

J'	K'	n'	F'	J''	K''	n''	F''	obs.	calc.	obs. - calc.
2	0	3	5	1	0	3	4	7513.699	7513.700	-0.001
2	0	3	4	1	0	3	3	7513.626	7513.623	0.003
2	0	1	3	1	0	3	3	7512.975	7512.980	-0.006
2	0	0	2	1	0	3	3	7512.459	7512.452	0.007
2	0	3	3	1	0	3	2	7513.995	7513.997	-0.002
2	0	1	1	1	0	3	2	7512.626	7512.628	-0.002
2	1	3	5	1	1	3	4	7513.552	7513.552	0.000
2	1	3	4	1	1	3	4	7513.928	7513.942	-0.015
2	1	3	4	1	1	2	3	7514.373	7514.371	0.002
2	1	2	4	1	1	3	3	7513.777	7513.782	-0.004
2	1	3	3	1	1	2	3	7514.436	7514.436	0.000
2	1	3	3	1	1	1	2	7514.319	7514.315	0.004
2	1	2	2	1	1	1	2	7514.019	7514.009	0.010
2	1	1	1	1	1	3	2	7513.033	7513.035	-0.002
3	0	3	6	2	0	3	5	11270.463	11270.452	0.012
3	1	3	6	2	1	3	5	11270.409	11270.414	-0.005
3	1	3	5	2	1	3	4	11270.572	11270.580	-0.008
3	2	3	6	2	2	3	5	11270.305	11270.302	0.003
3	2	3	3	2	2	3	2	11269.915	11269.912	0.003
3	2	2	3	2	2	2	2	11270.119	11270.118	0.002
3	2	1	2	2	2	1	1	11271.088	11271.059	0.029
3	2	3	1	2	2	3	1	11269.843	11269.845	-0.002
4	1	3	7	3	1	3	6	15026.974	15026.965	0.009
4	1	3	6	3	1	3	5	15027.017	15027.020	-0.002
4	1	2	6	3	1	2	5	15027.017	15027.015	0.002
4	1	3	5	3	1	3	4	15027.066	15027.088	-0.022
4	1	2	4	3	1	2	3	15027.109	15027.140	-0.032
4	2	2	5	3	2	2	4	15027.153	15027.154	-0.001
4	3	2	6	3	3	2	5	15027.662	15027.666	-0.004
4	3	1	5	3	3	1	4	15027.875	15027.872	0.003
4	3	1	4	3	3	1	3	15027.494	15027.494	0.000
4	3	0	4	3	3	0	3	15027.797	15027.796	0.000

Table 3.A1.8 The observed frequencies of the $\text{Na}^{37}\text{Cl}-(\text{H}_2\text{O})_5$ complex used in the fitting procedure (in MHz)

J'	K'	n'	F'	J''	K''	n''	F''	obs.	calc.	obs. - calc.
2	0	3	5	1	0	3	4	7382.510	7382.509	0.0010
2	0	2	4	1	0	2	3	7382.572	7382.573	-0.0012
2	1	3	5	1	1	3	4	7382.377	7382.371	0.0063
2	1	3	4	1	1	3	4	7382.745	7382.747	-0.0022
2	1	2	4	1	1	3	3	7382.572	7382.568	0.0034
3	1	3	6	2	1	3	5	11073.636	11073.636	0.0003
3	1	3	5	2	1	3	4	11073.805	11073.800	0.0044
3	2	3	6	2	2	3	5	11073.537	11073.531	0.0059
3	2	2	5	2	2	2	4	11074.284	11074.283	0.0004
3	2	1	4	2	2	1	3	11074.389	11074.392	-0.0031
3	2	3	3	2	2	3	2	11073.128	11073.129	-0.0004
3	2	0	3	2	2	0	2	11074.348	11074.359	-0.0112
3	2	1	2	2	2	1	1	11074.254	11074.259	-0.0048
4	1	3	7	3	1	3	6	14764.610	14764.607	0.0030
4	2	3	7	3	2	3	6	14764.610	14764.617	-0.0065
4	3	2	6	3	3	2	5	14765.289	14765.287	0.0011
4	3	1	5	3	3	1	4	14765.473	14765.460	0.0131
4	3	3	4	3	3	3	3	14764.360	14764.369	-0.0084
4	3	0	4	3	3	0	3	14765.395	14765.395	0.0003

Appendix II.

The calculation of the electric field gradient using the electrostatic model

Now we consider that there is a charge with magnitude C at the origin in the coordinate system as shown in Fig. 3.8. The electric field at the point (r, θ) arising from the charge is written as the sum of following two components,

$$E_a = \frac{C}{r^2} \sin \theta, \quad (3.A2.1)$$

and

$$E_b = \frac{C}{r^2} \cos \theta. \quad (3.A2.2)$$

As we can relate the variables (a, b) to (r, θ) as following equations,

$$(a, b) = (r \sin \theta, r \cos \theta). \quad (3.A2.3)$$

Therefore, we can calculate the electric field gradients at the point (r, θ) as follows,

$$\begin{aligned} \frac{\partial E_a}{\partial a} &= \frac{\partial E_a}{\partial r} \cdot \frac{\partial r}{\partial a} + \frac{\partial E_a}{\partial \theta} \cdot \frac{\partial \theta}{\partial a} \\ &= \frac{C}{r^3} (3 \cos^2 \theta - 2) \end{aligned} \quad (3.A2.4)$$

and, similarly,

$$\begin{aligned} \frac{\partial E_b}{\partial b} &= \frac{\partial E_b}{\partial r} \cdot \frac{\partial r}{\partial b} + \frac{\partial E_b}{\partial \theta} \cdot \frac{\partial \theta}{\partial b} \\ &= -\frac{C}{r^3} (3 \cos^2 \theta - 1) \end{aligned} \quad (3.A2.5)$$

Next we consider that there is a dipole moment with magnitude μ at the origin in the coordinate system as shown in Fig. 3.8. The electric field at the point (r, θ) arising from the dipole moment is written as the sum of following two components,

$$E_r = \frac{2\mu}{r^3} \cos \theta, \quad (3.A2.6)$$

and

$$E_{\theta} = \frac{\mu}{r^3} \sin \theta \quad (3.A2.7)$$

where E_r and E_{θ} represent the radial part and the angular part of the electric field, respectively. Therefore, the partial differentials of two components of the electric field on the variables, r and θ , are written as follows,

$$\frac{\partial E_r}{\partial r} = -\frac{6\mu}{r^4} \cos \theta, \quad \frac{\partial E_r}{\partial \theta} = -\frac{2\mu}{r^3} \sin \theta, \quad \frac{\partial E_{\theta}}{\partial r} = -\frac{3\mu}{r^4} \sin \theta, \quad \text{and} \quad \frac{\partial E_{\theta}}{\partial \theta} = \frac{\mu}{r^3} \cos \theta \quad (3.A2.8)$$

As the angle between the direction of component E_r and b -axis is $(\theta - \alpha)$, the projections along a - and b -axis at the point (r, θ) are written as follows,

$$E_a = E_r \sin(\theta - \alpha) + E_{\theta} \cos(\theta - \alpha) \quad (3.A2.9)$$

$$E_b = E_r \cos(\theta - \alpha) - E_{\theta} \sin(\theta - \alpha) \quad (3.A2.10)$$

As we can relate the variables (a, b) to (r, θ) as following equations,

$$r^2 = a^2 + b^2, \quad (3.A2.11)$$

and

$$\tan(\theta - \alpha) = \frac{a}{b} \quad (3.A2.12)$$

we obtain the following relations,

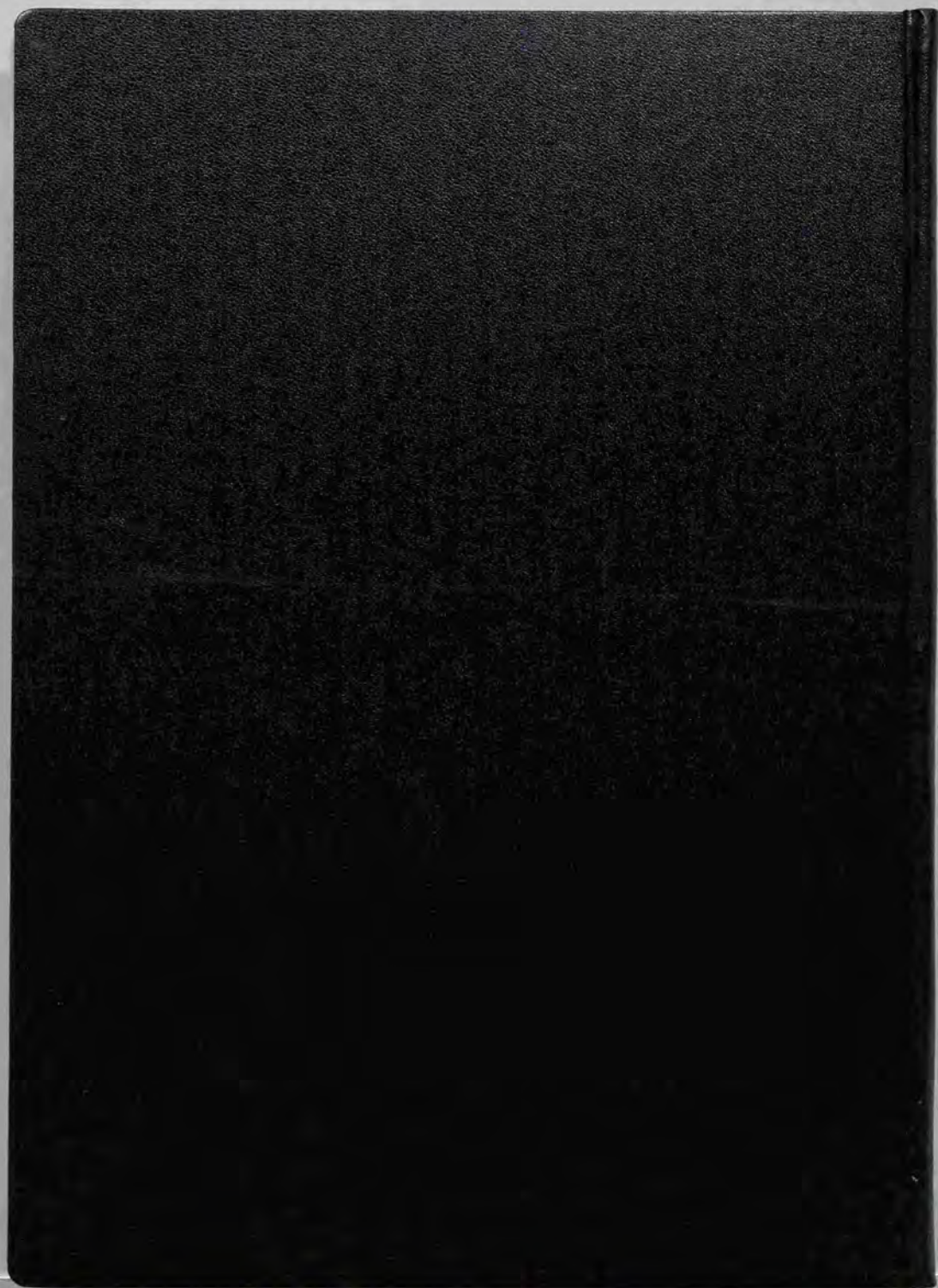
$$\frac{\partial r}{\partial a} = \sin(\theta - \alpha), \quad \frac{\partial r}{\partial b} = \cos(\theta - \alpha), \quad \frac{\partial \theta}{\partial a} = \frac{\cos(\theta - \alpha)}{r}, \quad \text{and} \quad \frac{\partial \theta}{\partial b} = -\frac{\sin(\theta - \alpha)}{r} \quad (3.A2.13)$$

Therefore, we can calculate the electric field gradients at the point (r, θ) as follows,

$$\begin{aligned} \frac{\partial E_a}{\partial a} &= \frac{\partial E_a}{\partial r} \cdot \frac{\partial r}{\partial a} + \frac{\partial E_a}{\partial \theta} \cdot \frac{\partial \theta}{\partial a} \\ &= -\frac{3\mu}{r^4} [\cos \theta \{3 \sin^2(\theta - \alpha) - 1\} + \sin \theta \sin 2(\theta - \alpha)] \end{aligned} \quad (3.A2.14)$$

and, similarly,

$$\begin{aligned} \frac{\partial E_b}{\partial b} &= \frac{\partial E_b}{\partial r} \cdot \frac{\partial r}{\partial b} + \frac{\partial E_b}{\partial \theta} \cdot \frac{\partial \theta}{\partial b} \\ &= -\frac{3\mu}{r^4} [\cos \theta \{3 \cos^2(\theta - \alpha) - 1\} - \sin \theta \sin 2(\theta - \alpha)] \end{aligned} \quad (3.A2.15)$$





Kodak Color Control Patches

Blue Cyan Green Yellow Red Magenta White 3/Color Black

Kodak Gray Scale

A 1 2 3 4 5 6 M 8 9 10 11 12 13 14 15 B 17 18 19

C **Y** **M**

© Kodak, 2007 TM Kodak